# Chapter 3

# Optical Properties of Water[1]

We now have learned how to quantitatively describe light fields. It remains to learn how to measure and describe the optical properties of the *medium* through which the light propagates.

Natural waters, both fresh and saline, are a witch's brew of dissolved and particulate matter. These solutes and particles are both optically significant and highly variable in kind and concentration. Consequently, the optical properties of natural waters show large temporal and spatial variations and seldom resemble those of pure water.

The great variability of the optical properties of natural waters is the bane of those who desire precise and easily tabulated data. However, it is the connections between the optical properties and the biological, chemical and geological constituents of natural water and the physical environment that define the critical role of optics in aquatic research. For just as hydrologic optics utilizes results from the biological, chemical, geological and physical subdisciplines of limnology and oceanography, so do those subdisciplines incorporate optics. This synergism is seen in such areas as bio-optical oceanography, marine photochemistry, mixed-layer dynamics, laser bathymetry, and remote sensing of biological productivity, sediment load, or pollutants.

The *bulk*, or large-scale, optical properties of water are conveniently divided into two mutually exclusive classes: inherent and apparent. *Inherent optical properties* (IOP's) *are those properties that depend only upon the medium*, and therefore are independent of the ambient light field within the medium. The two fundamental IOP's are the absorption coefficient and the volume scattering function. Other IOP's include the index of refraction, the beam attenuation coefficient and the single-scattering albedo. *Apparent optical properties* (AOP's) *are those properties that depend both on the medium* (the IOP's) *and on the geometric* (directional) *structure of the*

---

[1]Substantial parts of this chapter are reproduced from "Optical Properties of Water" by C.D. Mobley, in *Handbook of Optics, Second Edition*, M. Bass, editor, copyright 1994 by McGraw-Hill, Inc. Reproduced by permission of McGraw-Hill, Inc.

*ambient light field, and that display enough regular features and stability to be useful descriptors of the water body*.  Commonly used AOP's are the irradiance reflectance, the average cosines, and the various diffuse attenuation coefficients.  All of these quantities are defined below.

Radiative transfer theory provides the connection between the IOP's and the AOP's.  The physical environment of a water body – waves on its surface, the character of its bottom, the incident radiance from the sky – enters the theory via the boundary conditions necessary for solution of the equations arising from the theory.

The goal of this chapter is to survey the bulk optical properties of natural waters.  Our discussion of these properties is tailored to meet the needs of radiative transfer theory as applied to hydrologic optics, and we shall draw upon this information throughout the remainder of the book.  We comment only briefly on the reasons why the various optical properties have their observed values.  However, we shall discuss in some detail the presently available models that seek to predict bulk optical properties from parameters of biological or geological significance, such as chlorophyll concentration or particle mass concentration.  The unseverable connections between optics and biology, chemistry, and geology thus will be made obvious.  We close the chapter with an overview of "single-particle" optics, in order to show how the transition is made from a collection of diverse particles to the needed bulk optical properties.

# 3.1  Inherent Optical Properties

The inherent optical properties (IOP's) specify the optical properties of natural waters in a form suited to the needs of radiative transfer theory.  We shall define these properties here, and discuss their measurement and values in Sections 3.6-3.9, below.

Consider a small volume $\Delta V$ of water, of thickness $\Delta r$, illuminated by a narrow collimated beam of monochromatic light of spectral radiant power $\Phi_i(\lambda)$, W nm$^{-1}$, as schematically illustrated in Fig. 3.1.  Some part $\Phi_a(\lambda)$ of the incident power $\Phi_i(\lambda)$ is absorbed within the volume of water.  Some part $\Phi_s(\psi;\lambda)$ is scattered out of the beam at an angle $\psi$, and the remaining power $\Phi_t(\lambda)$ is transmitted through the volume with no change in direction.  Let $\Phi_s(\lambda)$ be the total power that is scattered into all directions.  Furthermore, assume that no inelastic scattering occurs, i.e. assume that no photons undergo a change in wavelength during the scattering process.  Then by conservation of energy,
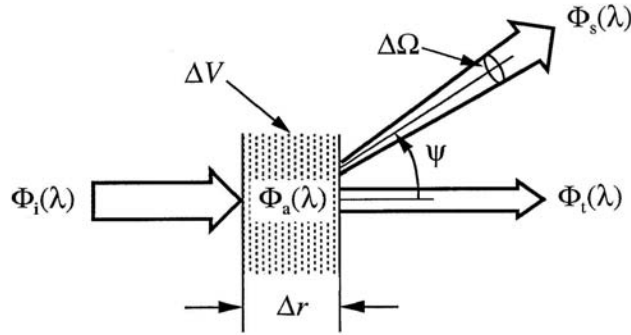
Fig. 3.1.  Geometry used to define inherent optical properties.  [reproduced from Mobley (1994), by permission]

$$\Phi_i(\lambda) = \Phi_a(\lambda) + \Phi_s(\lambda) + \Phi_t(\lambda).$$

The *spectral absorptance A(λ)* is the fraction of incident power that is absorbed within the volume:

$$A(\lambda) \equiv \frac{\Phi_a(\lambda)}{\Phi_i(\lambda)}.$$

We are now using "spectral" to mean "as a function of wavelength."  Spectral IOP's and AOP's do *not* have units of nm$^{-1}$ appended.  Likewise, the *spectral scatterance B(λ)* is the fractional part of the incident power that is scattered out of the beam,

$$B(\lambda) \equiv \frac{\Phi_s(\lambda)}{\Phi_i(\lambda)},$$

and the *spectral transmittance T(λ)* is

$$T(\lambda) \equiv \frac{\Phi_t(\lambda)}{\Phi_i(\lambda)}.$$

Clearly, $A(\lambda) + B(\lambda) + T(\lambda) = 1$.

A quantity easily confused with the absorptance $A(\lambda)$ is the *absorbance D(λ)* (also called the *optical density)*, which is defined as

$$D(\lambda) \equiv \log_{10} \frac{\Phi_i(\lambda)}{\Phi_s(\lambda) + \Phi_t(\lambda)} = -\log_{10}[1 - A(\lambda)].$$

$D(\lambda)$ is the quantity actually measured in a spectrophotometer (Kirk, 1983).

The inherent optical properties usually employed in hydrologic optics are the spectral absorption and scattering coefficients, which are respectively the spectral absorptance and scatterance *per unit distance* in the medium.  In the geometry of Fig. 3.1, the *spectral absorption coefficient* a($\lambda$) is defined as

$$a(\lambda) \equiv \lim_{\Delta r \to 0} \frac{A(\lambda)}{\Delta r} \qquad (\text{m}^{-1}),$$

(3.1)

and the *spectral scattering coefficient* b($\lambda$) is

$$b(\lambda) \equiv \lim_{\Delta r \to 0} \frac{B(\lambda)}{\Delta r} \qquad (\text{m}^{-1}).$$

(3.2)

The *spectral beam attenuation coefficient c($\lambda$)* is defined as

$$c(\lambda) \equiv a(\lambda) + b(\lambda) \qquad (\text{m}^{-1}).$$

(3.3)

Now take into account the angular distribution of the scattered power, with $B(\psi;\lambda)$ being the fraction of incident power scattered out of the beam through an angle $\psi$ into a solid angle $\Delta\Omega$ centered on $\psi$, as shown in Fig. 3.1. The angle $\psi$ is called the *scattering angle*; its values lie in the interval $0 \le \psi \le \pi$.  Then the angular scatterance per unit distance and unit solid angle, $\beta(\psi;\lambda)$, is

$$\beta(\psi;\lambda) \equiv \lim_{\Delta r \to 0} \lim_{\Delta\Omega \to 0} \frac{B(\psi;\lambda)}{\Delta r \, \Delta\Omega} = \lim_{\Delta r \to 0} \lim_{\Delta\Omega \to 0} \frac{\Phi_s(\psi;\lambda)}{\Phi_i(\lambda) \, \Delta r \, \Delta\Omega} \qquad (\text{m}^{-1}\,\text{sr}^{-1}).$$

The spectral power scattered into the given solid angle $\Delta\Omega$ is just the spectral radiant intensity scattered into direction $\psi$ times the solid angle: $\Phi_s(\psi;\lambda) = I_s(\psi;\lambda)\Delta\Omega$.  Moreover, if the incident power $\Phi_i(\lambda)$ falls on an area $\Delta A$, then the corresponding incident irradiance is $E_i(\lambda) = \Phi_i(\lambda)/\Delta A$.  Noting that $\Delta V = \Delta r \Delta A$ is the volume of water that is illuminated by the incident beam gives

$$\beta(\psi;\lambda) = \lim_{\Delta V \to 0} \frac{I_s(\psi;\lambda)}{E_i(\lambda) \, \Delta V}.$$

(3.4)

This form of $\beta(\psi;\lambda)$ suggests the name *spectral volume scattering function* and the physical interpretation of scattered intensity per unit incident irradiance per unit volume of water.  In the language of a physicist, $\beta(\psi;\lambda)$ also can be interpreted as the differential scattering cross section per unit volume.

Integrating $\beta(\psi;\lambda)$ over all directions (solid angles) gives the total scattered power per unit incident irradiance and unit volume of water, in other words the spectral scattering coefficient:

$$b(\lambda) = \int_{\Xi} \beta(\psi;\lambda)\, d\Omega = 2\pi \int_{0}^{\pi} \beta(\psi;\lambda)\, \sin\psi\, d\psi \,. \tag{3.5}$$

The last equation follows because scattering in natural waters is azimuthally symmetric about the incident direction (for unpolarized sources and for randomly oriented scatterers). This integration is often divided into forward scattering, $0 \le \psi \le \pi/2$, and backward scattering, $\pi/2 \le \psi \le \pi$, parts. The corresponding spectral forward and backward scattering coefficients are, respectively,

$$b_{\mathrm{f}}(\lambda) \equiv 2\pi \int_{0}^{\pi/2} \beta(\psi;\lambda)\, \sin\psi\, d\psi \tag{3.6a}$$

$$b_{\mathrm{b}}(\lambda) \equiv 2\pi \int_{\pi/2}^{\pi} \beta(\psi;\lambda)\, \sin\psi\, d\psi \,. \tag{3.6b}$$

The *spectral volume scattering phase function*, $\tilde{\beta}(\psi,\lambda)$, is defined by

$$\tilde{\beta}(\psi;\lambda) \equiv \frac{\beta(\psi;\lambda)}{b(\lambda)} \qquad (\mathrm{sr}^{-1}) \,. \tag{3.7}$$

Writing the volume scattering function $\beta(\psi;\lambda)$ as the product of the scattering coefficient $b(\lambda)$ and the phase function $\tilde{\beta}(\psi,\lambda)$ partitions $\beta(\psi;\lambda)$ into a factor giving the *strength* of the scattering, $b(\lambda)$ with units of $\mathrm{m}^{-1}$, and a factor giving the *angular distribution* of the scattered photons, $\tilde{\beta}(\psi,\lambda)$ with units of $\mathrm{sr}^{-1}$. Combining Eqs. (3.5) and (3.7) gives the normalization condition for the phase function:

$$2\pi \int_{0}^{\pi} \tilde{\beta}(\psi;\lambda)\, \sin\psi\, d\psi = 1 \,. \tag{3.8}$$

The term "phase function" has its historical origins in astronomy; $\tilde{\beta}$ has nothing whatsoever to do with the phase of an electromagnetic wave.

The average over all scattering directions of the cosine of the scattering angle $\psi$,

$$g \equiv 2\pi \int_{0}^{\pi} \tilde{\beta}(\psi)\, \cos\psi\, \sin\psi\, d\psi \,, \tag{3.8b}$$

is a convenient measure of the "shape" of the phase function. For example,

if $\tilde{\beta}(\psi)$ is very large for small $\psi$, then $g$ is near one. If $\tilde{\beta}(\psi)$ is symmetric about $\psi = 90°$, then $g = 0$. The average cosine $g$ often is called the *asymmetry parameter* of the phase function.

Another inherent optical property commonly used in hydrologic optics is the *spectral single-scattering albedo* $\omega_o(\lambda)$, defined by

$$\omega_o(\lambda) \equiv \frac{b(\lambda)}{c(\lambda)}. \qquad (3.9)$$

In waters where the beam attenuation is due primarily to scattering, $\omega_o$ is near one. In waters where the beam attenuation is due primarily to absorption, $\omega_o$ is near zero. As we shall see in Section 6.1, the single-scattering albedo is the probability that a photon will be scattered (rather than absorbed) in any given interaction, hence $\omega_o(\lambda)$ is also known as the *probability of photon survival*.

Just as with the radiometric quantities, there is an "historic" set of symbols in addition to the IAPSO recommended symbols, which we have used above. Table 3.1 summarizes the IOP's as they are commonly employed in hydrologic optics.

The preceding discussion has assumed that no inelastic (transpectral) scattering processes are present. However, transpectral scattering does occur in natural waters, attributable to fluorescence by dissolved matter or chlorophyll, and to Raman or Brillouin scattering by the water molecules themselves. Power lost from wavelength $\lambda_1$ by scattering into wavelength $\lambda_2 \neq \lambda_1$ appears in the above formalism as an increase in the spectral absorption at $\lambda_1$. In this case, $a(\lambda_1)$ accounts for "true" absorption (e.g.

Table 3.1. Terms, units, and symbols for inherent optical properties.

| Quantity | SI units | Recommended symbol | Historic symbol |
|---|---|---|---|
| (real) index of refraction | dimensionless | $n$ | $m$ |
| absorption coefficient | $m^{-1}$ | $a$ | $a$ |
| volume scattering function | $m^{-1} sr^{-1}$ | $\beta$ | $\sigma$ |
| scattering phase function | $sr^{-1}$ | $\tilde{\beta}$ | $p$ |
| scattering coefficient | $m^{-1}$ | $b$ | $s$ |
| backward scattering coefficient | $m^{-1}$ | $b_b$ | $b$ |
| forward scattering coefficient | $m^{-1}$ | $b_f$ | $f$ |
| beam attenuation coefficient | $m^{-1}$ | $c$ | $\alpha$ |
| single-scattering albedo | dimensionless | $\tilde{\omega}$ or $\omega_o$ | $\rho$ |

conversion of radiant energy into heat) as well as for the loss of power at wavelength $\lambda_1$ by inelastic scattering to other wavelengths. The gain in power at $\lambda_2$ appears as a source term in the radiative transfer formalism. These matters are discussed in detail in Chapter 5.

The IOP's as just defined give us a full description of the optical properties of a water body as needed for the interpretation and prediction of underwater light fields within the framework of radiative transfer theory. Note that the IOP's can be measured using small samples of water; they are independent of the environment where the sample was taken. However, nature has not been kind to us. It is usually quite difficult to measure the IOP's, especially *in situ*. Indeed, the only IOP that is routinely and accurately measured *in situ* is the beam attenuation coefficient $c(\lambda)$, and even then it is usually measured at only one wavelength, $\lambda \approx 660$ nm. The optical measurements commonly made are of various apparent optical properties, which we discuss in Section 3.2.

## *Modeling IOP's*

*It is the total values of the various IOP's that are relevant to radiative transfer.* However, each of these quantities is a sum of contributions by the various constituents of a water body. For example, the total absorption coefficient $a$ is the sum of absorption by the water itself, by various biological particles, by dissolved substances, by mineral particles, and so on. Since the composition of natural water bodies varies with location $\vec{x}$ and time $t$, so do the IOP's.

It is often desirable to model, or predict, the IOP's in terms of the constituent contributions. Thus we write

$$a(\vec{x};t;\lambda) \;=\; \sum_{i=1}^{N_a} a_i(\vec{x};t;\lambda)\,, \tag{3.10}$$

if there are $N_a$ different substances contributing to the absorption. Typically, $a_1$ is taken to be absorption by pure sea water, so that $a_1(\vec{x};t;\lambda) \equiv a_w(\lambda)$ depends only on wavelength. Likewise we write

$$b(\vec{x};t;\lambda) \;=\; b_w(\lambda) \;+\; \sum_{i=2}^{N_s} b_i(\vec{x};t;\lambda) \tag{3.11}$$

and

$$\beta(\vec{x};t;\psi;\lambda) \;=\; \beta_w(\psi,\lambda) \;+\; \sum_{i=2}^{N_s} \beta_i(\vec{x};t;\psi;\lambda)\,, \tag{3.12}$$

where $N_s$ is the number of constituents contributing to scattering.

Each of the component volume scattering functions can be written in terms of a phase function. Thus

$$\beta_i(\vec{x};t;\psi;\lambda) \equiv b_i(\vec{x};t;\lambda)\,\tilde{\beta}_i(\psi;\lambda)\,,$$

in which case Eq. (3.12) can be written as

$$\tilde{\beta}(\vec{x};t;\psi;\lambda) = \frac{b_w(\lambda)}{b(\vec{x};t;\lambda)}\,\tilde{\beta}_w(\psi) + \sum_{i=2}^{N_s} \frac{b_i(\vec{x};t;\lambda)}{b(\vec{x};t;\lambda)}\,\tilde{\beta}_i(\psi;\lambda)\,. \qquad (3.13)$$

There are two points to note in Eq. (3.13). First, if each of the constituent $\tilde{\beta}_i$'s satisfies the normalization requirement (3.8), then so does the total $\tilde{\beta}$. Second, we have *assumed* that the spatial and temporal variability of the constituent $\beta_i$'s are contained in the corresponding scattering coefficients $b_i$. This is usually reasonable, since the directional ($\psi$) nature of the scattering is largely determined by the *type* of particles (e.g. water molecules, small mineral particles, or large biological particles), and the strength of scattering is determined by the *concentration* of particles, which varies with location and time. We can imagine exceptions to this statement, such as a change in $\tilde{\beta}_i$ induced by a change in the particle size distribution while $b_i$ stays constant, but Eq. (3.13) is generally a good approximation of nature. The assumption that the $\tilde{\beta}_i$'s are independent of position and time yields major computational savings (see Section 8.2), and we shall make the assumption in the numerical simulation of Section 11.8. Examples of Eqs. (3.10) to (3.13) will be seen in Sections 3.7 and 3.8.

## 3.2 Apparent Optical Properties

Apparent optical properties (AOP's) arise when we use radiometric quantities other than radiance to describe the light field in a water body. As we already have stated, the AOP's depend both on the medium (i.e. on the IOP's) and on the directional structure of the ambient light field. Any radiometric quantity such as an irradiance satisfies this half of the definition. However, the second half of the definition requires that the quantity also display enough regular features and stability to be useful for describing a water body. An irradiance, for example, can change greatly in magnitude in a matter of seconds if a cloud passes in front of the sun, or if a gust of wind changes the sea surface from glassy smooth to rippled. However, observation shows that certain *ratios* of radiometric quantities are relatively

insensitive to environmental factors such as sea state.  Likewise, the *rate of change with depth* of a radiometric quantity is often well behaved.  It is these ratios and depth derivatives that are candidates for consideration as AOP's.

An ideal AOP changes only slightly with external environmental changes, but changes enough from one water body to the next to be useful in characterizing the different optical properties of the two water bodies.  Note that, unlike IOP's, AOP's cannot be measured on water samples, because they depend on the ambient radiance distribution found in the water body itself.

Table 3.2 lists the most commonly used AOP's, along with their recommended and historic symbols.  We define these AOP's in the remainder of this section.  We shall have ample opportunity in the course of our studies to further examine the AOP's and to illustrate their dependence on the IOP's and on environmental conditions.

Table 3.2.  Terms, units, and symbols for apparent optical properties.

| Quantity | SI units | Recommen-ded symbol | Historic symbol |
|---|---|---|---|
| distribution function | dimensionless | $D$ | $D$ |
| average cosine of light field | dimensionless | $\bar{\mu}$ | $D = 1/\bar{\mu}$ |
| of downwelling light | dimensionless | $\bar{\mu}_d$ | $D(-) = 1/\bar{\mu}_d$ |
| of upwelling light | dimensionless | $\bar{\mu}_u$ | $D(+) = 1/\bar{\mu}_u$ |
| irradiance reflectance | dimensionless | $R$ | $R(-)$ |
| remote sensing reflectance | $sr^{-1}$ | $R_{rs}$ | — |
| (vertical) diffuse attenuation coefficients (*K*-functions): | | | |
| of radiance $L(z;,\theta,\phi)$ | $m^{-1}$ | $K(\theta,\phi)$ | $K(\theta,\phi)$ |
| of downward irradiance $E_d(z)$ | $m^{-1}$ | $K_d$ | $K(-)$ |
| of upward irradiance $E_u(z)$ | $m^{-1}$ | $K_u$ | $K(+)$ |
| of downward scalar irradiance $E_{od}(z)$ | $m^{-1}$ | $K_{od}$ | $k(-)$ |
| of upward scalar irradiance $E_{ou}(z)$ | $m^{-1}$ | $K_{ou}$ | $k(+)$ |
| of total scalar irradiance $E_o(z)$ | $m^{-1}$ | $K_o$ | $k$ |
| of PAR$(z)$ | $m^{-1}$ | $K_{PAR}$ | — |

*Average cosines*

Let us consider the case of horizontally homogeneous water bodies. Let us also measure the geometric depth $z$ (in meters) as positive downward from the mean sea surface (i.e., $z = x_3$ in the coordinate system of Fig. 1.3). Then the quantity

$$\bar{\mu}_d(z;\lambda) \equiv \frac{\int_{\Xi_d} L(z;\theta,\phi;\lambda)\cos\theta\, d\Omega}{\int_{\Xi_d} L(z;\theta,\phi;\lambda)\, d\Omega} \equiv \frac{E_d(z;\lambda)}{E_{od}(z;\lambda)} \tag{3.14}$$

is called the *spectral downwelling average cosine*. The definition shows that $\bar{\mu}_d(z;\lambda)$ is the average value of the cosine of the polar angle of all the photons contributing to the downwelling radiance at the given depth and wavelength. The *spectral upwelling average cosine* is defined analogously:

$$\bar{\mu}_u(z;\lambda) \equiv \frac{E_u(z;\lambda)}{E_{ou}(z;\lambda)} . \tag{3.15}$$

The average cosines are crude but useful one-parameter measures of the directional structures of the downwelling and upwelling light fields. For example, if the radiance distribution is collimated in direction $(\theta_o,\phi_o)$, with $0 \leq \theta_o \leq \pi/2$, then $\bar{\mu}_d = \cos\theta_o$. (In this case, $\bar{\mu}_u$ is undefined since there are no photons heading upward.) If the radiance distribution is isotropic, then $\bar{\mu}_d = \bar{\mu}_u = 1/2$. Typical values of the average cosines for natural waters illuminated by the sun and sky are $\bar{\mu}_d \approx 3/4$ and $\bar{\mu}_u \approx 3/8$. A useful definition of an average cosine for the entire light field can be make by integrating over all directions $\Xi$ in Eq. (3.14):

$$\bar{\mu}(z;\lambda) \equiv \frac{\int_{\Xi} L(z;\theta,\phi;\lambda)\cos\theta\, d\Omega}{\int_{\Xi} L(z;\theta,\phi;\lambda)\, d\Omega} \equiv \frac{E_d(z;\lambda) - E_u(z;\lambda)}{E_o(z;\lambda)} .$$

This quantity varies from $\bar{\mu} = 0$ for an isotropic radiance distribution to $\bar{\mu} = \cos\theta_o$ for a collimated beam in direction $(\theta_o,\phi_o)$; thus $-1 \leq \bar{\mu} \leq 1$. In natural, sunlit waters, $\bar{\mu}$ is always positive. Note that $\bar{\mu}$ is *not* equal to the sum of $\bar{\mu}_d$ and $\bar{\mu}_u$.

Older literature generally refers to *distribution functions*, $D_d$ and $D_u$, rather than to average cosines. The distribution functions are just reciprocals of the average cosines:

$$D_d(z;\lambda) \equiv \frac{1}{\bar{\mu}_d(z;\lambda)} \quad \text{and} \quad D_u(z;\lambda) \equiv \frac{1}{\bar{\mu}_u(z;\lambda)} . \tag{3.16}$$

## Reflectances

Another commonly used AOP is the *spectral irradiance reflectance* (or *irradiance ratio*) $R(z;\lambda)$, defined as the ratio of spectral upwelling to downwelling plane irradiances:

$$R(z;\lambda) \equiv \frac{E_u(z;\lambda)}{E_d(z;\lambda)} . \qquad (3.17)$$

$R(z;\lambda)$ is often evaluated in the water just below the surface; we denote this depth by $z = w \approx 0$.

The *spectral remote-sensing reflectance $R_{rs}$* is defined as

$$R_{rs}(\theta,\phi;\lambda) \equiv \frac{L(z=a;\theta,\phi;\lambda)}{E_d(z=a;\lambda)} \qquad (sr^{-1}) . \qquad (3.18)$$

Here depth $z = a$ indicates that $R_{rs}$ is evaluated using $L$ and $E_d$ in the air, just above the water surface; this $L$ is often called the "water-leaving" radiance. The remote-sensing reflectance is a measure of how much of the downwelling light that is incident onto the water surface is eventually returned through the surface in direction $(\theta,\phi)$, so that it can be detected by a radiometer pointed in the opposite direction. Both $R$ and $R_{rs}$ are of great use in optical oceanography, and we shall encounter them again.

## Diffuse attenuation coefficients

Under typical oceanic conditions, for which the incident lighting is provided by the sun and sky, the various radiances and irradiances all decrease *approximately* exponentially with depth, at least when far enough below the surface (and far enough above the bottom, in shallow water) to be free of boundary effects. It is therefore convenient to write the depth dependence of, say, $E_d(z;\lambda)$ as

$$E_d(z;\lambda) \equiv E_d(0;\lambda) \exp\left[ -\int_0^z K_d(z';\lambda) \, dz' \right], \qquad (3.19)$$

where $K_d(z;\lambda)$ is the *spectral diffuse attenuation coefficient* for spectral downwelling plane irradiance. Solving for $K_d(z;\lambda)$ gives

$$K_d(z;\lambda) = -\frac{d \ln E_d(z;\lambda)}{dz} = -\frac{1}{E_d(z;\lambda)} \frac{d E_d(z;\lambda)}{dz} \qquad (m^{-1}), \qquad (3.20)$$

which is generally the equation used to define $K_d(z;\lambda)$. If we define $\overline{K}_d(z;\lambda)$

as the average of $K_d(z;\lambda)$ over the depth interval from 0 to $z$, i.e.

$$\bar{K}_d(z;\lambda) \equiv \frac{1}{z} \int_0^z K_d(z';\lambda)\, dz' ,$$

then we can write Eq. (3.19) as

$$E_d(z;\lambda) \equiv E_d(0;\lambda) \exp\left[ -\bar{K}_d(z;\lambda)\, z \right]. \qquad (3.21)$$

Other diffuse attenuation coefficients, e.g. $K_u$, $K_{od}$, $K_{ou}$, $K_{PAR}$ and $K(\theta,\varphi)$, are defined by equations analogous to Eqs. (3.19) and (3.20), using the corresponding radiometric quantities.  For example, $K(\theta,\varphi) \equiv K(z;,\theta,\varphi;\lambda)$ refers to the diffuse attenuation of the radiance $L(z;\theta,\varphi;\lambda)$, i.e. to

$$K(\theta,\varphi) \equiv -\frac{1}{L(z;\theta,\varphi;\lambda)} \frac{dL(z;\theta,\varphi;\lambda)}{dz} . \qquad (3.22)$$

The distinction between *beam* and *diffuse* attenuation coefficients is important.  The beam attenuation coefficient $c(\lambda)$ is defined in terms of the radiant power lost from a single, narrow, collimated beam of photons.  The downwelling diffuse attenuation coefficient $K_d(z;\lambda)$ is defined in terms of the decrease with depth of the ambient downwelling irradiance $E_d(z;\lambda)$, which comprises photons heading in all downward directions (a diffuse, or uncollimated, light field).  $K_d(z;\lambda)$ clearly depends on the directional structure of the ambient light field, hence its classification as an apparent optical property.

The various diffuse attenuation coefficients, or "*K*-functions," are conceptually distinct.  In practice, though, they often have nearly the same numerical values except, perhaps, near the surface, and they all asymptotically approach the same value at great depth.  In *homogeneous* (vertically well mixed) waters, the *K*-functions depend only weakly on depth and therefore can serve as convenient, if imperfect, descriptors of the water body.  Smith and Baker (1978) have pointed out other reasons why the *K*-functions are useful:

- The *K*'s are defined as ratios and therefore do not require absolute radiometric measurements.
- The *K*'s are strongly correlated with phytoplankton chlorophyll concentration, thus they provide a connection between biology and optics.
- About 90% of the diffusely reflected light from a water body comes from a surface layer of water of depth $1/K_d$; thus $K_d$ has implications for remote sensing.

- Radiative transfer theory provides several useful relations between the *K*'s and other quantities of interest, such as the absorption and beam attenuation coefficients and other AOP's.
- Instruments are commercially available for the routine determination of the *K*'s.

## *Gordon's normalization of $K_d$*

Gordon (1989a) developed a simple way to normalize measured $K_d$ values. His normalization for all practical purposes *removes the effects of the sea state and incident sky radiance distribution from $K_d$, so that the normalized $K_d$ can be regarded as an IOP.* The theory behind the normalization is given in the above paper and in Gordon (1976); the mechanics of the normalizing process are as follows.

Let $E_d$(sun) be the irradiance incident onto the sea surface due to the sun's direct beam, and let $E_d$(sky) be the irradiance due to diffuse sky radiance. Then the fraction *f* of the direct sunlight in the incident irradiance that is transmitted through the surface into the water is

$$f = \frac{t(\text{sun})\,E_d(\text{sun})}{t(\text{sun})\,E_d(\text{sun}) + t(\text{sky})\,E_d(\text{sky})} \ .$$

Here $t$(sun) and $t$(sky) are respectively the fractions of the direct beam and of the diffuse irradiance transmitted through the surface; these quantities can be computed using methods to be developed in Chapter 4 [where they are denoted by $t(a,w)$]. However, if the solar zenith angle $\theta_s$ is less than 45°, then $t$(sun) $\approx 0.97$. If the sky radiance distribution is nearly uniform (as it is for a clear sky), then $t$(sky) $\approx 0.94$. In this case, we can accurately estimate *f* from measurements made just above the sea surface:

$$f \approx \frac{E_d(\text{sun})}{E_d(\text{sun}) + E_d(\text{sky})} \ .$$

The sun and sky irradiances are easily obtained from an instrument on the deck of a ship. When both direct and diffuse light fall onto the instrument, it records $E_d$(sun) + $E_d$(sky). When the direct solar beam is blocked, the instrument records $E_d$(sky). (Advanced technology is not required here: just hold your hat so that its shadow falls on the instrument.)

Next compute the nadir angle of the transmitted solar beam, $\theta_{sw}$, using Snell's law [see Eq. (4.8)]:

$$\theta_{sw} = \sin^{-1}\left(\frac{\sin\theta_s}{1.34}\right) \ .$$

Finally, compute the quantity

$$D_o = \frac{f}{\cos\theta_{sw}} + 1.197(1 - f).$$

This value of $D_o$ is valid for flat or rough sea surfaces as long as $\theta_s \leq 50°$. For larger values of $\theta_s$, or for an overcast sky, a correction must be applied to $D_o$ to account for surface wave effects on the transmitted light; the correction factors are given in Gordon (1989a, his Fig. 6).

Gordon's normalization then consists simply of dividing the measured $K_d$ by $D_o$:

$$K_d(\text{normalized}) = \frac{K_d(\text{measured})}{D_o}.$$

Physically, $D_o$ is a distribution function $(1/\bar{\mu}_d)$ that *reduces $K_d$ values to the values that would be measured if the sun were at the zenith, if the sea surface were level, and if the sky were black* (i.e. if there were no atmosphere). The zenith-sun, level-surface, black-sky case is the only physical situation for which $D_o = 1$. In other words, normalization by $D_o$ removes the influence of incident lighting and sea state on $K_d$. The same normalization can be applied to depth-averaged values $\bar{K}_d$.

We recommend that, whenever possible, experimentalists routinely make the simple measurements necessary to determine $D_o$. When making hydrographic casts, the above-surface $E_d$ measurements can be made on deck with the underwater instrument, just before the instrument is placed in the water. Normalization of $K_d$ greatly enhances its value in the recovery of IOP's from irradiance measurements; these matters are discussed in Section 10.4.

# 3.3 Optically Significant Constituents of Natural Waters

In order to motivate our subsequent studies of the absorbing and scattering properties of natural waters, we need to have some knowledge of the composition of those waters. Natural waters contain a continuous size distribution of particles ranging from water molecules of size ~0.1 nm, to small organic molecules of size ~1 nm, to large organic molecules of size ~10 nm, to viruses of size ~100 nm, to ..., to whales of size ~10 m, to submarines of size ~100 m. Thus, strictly speaking, water is composed entirely of particles. However, the constituents of natural waters are

traditionally divided into "dissolved" and "particulate" matter, of organic and inorganic origins, living and nonliving.

When filtering a water sample, everything that passes through a filter whose pore size is roughly 0.4 μm is called dissolved matter, and everything retained on the filter is called a particle. This dividing line is determined more by our ability to examine the material left on the filter pad than by any distinguishing features of the chemical, biological or optical properties of the matter. Note that 0.4 μm = 400 nm, the shortest wavelength of visible light. Thus optical microscopy is unable to resolve individual particles smaller than the historical dividing line between dissolved and particulate matter.

Each of the components of natural water, regardless of how they are classified, contributes in some fashion to the values of the optical properties of a given water body.

Pure sea water consists of pure water plus various dissolved salts, which average about 35 parts per thousand (35‰) by weight. These salts increase scattering above that of pure water by about 30% (see Table 3.8, below). These salts have a negligible effect on absorption at visible wavelengths, but it is likely that they increase absorption somewhat at ultraviolet wavelengths. They increase absorption tremendously at extremely long ($\lambda \geq 0.1$ m) wavelengths.

Both fresh and saline waters contain varying concentrations of dissolved organic compounds. These compounds are produced during the decay of plant matter and consist mostly of various humic and fulvic acids (Kirk, 1983). These compounds are generally brown in color, and in sufficient concentrations can color the water yellowish brown. For this reason the compounds are generically referred to as *yellow matter* or CDOM, *colored dissolved organic matter*. Other common names are *gelbstoff* and *gilvin*. Yellow matter absorbs very little in the red, but its absorption increases rapidly with decreasing wavelength and can be significant at blue and ultraviolet wavelengths. One of its main sources is decayed terrestrial vegetation. Concentrations are thus generally greatest in lakes, rivers, and coastal waters influenced by river runoff. In such waters, yellow matter can be the dominant absorber at the blue end of the spectrum. In mid-ocean waters, absorption by yellow matter is usually small compared to absorption by other constituents, but some yellow matter is likely to be present as the result of decaying phytoplankton, especially at the end of a bloom.

Particulate matter in the oceans has two distinct origins: biological and physical. The organic particles of optical importance are created as bacteria, phytoplankton, and zooplankton grow and reproduce. Particles of

a given size are destroyed by breaking apart after death, by flocculation into larger aggregate particles, or by settling out of the water column.  Inorganic particles are created primarily by weathering of terrestrial rocks and soils.  These particles can enter the water as wind-blown dust settles on the sea surface, as rivers carry eroded soil to the sea, or as currents resuspend bottom sediments.  Inorganic particles are removed from the water by settling, aggregating, or dissolving.  This particulate matter usually is the major determiner of both the absorption and scattering properties of natural waters and is responsible for most of the temporal and spatial variability in these optical properties.

     *Organic particles* occur in many forms:

VIRUSES.  Natural marine waters contain virus particles in concentrations of $10^{12}$ to $10^{15}$ particles m$^{-3}$ (Suttle, *et al.* 1990).  These particles are generally much smaller (20–250 nm) than the wavelength of visible light.  In spite of their large numbers, it is unlikely that viruses contribute significantly to the absorption and total scattering properties of natural waters, because they are very inefficient absorbers and scatterers on a per-particle basis.  However, very small particles can be efficient backscatterers, and there is speculation that viruses sometimes may contribute significantly to the backscatter coefficient $b_b$, at least at blue wavelengths in very clear waters.  Note that viruses would be considered dissolved matter by the traditional definition.

COLLOIDS.  Nonliving colloidal particles in the size range 0.4–1.0 μm are found in typical number concentrations of $10^{13}$ m$^{-3}$, and colloids of size $\leq$ 0.1 μm are found in abundances of $10^{15}$ m$^{-3}$ (Koike, *et al.*, 1990; Wells and Goldberg, 1991).  Part of the absorption traditionally attributed to dissolved matter probably is due to colloids, some of which strongly resemble fulvic acids in electron micrographs. Modeling results based on Mie scattering theory (e.g. Stramski and Kiefer, 1991) suggest that colloids contribute significantly to backscattering.

BACTERIA.  Living bacteria in the size range 0.2–1.0 μm occur in typical number concentrations of $10^{11}$–$10^{13}$ m$^{-3}$.  It only recently has been recognized that bacteria can be significant scatterers and absorbers of light, especially at blue wavelengths and in clear oceanic waters, where the larger phytoplankton are relatively scarce (Spinrad, *et. al.*, 1989; Morel and Ahn, 1990; Stramski and Kiefer, 1991).  Bacteria are likely the most important microorganisms contributing to particulate backscatter.

PHYTOPLANKTON.  These ubiquitous microscopic plants occur with incredible diversity of species, size, shape, and concentration.  They range in cell size from less than 1 μm to more than 200 μm, and some

species form even larger chains of individual cells. It has long been recognized that phytoplankton are the particles primarily responsible for determining the optical properties of most oceanic waters. Their chlorophyll and related pigments strongly absorb light in the blue and red and thus, when concentrations are high, predominate in determining the spectral absorption of sea water. These particles are generally much larger than the wavelength of visible light and are efficient scatterers, especially via diffraction, thus strongly influencing the total scattering properties of sea water. Although large particles scatter strongly at small scattering angles, and thus contribute to $b$, they scatter only weakly at large angles. Therefore the larger phytoplankton contribute relatively little to $b_b$.

ORGANIC DETRITUS. Nonliving organic particles of various sizes are produced, for example, when phytoplankton die and their cells break apart, and when zooplankton graze on phytoplankton and leave cell fragments and fecal pellets. Even if these detrital particles contain pigments at the time of their production, they can be rapidly photo-oxidized and lose the characteristic absorption spectrum of living phytoplankton, leaving significant absorption only at blue wavelengths. There is circumstantial evidence (Stramski and Kiefer, 1991) that sub-micrometer, low-index-of-refraction, detrital particles are the major backscatterers in the ocean.

LARGE PARTICLES. Particles larger than 100 μm include zooplankton (living animals with sizes from tens of micrometers to two centimeters) and fragile amorphous aggregates of smaller particles ("marine snow," with sizes from 0.5 mm to tens of centimeters). Such particles occur in highly variable numbers from almost none to thousands per cubic meter. Even at relatively large concentrations, these large particles tend to be missed by optical instruments that randomly sample only a few cubic centimeters of water or that generate turbulence, which can break apart the aggregates. Large "fluffy" particles can be efficient scatterers of light at all scattering angles. Aggregates therefore may significantly affect the optical properties (especially backscatter) of large volumes of water, as are seen by remote sensing instruments. Although such optical effects are recognized, they have not been quantified (Alldredge and Silver, 1988; Carder and Costello, 1994).

*Inorganic* particles generally consist of finely ground quartz sand, clay minerals, or metal oxides in the size range from much less than 1 μm to several tens of micrometers. Insufficient attention has been paid to the optical effects of such particles in sea water, although it is recognized that inorganic particles are sometimes optically more important than organic

particles.  Such situations can occur both in turbid coastal waters carrying a heavy sediment load and in very clear oceanic waters that are receiving wind-blown dust (Carder, *et al.*, 1986).

At certain stages of its life, the phytoplankton coccolithophore species *Emiliania huxleyi* is a most remarkable biological source of crystalline particles.  During blooms, *E. huxleyi* produces and sheds enormous numbers of small $(2-4\,\mu m)$ calcite plates; concentrations of $3 \times 10^{11}$ plates m$^{-3}$ have been observed (Balch, *et al.*, 1991).  Although they have a negligible effect on light absorption, these calcite plates are extremely efficient light scatterers: irradiance reflectances of $R = 0.39$ have been observed at blue wavelengths during blooms (compared with $R = 0.02$ to 0.05 in the blue for typical ocean waters).  Such coccolithophore blooms give the ocean a milky white or turquoise appearance.

Stramski and Kiefer (1991) and Morel (1991a) give excellent reviews of the optical properties of marine particles.  We postpone until Section 3.11 discussion of how the optical properties of individual particles combine to determine the bulk (water plus many particles) optical properties.

## 3.4  Particle Size Distributions

The sizes of the particles just discussed are measured in various ways.  Visible microscopy can be used for particles greater in size than a few wavelengths of light; electron microscopy can be used for particles as small as nanometers in size.  Both methods are exceedingly tedious and time consuming if large numbers of particles must be counted and sized.  Most size data have been obtained using electrical resistance methods (e.g. Coulter® counters).  These instruments measure the change in voltage induced (at constant current) between two small electrodes when a particle, whose resistance is different from that of the water, passes between the electrodes.  Assuming that the particle is a dielectric, the change in voltage is proportional to the particle's volume, all else being equal.  These instruments enable the rapid, automated evaluation of large numbers of particles, for particle sizes greater that ~1 µm.  *In situ* sizing of particles has been done with video cameras (Eisma, *et al.*, 1990), with laser-light diffraction techniques (Bale and Morris, 1987), and with laser holography (Costello, *et al.*, 1989).  These techniques work best for large particles, and they are especially valuable in the analysis of delicate aggregate particles, which break apart if disturbed.  New techniques for image analysis and pattern recognition may enhance the utility of both microscopy and *in situ* observations in coming years.

For instrumentation reasons, then, most of the available data is for particles larger than ~1 μm in size. Only recently has information become available on sub-micrometer particles.

A single family of particle size distributions sometimes suffices to describe oceanic particulate matter in the optically important size range from 0.1 to 100 μm. Let $N(x)$ be the number of particles per unit volume with "size" greater than $x$ in a sample of particles. Since only a sphere has a unique size (its diameter), $x$ usually represents equivalent spherical diameter computed from particle volume, but also can represent particle volume or surface area. The Junge (also called hyperbolic) cumulative size distribution is then (Bader, 1970)

$$N(x) = k \left( \frac{x}{x_o} \right)^{-m} \qquad (\text{m}^{-3}),$$

where $k$ sets the scale, $x_o$ is a reference size, and $-m$ is the slope of the distribution when $\log N$ is plotted versus $\log x$; $k$, $x_o$ and $m$ are positive constants. Oceanic particle size distributions usually have $m$ values between 2 and 5, with $m = 3$ to 4 being typical; such spectra can be seen in McCave (1983, his Fig. 7).

As we shall see in Section 3.11, the quantity most relevant to optics is not the *cumulative* size distribution $N(x)$, but rather the *number* size distribution $n(x)$. The number distribution is defined such that $n(x)dx$ is the number of particles per unit volume in the size interval from $x$ to $x + dx$. The number distribution is related to the cumulative distribution by $n(x) = |dN(x)/dx|$. Thus, for the Junge distribution,

$$n(x) = k m x_o^m x^{-m-1} \equiv K x^{-s} \qquad (\text{m}^{-4}), \tag{3.23}$$

where $K \equiv kmx_o^m$ and $s \equiv m + 1$; the slope of $\log n(x)$ vs. $\log x$ is $-s$. Figure 3.2 shows the number distribution of biological particles typical of open ocean waters; note that a value of $s = 4$ gives a reasonable fit to the plotted points.

Although Fig. 3.2 is representative of average values, the particle size distribution can be considerably different at a particular time and location. This is to be expected, considering the many types of oceanic particles and the various mechanisms for particle production and removal. Observation shows that oceanic particle size spectra often are best described by a segmented distribution, in which a smaller value of $m$ is used for $x$ less than a certain value, and a larger value of $m$ is used for $x$ greater than that value. Such segmented spectra can be seen in Bader (1970, his Fig. 9) and
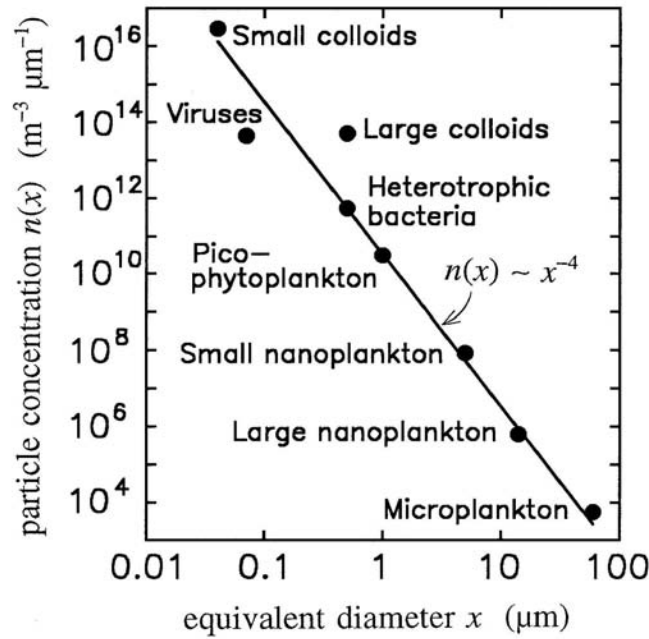
Fig. 3.2. Number size distribution typical of biological particles in the open ocean. [figure courtesy of D. Stramski]

in McCave (1983, his Fig. 8). However, even segmented Junge distributions are often inadequate. In particular, the Junge distributions tend to overestimate the number of small particles [note that $n(x) \rightarrow \infty$ as $x \rightarrow 0$] and to underestimate the number of large particles.

Risović (1993) shows that a segmented, generalized gamma distribution

$$n(x) = C_A x^2 \exp\left(-52 x^{\gamma_A}\right) + C_B x^2 \exp\left(-17 x^{\gamma_B}\right), \qquad (3.24)$$

gives a better fit to observations than does a segmented Junge distribution. Here $x$ is measured in micrometers. $C_A$ and $C_B$ are constants with units of $\mu m^{-6}$, which can be obtained from the concentrations (numbers per unit volume) of particle components "A" and "B"; details are given in Risović's paper. Component A refers to those particles whose distribution has a "steep" slope (that is, their number decreases rapidly as $x$ increases); these are generally the small particles with $x < 1$ $\mu m$. Component B consists of the generally larger particles that decrease less rapidly in number as $x$ increases. Fitting Eq. (3.24) to over 70 size distributions measured in a

variety of waters showed that the two parameters $\gamma_A$ and $\gamma_B$ fall in the ranges $0.145 \leq \gamma_A \leq 0.195$ and $0.192 \leq \gamma_B \leq 0.322$, with mean values of 0.157 and 0.226, respectively.

It should be noted, however, that a simple distribution like Eq. (3.24) sometimes fails to represent oceanic conditions. For example, during the growth phase of a phytoplankton bloom the rapid increase in population of a particular species may give abnormally large numbers of particles in a particular size range. Such bloom conditions therefore give a "bump" in $n(x)$ that is not well modeled.

## 3.5  Electromagnetic Properties of Water

In studies of electromagnetic wave propagation at the level of Maxwell's equations, it is convenient to specify the bulk electromagnetic properties of the medium via the electrical permittivity $\epsilon$, the magnetic permeability $\mu$, and the electrical conductivity $\sigma$. Since water displays no significant magnetic properties, the permeability can be taken equal to the free-space (*in vacuo*) value at all frequencies: $\mu = \mu_o = 4\pi \times 10^{-7} \, N \, A^{-2}$. Both $\epsilon$ and $\sigma$ depend on the frequency $\nu$ of the propagating electromagnetic wave, as well as on the water temperature, pressure, and salinity. Low frequency ($\nu \to 0$) values for the permittivity are of order $\epsilon \approx 80\epsilon_o$, where $\epsilon_o = 8.85 \times 10^{-12} \, A^2 \, s^2 \, N^{-1} \, m^{-2}$ is the free-space value. This value decreases to $\epsilon \approx 1.8\epsilon_o$ at optical frequencies. Extensive tabulations of $\epsilon/\epsilon_o$ as a function of temperature and pressure are given for pure water in Archer and Wang (1990). The low frequency conductivity ranges from $\sigma \approx 4 \times 10^{-6}$ Siemen $m^{-1}$ ($4 \times 10^{-6} \, s^{-1}$) for pure water to $\sigma \approx 4.4$ Siemen $m^{-1}$ for sea water.

The effects of $\epsilon$, $\mu$ and $\sigma$ on electromagnetic plane-wave propagation are compactly summarized in terms of the *complex index of refraction, m = n − ik*, where $i = \sqrt{(-1)}$. The real part $n$ of $m$ is usually called "the index of refraction"; $k$ is sometimes called the (dimensionless) electrodynamic absorption coefficient, but usually is called just "the imaginary part of the (complex) index of refraction." Although $n$ and $k$ are collectively called the *optical constants* of water, they depend strongly on wavelength. The explicit dependence of $m$ on $\epsilon$, $\mu$ and $\sigma$ is given by (Kerker, 1969)

$$m^2 = \mu\epsilon c^2 - i \frac{2\pi\mu\sigma c^2}{\nu}$$
$$= (n - ik)^2 = n^2 - k^2 - i2nk \, ,$$

where $c = (\epsilon_o\mu_o)^{-\frac{1}{2}}$ is the speed of light *in vacuo*. These equations can be

used to relate $n$ and $k$ to the bulk electromagnetic properties.  The optical constants are convenient because they are directly related to the scattering and absorbing properties of water.  The real index of refraction $n(\lambda)$ governs scattering both at interfaces (via the laws of reflection and refraction) and within the medium (via thermal or other fluctuations of $n(\lambda)$ at molecular and larger scales).  The spectral absorption coefficient $a(\lambda)$ is related to $k(\lambda)$ by (Kerker, 1969)

$$a(\lambda) \ = \ \frac{4\pi k(\lambda)}{\lambda} \ .$$

Here $\lambda$ refers to the wavelength *in vacuo* corresponding to a given frequency $\nu$ of electromagnetic wave.

Figure 3.3 shows the wavelength dependence of the optical constants $n$ and $k$ for pure water.  The extraordinary feature seen in this figure is the narrow "window" in $k(\lambda)$, where $k(\lambda)$ decreases by over nine orders of magnitude between the near ultraviolet and the visible, and then quickly rises again in the near infrared.  This behavior in $k(\lambda)$ gives a corresponding window in the spectral absorption coefficient $a(\lambda)$, as seen in Fig. 3.4.

The shape of the absorption curve of pure water can be crudely explained as follows.  At blue wavelengths, photons are barely energetic enough to boost electrons into higher energy levels of the water molecule,
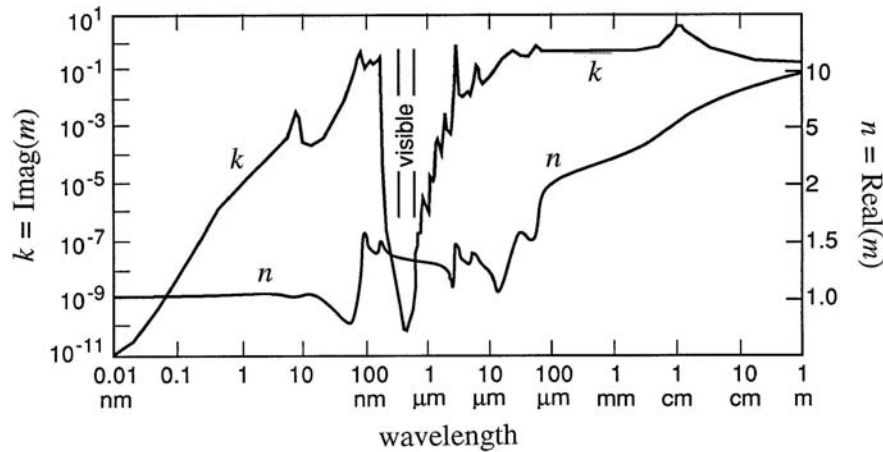


Fig. 3.3.  The optical constants of pure water.  The left axis gives the imaginary part of $m$, and the right axis gives the real part of $m$, where $m$ is the complex index of refraction.  [redrawn from Zoloratev and Demin (1977), with permission]
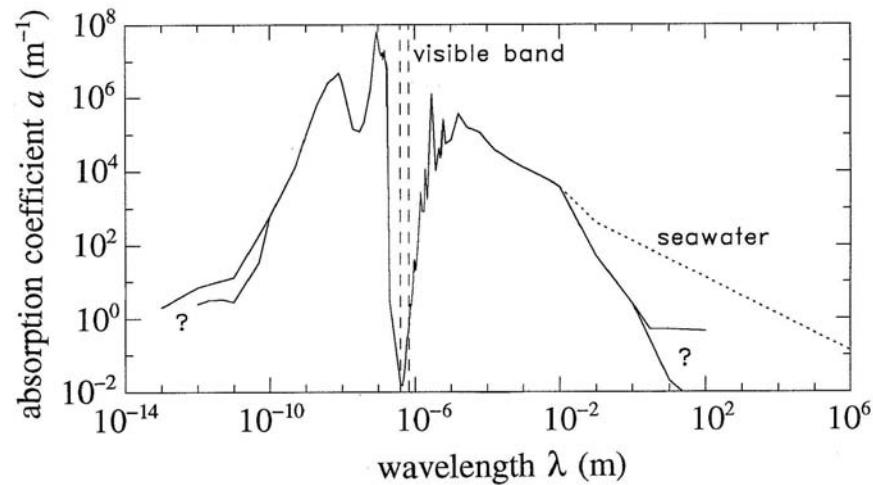
Fig. 3.4. Spectral absorption coefficient of pure water (solid line) and of pure sea water (dotted line) as a function of wavelength. [drawn from data compiled in Hale and Querry (1973), Jackson (1975), Smith and Baker (1981), and Zoloratev and Demin (1977)]

and the photons do not have the right energy to interact easily with the molecule as a whole (although some vibrational modes of the molecule can be excited). The photons therefore do not interact strongly with the water molecules, and $a(\lambda)$ is at its minimum. As the wavelength decreases toward the ultraviolet, the photons become sufficiently energetic to excite atomic transitions, and the absorption rapidly increases. At extremely small wavelengths, processes such as Compton scattering (scattering of high-energy photons by electrons) come in to play, and the relevant parameter is just the density of the material, not its structure as a water molecule. As the wavelength increases from blue to red and beyond, the photons begin having just the right energy to excite first the fundamental vibrational and then the rotational modes of the water molecules, and absorption once again increases rapidly in the infrared. The prominent peaks in $a(\lambda)$ in the infrared result from these resonant excitations of molecular motions. At very long wavelengths, the photons are not energetic enough to excite molecular motions, and the absorption decreases.

Ions resulting from the dissolved salts make seawater a much better conductor of electricity than is pure water (recall that the conductivity $\sigma$ of sea water is about one million times that of pure water). These ions do not appreciably affect the absorption at most wavelengths. However, the behavior of sea water as a conductor gives it a much higher absorption than

pure water at very long wavelengths, as shown by the dotted line in Fig 3.4. Not until the wavelength of the electromagnetic radiation is on the order of thousands of kilometers does sea water once again have an absorption comparable to the low values at visible wavelengths.

Because of the opaqueness of water outside the near-ultraviolet to near-infrared wavelengths, we can henceforth restrict our attention to this narrow band. These wavelengths overlap with the wavelengths of the sun's maximum energy output (recall Fig. 1.1) and with a corresponding window in atmospheric absorption. It is this astounding overlap of energy source and "open windows" that has enabled aquatic life to develop in the form we see on earth.

# 3.6 Real Index of Refraction

As we have stated, the real part $n$ of the index of refraction determines the scattering properties of a medium. If $n$ were truly constant, there would be no scattering. However, there are always variations of $n$ within a material medium. Even in absolutely pure water, random thermal fluctuations give rise to varying numbers of molecules in any given small volume $\Delta V$, where $\Delta V$ is small compared to the wavelength of light but large compared to atomic scales. These molecule number density fluctuations result in small-scale fluctuations in the index of refraction. In pure sea water, the ions of dissolved salts cause additional molecular-scale fluctuations in $n$, and hence greater scattering. Proper treatment of this fluctuation theory of $n$ is a difficult problem in statistical thermodynamics, which was solved by Einstein and Smoluchowski between 1908 and 1910. Morel (1974) and Shifrin (1988) give excellent reviews of the associated physics and mathematics.

Austin and Halikas (1976) exhaustively reviewed the literature on measurements of the real index of refraction of bulk samples of sea water. Their report contains extensive tables and interpolation algorithms for the index of refraction (relative to air), $n(\lambda,S,T,p)$, as a function of wavelength ($\lambda = 400-700$ nm), salinity ($S = 0-43‰$), temperature ($T = 0-30°C$), and pressure ($p = 10^5-10^8$ Pa, or 1 to 1080 atm). Figure 3.5 illustrates the general dependence of $n$ on these four parameters: $n$ decreases with increasing wavelength or temperature, and $n$ increases with increasing salinity or pressure. Table 3.3 gives the values of $n$ for the extreme values of each parameter. The extreme values of $n$, 1.329128 and 1.366885, show that $n$ varies by less than 3% over the entire parameter range relevant to hydrologic optics. Table 3.4 gives selected values of $n(\lambda,T)$ for fresh water
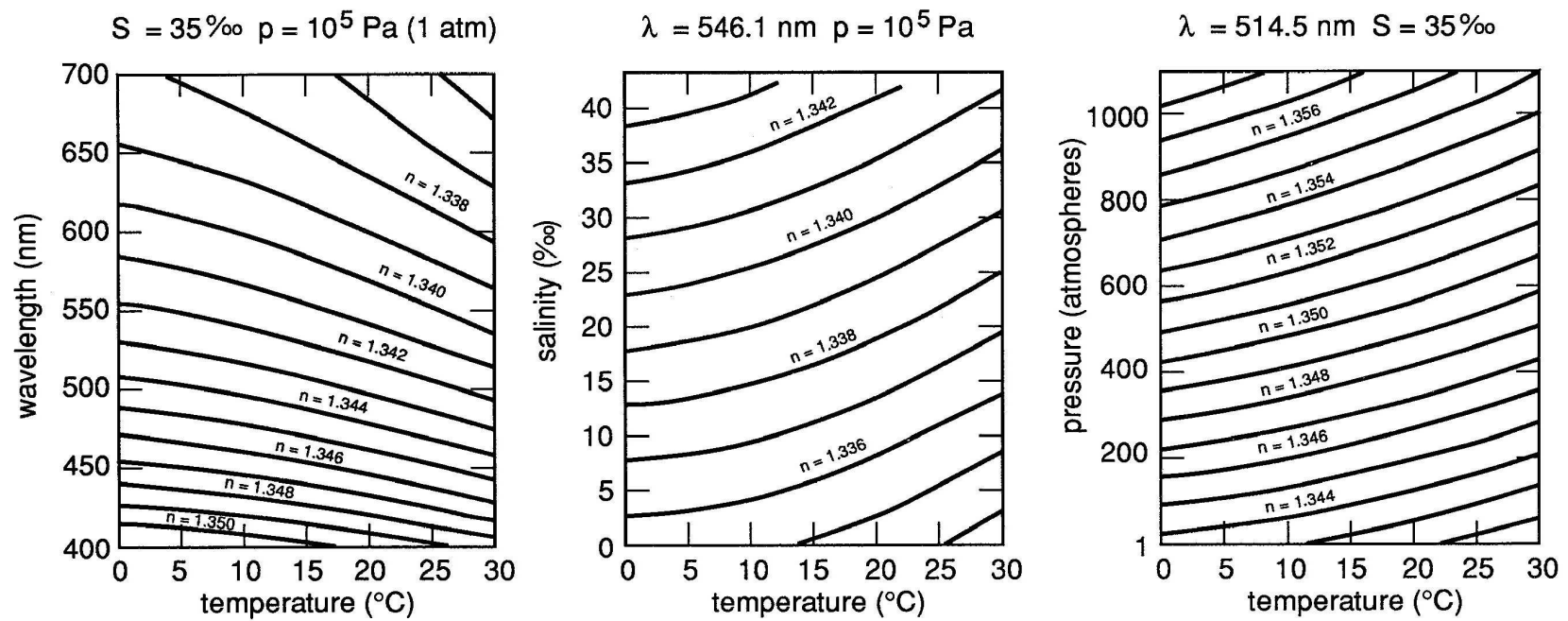
Fig. 3.5. Real index of refraction of water for selected values of pressure, temperature, and salinity. [adapted from Austin and Halikas (1976)]

Table 3.3.  Index of refraction of water, $n$, for the extreme values
of pressure $p$, temperature $T$, salinity $S$, and wavelength $\lambda$
encountered in hydrologic optics.[a]

| $p$ (Pa) | $T$ (°C) | $S$ (‰) | $\lambda$ (nm) | $n$ |
|---|---|---|---|---|
| $1.01\times10^5$ | 0 | 0 | 400 | 1.344186 |
| 1.01 | 0 | 0 | 700 | 1.331084 |
| 1.01 | 0 | 35 | 400 | 1.351415 |
| 1.01 | 0 | 35 | 700 | 1.337906 |
| 1.01 | 30 | 0 | 400 | 1.342081 |
| 1.01 | 30 | 0 | 700 | 1.329128 |
| 1.01 | 30 | 35 | 400 | 1.348752 |
| 1.01 | 30 | 35 | 700 | 1.335316 |
| $1.08\times10^8$ | 0 | 0 | 400 | 1.360076 |
| 1.08 | 0 | 0 | 700 | 1.346604 |
| 1.08 | 0 | 35 | 400 | 1.366885 |
| 1.08 | 0 | 35 | 700 | 1.352956 |
| 1.08 | 30 | 0 | 400 | 1.356281 |
| 1.08 | 30 | 0 | 700 | 1.342958 |
| 1.08 | 30 | 35 | 400 | 1.362842 |
| 1.08 | 30 | 35 | 700 | 1.348986 |

[a] Reproduced from Austin and Halikas (1976).

($S = 0$) and for typical sea water ($S = 35$‰) at atmospheric pressure ($p = 10^5$ Pa).  The values in Table 3.4 can be multiplied by 1.000293 (the index of refraction of dry air at STP and $\lambda = 538$ nm) if values relative to vacuum are desired.  Millard and Seaver (1990) have developed a 27-term formula that gives the index of refraction to part-per-million accuracy over most of the oceanographic parameter range.

The index of refraction of a sample of natural water is also influenced by the presence of suspended particulate matter.  The particles found in natural waters often have a bimodal index of refraction distribution.  Living phytoplankton typically have "low" indices of refraction, in the range 1.01 to 1.09 relative to the index of refraction of pure seawater. Detritus and inorganic particles generally have "high" indices, in the range of 1.15 to 1.20 relative to seawater (Jerlov, 1976).  Typical values are 1.05 for

Table 3.4.  Index of refraction of fresh water and of sea water at
atmospheric pressure, for selected temperatures and wavelengths.[a]

**Fresh Water ($S = 0$)**

| Temp (°C) | Wavelength (nm) | | | | | | |
|---|---|---|---|---|---|---|---|
| | 400 | 450 | 500 | 550 | 600 | 650 | 700 |
| 0 | 1.34419 | 1.34024 | 1.33741 | 1.33530 | 1.33362 | 1.33225 | 1.33108 |
| 10 | 1.34390 | 1.33997 | 1.33714 | 1.33503 | 1.33336 | 1.33199 | 1.33084 |
| 20 | 1.34317 | 1.33924 | 1.33643 | 1.33433 | 1.33267 | 1.33130 | 1.33016 |
| 30 | 1.34208 | 1.33816 | 1.33537 | 1.33327 | 1.33162 | 1.33026 | 1.32913 |

**Sea Water ($S = 35\%o$)**

| Temp (°C) | Wavelength (nm) | | | | | | |
|---|---|---|---|---|---|---|---|
| | 400 | 450 | 500 | 550 | 600 | 650 | 700 |
| 0 | 1.35141 | 1.34734 | 1.34442 | 1.34224 | 1.34050 | 1.33911 | 1.33791 |
| 10 | 1.35084 | 1.34678 | 1.34385 | 1.34167 | 1.33997 | 1.33855 | 1.33738 |
| 20 | 1.34994 | 1.34586 | 1.34295 | 1.34077 | 1.33904 | 1.33765 | 1.33644 |
| 30 | 1.34875 | 1.34469 | 1.34179 | 1.33962 | 1.33790 | 1.33649 | 1.33532 |

[a] Data extracted from Austin and Halikas (1976).

phytoplankton and 1.16 for inorganic particles.  We shall say more about the
refractive properties of individual particles in Section 3.11.

# 3.7  Absorption

We now turn our attention to the imaginary part of the complex index
of refraction, i.e. to absorption.

## *Measurement of absorption*

Determination of the spectral absorption coefficient $a(\lambda)$ for natural
waters is a difficult task for several reasons.  First, water itself absorbs only
weakly at near-UV and blue wavelengths, so that very sensitive instruments are
required.  More importantly, scattering is never negligible, so that

careful consideration must be made of the possible aliasing of the absorption measurements by scattering effects. In pure water at wavelengths of $\lambda = 370$ to 450 nm, molecular scattering provides 20–25% of the total beam attenuation, $c(\lambda) = a(\lambda) + b(\lambda)$, (see Table 3.5). Scattering effects can dominate absorption at all visible wavelengths in waters with high particulate loads. Additional complications arise in determining the absorption of pure water because of the difficulty of preparing uncontaminated samples. Many techniques have been employed in attempts to determine the spectral absorption coefficient for pure water, $a_w(\lambda)$; these are reviewed in Smith and Baker (1981).

The absorption by water itself usually is taken as known. Our real interest is directed towards measuring the absorption due to the various particulate and dissolved substances in a given water sample. The highly variable absorption by the constituents of a water body helps connect the optical properties of the water body with its biogeochemical character.

Because these constituents usually occur in low concentrations, it is necessary to concentrate samples before making absorption measurements. This is commonly done by filtering a sample of water to retain the particulate matter on a filter pad. The spectral absorption of the particulate matter, $a_p(\lambda)$, is then determined in a spectrophotometer, which measures the light transmitted through the filter pad and collected matter. The filter-pad method is the standard way of measuring absorption at sea.

Even though this technique for determining particulate absorption has been in use for many years, the methodology is still evolving because of the many types of errors inherent in the filter-pad measurements. The major problem with filter-pad measurements is that the intense scattering within the filter pad and collected particles increases the average distance travelled by the photons passing through the sample, which increases the apparent absorption. Corrections must be applied for this increase in photon path length, and this is an uncertain process. Other sources of error in filter-pad measurements include the inability of filters to retain all particles, absorption by dissolved matter retained on the filter pad, and decomposition of pigments during the filtration process. The state of the filter-pad art can be seen in Bannister (1988), Mitchell (1990), Stramski (1990), and Cleveland and Weidemann (1993). It is also possible to determine the absorption from measurements of light reflected by the filter pad, as opposed to transmitted through it. These two methods are compared in Balch and Kilpatrick (1992).

Laboratory methods for the measurement of absorption in dilute suspensions of particles (contained in cuvettes) generally employ spectrophotometers (Bricaud, *et al.*, 1983), although photoacoustic effects

have been investigated (Trees and Voss, 1990). These methods give good accuracy but are not well suited for the rigors of shipboard use.

The absorption of pure water, $a_w(\lambda)$, can be added to $a_p(\lambda)$ in order to obtain the total absorption of an oceanic water sample, *assuming* that absorption by dissolved organic matter (yellow substances) is negligible. However, this assumption is not always valid even in the open ocean, and it is seldom justified in near-shore waters. If the absorption by yellow matter, $a_y(\lambda)$, is desired, the sample is first filtered to remove the particles. Then the absorption of the *filtrate* is measured, and $a_y(\lambda)$ is taken to be $a_{filtrate}(\lambda) - a_w(\lambda)$.

Several novel instruments for the measurement of $a(\lambda)$ are now under development. Some of these attempt to circumvent scattering effects by the use of reflecting tubes (Zaneveld, *et al.*, 1990) or integrating cavities (Fry, *et al.*, 1992a). Another (Doss and Wells, 1992) obtains the absorption from measurements of certain integrals of the radiance distribution (see Section 10.2). Maffione, *et al.* (1993) used an isotropically emitting source to measure the average absorption between the source and the detector. These instruments show promise for avoiding the problems inherent in the filter-pad technique. Except for the integrating cavity of Fry, *et al.*, these instruments make *in-situ* measurements of the total absorption, which at present is very difficult (Voss, 1989). The extent to which these prototype instruments can be perfected for use in routine oceanographic measurements remains to be seen.

## *Absorption by pure sea water*

Smith and Baker (1981) made a careful, but indirect, determination of the *upper bound* of the spectral absorption coefficient of pure sea water, $a_w(\lambda)$, in the wavelength range of oceanographic interest, 200 nm $\leq \lambda \leq$ 800 nm. Their work assumed that for the clearest natural waters, (1) absorption by salt or other dissolved substances was negligible, (2) the only scattering was by water molecules and salt ions, and (3) there was no inelastic scattering (i.e. no fluorescence). With these assumptions, the inequality (derived from radiative transfer theory)

$$a_w(\lambda) \leq K_d(\lambda) - \tfrac{1}{2} b_{sw}(\lambda)$$

holds. Here $b_{sw}(\lambda)$ is the spectral scattering coefficient for pure sea water; $b_{sw}(\lambda)$ was taken as known (from Table 3.8). Smith and Baker then used measured values of the diffuse attenuation function $K_d(\lambda)$ from very clear waters (e.g. Crater Lake, Oregon, USA and the Sargasso Sea) to estimate
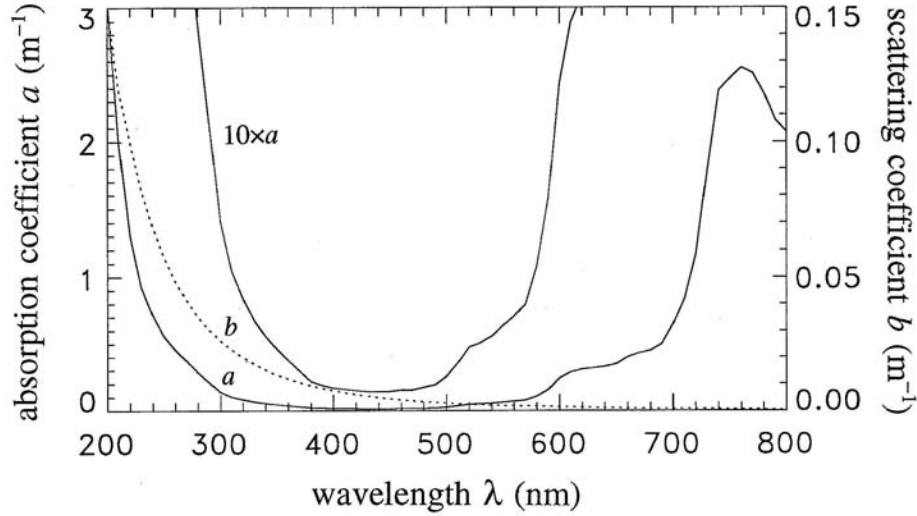
Fig. 3.6. Absorption (solid line) and scattering (dotted line) coefficients for pure sea water, as determined by Smith and Baker (1981).

$a_w(\lambda)$. Table 3.5 gives their self-consistent values of $a_w(\lambda)$, $K_d(\lambda)$, and $b_{sw}(\lambda)$; Fig. 3.6 shows $a_w(\lambda)$ and $b_{sw}(\lambda)$.

The Smith and Baker absorption values are widely used. However, it must be remembered that the values of $a_w(\lambda)$ in Table 3.5 are upper bounds; the true absorption of pure water is likely to be somewhat lower, at least at violet and blue wavelengths (Sogandares, *et al.*, 1991). Smith and Baker pointed out that there are uncertainties because $K_d$, an apparent optical property, is influenced by environmental conditions. They also commented that at wavelengths below 300 nm, their values are "merely an educated guess." They estimated the accuracy of $a_w(\lambda)$ to be within +25% and −5% between 300 and 480 nm, and +10% to −15% between 480 and 800 nm. It also should be noted that the Smith and Baker values inescapably contain the effects of Raman scattering by the water itself.

Numerical simulations by Gordon (1989a) indicate that a more restrictive inequality,

$$a_w(\lambda) \leq \frac{K_d(\lambda)}{D_o(\lambda)} - 0.62\, b_{sw}(\lambda),$$

could be used. Here $D_o(\lambda)$ is the measurable distribution function that corrects for the effects of sun angle and sea state on $K_d(\lambda)$, as described in Section 3.2. Use of the Gordon inequality could reduce the Smith and Baker absorption values by up to 20% at blue wavelengths. And finally, the

Table 3.5. Spectral absorption coefficient of pure sea water, $a_w$, as determined by Smith and Baker. Values of the molecular scattering coefficient of pure sea water, $b_{sw}$, and of the diffuse attenuation coefficient $K_d$ used in their computation of $a_w$ are also shown.[a]

| $\lambda$ (nm) | $a_w$ (m$^{-1}$) | $b_{sw}$ (m$^{-1}$) | $K_d$ (m$^{-1}$) | $\lambda$ (nm) | $a_w$ (m$^{-1}$) | $b_{sw}$ (m$^{-1}$) | $K_d$ (m$^{-1}$) |
|---|---|---|---|---|---|---|---|
| 200 | 3.07 | 0.151 | 3.14 | 500 | 0.0257 | 0.0029 | 0.0271 |
| 210 | 1.99 | 0.119 | 2.05 | 510 | 0.0357 | 0.0026 | 0.0370 |
| 220 | 1.31 | 0.0995 | 1.36 | 520 | 0.0477 | 0.0024 | 0.0489 |
| 230 | 0.927 | 0.0820 | 0.968 | 530 | 0.0507 | 0.0022 | 0.0519 |
| 240 | 0.720 | 0.0685 | 0.754 | 540 | 0.0558 | 0.0021 | 0.0568 |
| 250 | 0.559 | 0.0575 | 0.588 | 550 | 0.0638 | 0.0019 | 0.0648 |
| 260 | 0.457 | 0.0485 | 0.481 | 560 | 0.0708 | 0.0018 | 0.0717 |
| 270 | 0.373 | 0.0415 | 0.394 | 570 | 0.0799 | 0.0017 | 0.0807 |
| 280 | 0.288 | 0.0353 | 0.306 | 580 | 0.108 | 0.0016 | 0.109 |
| 290 | 0.215 | 0.0305 | 0.230 | 590 | 0.157 | 0.0015 | 0.158 |
| 300 | 0.141 | 0.0262 | 0.154 | 600 | 0.244 | 0.0014 | 0.245 |
| 310 | 0.105 | 0.0229 | 0.116 | 610 | 0.289 | 0.0013 | 0.290 |
| 320 | 0.0844 | 0.0200 | 0.0944 | 620 | 0.309 | 0.0012 | 0.310 |
| 330 | 0.0678 | 0.0175 | 0.0765 | 630 | 0.319 | 0.0011 | 0.320 |
| 340 | 0.0561 | 0.0153 | 0.0637 | 640 | 0.329 | 0.0010 | 0.330 |
| 350 | 0.0463 | 0.0134 | 0.0530 | 650 | 0.349 | 0.0010 | 0.350 |
| 360 | 0.0379 | 0.0120 | 0.0439 | 660 | 0.400 | 0.0008 | 0.400 |
| 370 | 0.0300 | 0.0106 | 0.0353 | 670 | 0.430 | 0.0008 | 0.430 |
| 380 | 0.0220 | 0.0094 | 0.0267 | 680 | 0.450 | 0.0007 | 0.450 |
| 390 | 0.0191 | 0.0084 | 0.0233 | 690 | 0.500 | 0.0007 | 0.500 |
| 400 | 0.0171 | 0.0076 | 0.0209 | 700 | 0.650 | 0.0007 | 0.650 |
| 410 | 0.0162 | 0.0068 | 0.0196 | 710 | 0.839 | 0.0007 | 0.834 |
| 420 | 0.0153 | 0.0061 | 0.0184 | 720 | 1.169 | 0.0006 | 1.170 |
| 430 | 0.0144 | 0.0055 | 0.0172 | 730 | 1.799 | 0.0006 | 1.800 |
| 440 | 0.0145 | 0.0049 | 0.0170 | 740 | 2.38 | 0.0006 | 2.380 |
| 450 | 0.0145 | 0.0045 | 0.0168 | 750 | 2.47 | 0.0005 | 2.47 |
| 460 | 0.0156 | 0.0041 | 0.0176 | 760 | 2.55 | 0.0005 | 2.55 |
| 470 | 0.0156 | 0.0037 | 0.0175 | 770 | 2.51 | 0.0005 | 2.51 |
| 480 | 0.0176 | 0.0034 | 0.0194 | 780 | 2.36 | 0.0004 | 2.36 |
| 490 | 0.0196 | 0.0031 | 0.0212 | 790 | 2.16 | 0.0004 | 2.16 |
|  |  |  |  | 800 | 2.07 | 0.0004 | 2.07 |

[a] Reproduced from Smith and Baker (1981), with permission.

Smith and  Baker measurements were not made in optically pure water, but rather in the "clearest natural waters."  Even these waters contain a small amount of dissolved and particulate matter, which will contribute something to both absorption and scattering.

There is evidence (Pegau and Zaneveld, 1992) that absorption by water is weakly dependent on temperature, at least in the red and near infrared ($\partial a/\partial T \approx 0.0015$ m$^{-1}$ °K$^{-1}$ at $\lambda = 600$ nm and $\partial a/\partial T \approx 0.01$ m$^{-1}$ °K$^{-1}$ at $\lambda = 750$ nm), and perhaps also slightly dependent on salinity.

## *Absorption by dissolved organic matter*

Absorption by yellow matter (CDOM or gelbstoff) is reasonably well described by the model (Bricaud, *et al.*, 1981)

$$a_y(\lambda) = a_y(\lambda_o) \exp\left[-0.014\,(\lambda - \lambda_o)\right] \tag{3.25}$$

over the range 350 nm $\leq \lambda \leq$ 700 nm.  Here $\lambda_o$ is a reference wavelength, often chosen to be $\lambda_o = 440$ nm, and $a_y(\lambda_o)$ is the absorption due to yellow matter at the reference wavelength.  The value of $a_y(\lambda)$ of course depends on the concentration of yellow matter in the water.  The exponential decay constant depends on the relative proportion of specific types of yellow matter; other studies have found exponent coefficients of $-0.014$ to $-0.019$ (Roesler, *et al.*, 1989, their Table 1).  Both total concentration and proportions are highly variable.

Table 3.6 gives measured values of $a_y(440)$ for selected waters. Because of the variability in yellow matter concentrations, the values found in Table 3.6 have little general validity even for the particular water bodies sampled, but they do serve to show representative values and the range of influence of yellow matter in determining the total absorption.  Although the above model allows the determination of spectral absorption by yellow matter if the absorption is known at one wavelength, no model yet exists that allows for the direct determination of $a_y(\lambda)$ from given concentrations of yellow matter constituents.

## *Absorption by phytoplankton*

Phytoplankton cells are strong absorbers of visible light and therefore play a major role in determining the absorption properties of natural waters. Absorption by phytoplankton occurs in various photosynthetic pigments, of which the chlorophylls are best known to nonspecialists.  Absorption by chlorophyll itself is characterized by strong absorption bands in the blue and

Table 3.6.  Measured absorption coefficient at $\lambda = 440$ nm due to yellow matter, $a_y(440)$, for selected waters.[a]

| Water body | $a_y(440)$ $(m^{-1})$ |
|---|---|
| Oceanic waters | |
| Sargasso Sea | $\approx$ .0 |
| off Bermuda | 0.01 |
| Gulf of Guinea | 0.024-0.113 |
| oligotrophic Indian Ocean | 0.02 |
| mesotrophic Indian Ocean | 0.03 |
| eutrophic Indian Ocean | 0.09 |
| Coastal and estuarine waters | |
| North Sea | 0.07 |
| Baltic Sea | 0.24 |
| Rhone River mouth, France | 0.086-0.572 |
| Clyde River estuary, Australia | 0.64 |
| Lakes and rivers | |
| Crystal Lake, Wisconsin, USA | 0.16 |
| Lake George, Australia | 0.69-3.04 |
| Lake George, Uganda | 3.7 |
| Carrao River, Venezuela | 12.44 |
| Lough Napeast, Ireland | 19.1 |

[a] Condensed from Kirk (1983), with permission of Cambridge University Press, copyright 1983.

in the red (peaking at $\lambda \approx 430$ and 665 nm, respectively, for chlorophyll *a*), with very little absorption in the green.  Chlorophyll occurs in all photosynthetic plants, and its concentration in milligrams of chlorophyll per cubic meter of water is commonly used as the relevant optical measure of phytoplankton abundance.  In practice, the term "chlorophyll concentration" usually refers to the sum of chlorophyll *a*, the main pigment in phytoplankton cells, and the related pigment pheophytin *a*.  This sum is often called the "pigment concentration." Chlorophyll concentrations for various waters range from 0.01 mg m$^{-3}$ in the clearest open ocean waters,

to 10 mg m$^{-3}$ in productive coastal upwelling regions, to 100 mg m$^{-3}$ in eutrophic estuaries or lakes. The globally averaged, near-surface, open-ocean value is in the neighborhood of 0.5 mg m$^{-3}$.

The absorbing pigments are not evenly distributed within phytoplankton cells, but are localized into small "packages" (chloroplasts), which are distributed nonrandomly throughout the cell. This localized distribution of pigments means that the spectral absorption by a phytoplankton cell, or by a collection of cells in water, is "flatter" (has less pronounced peaks and reduced overall absorption) than if the pigments were uniformly distributed throughout the cell, or throughout the water (Kirk, 1983). This so-called "pigment packaging effect" is a major source of both inter- and intra-species variability in spectral absorption by phytoplankton, because the details of the pigment packaging within cells depend not only on species but also on a cell's size and physiological state (which in turn depends on environmental factors such as ambient lighting and nutrient availability). Another source of variability in addition to chlorophyll *a* concentration and packaging is changes in pigment composition (the relative proportions of accessory pigments, namely chlorophylls *b* and *c*, pheopigments, biliproteins, and carotenoids), since each pigment displays a characteristic absorption curve. The spectral absorption characteristics of these accessory pigments can be seen in Kirk (1983); tabulated values are given in Bidigare, *et al.*, (1990).

A qualitative feel for the nature of phytoplankton absorption can be obtained from Fig. 3.7, which is based on absorption measurements from eight different single-species laboratory phytoplankton cultures (Sathyendranath, *et al.*, 1987). Measured spectral absorption coefficients for the eight cultures, $a_i(\lambda)$, $i = 1$ to 8, were first reduced by subtracting $a_i(737)$ to remove the effects of absorption by detritus and cell constituents other than pigments: the assumption is that pigments do not absorb at $\lambda = 737$ nm and that the residual absorption is wavelength independent (which is a crude approximation). The resulting curves were then normalized by the chlorophyll concentrations $C_i$ of the respective cultures to generate the *chlorophyll-specific spectral absorption* curves for phytoplankton, $a_i^*(\lambda)$:

$$a_i^*(\lambda) = \frac{a_i(\lambda) - a_i(737)}{C_i} \qquad \left( \frac{\text{m}^{-1}}{\text{mg m}^{-3}} = \text{m}^2\,\text{mg}^{-1} \right),$$

which are plotted in Fig. 3.7.

Several general features of phytoplankton absorption are seen in Fig. 3.7: there are distinct absorption peaks at $\lambda \approx 440$ and 675 nm; the blue peak is one to three times as high as the red one (for a given species) due
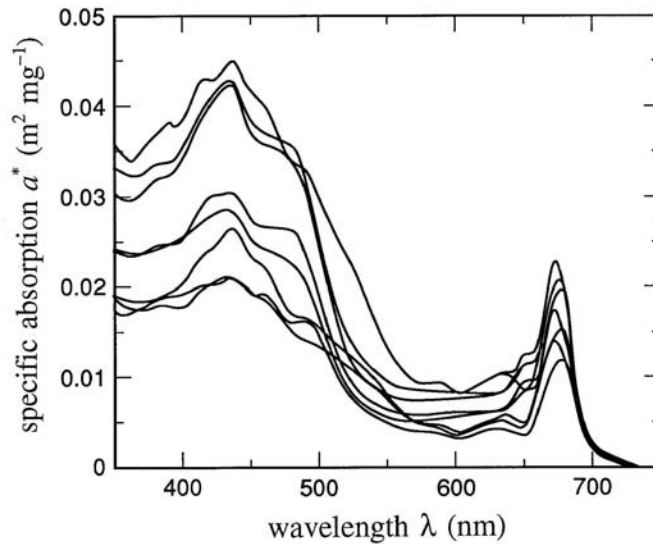
Fig. 3.7. Chlorophyll-specific spectral absorption coefficients for eight species of phytoplankton. [redrawn from Sathyendranath, *et al*. (1987), by permission]

to the contribution of accessory pigments to absorption in the blue; and there is relatively little absorption between 550 and 650 nm, with the absorption minimum near 600 nm being 10% to 30% of the value at 440 nm. There is clearly considerable variability in the phytoplankton absorption curves even for laboratory cultures. The variability of $a^*(\lambda)$ in naturally occurring populations of phytoplankton scarcely has been studied but likely is at least as great as that seen in Fig. 3.7. Similar curves can be seen in Bricaud, *et al.*, (1988), along with the corresponding chlorophyll-specific scattering and attenuation coefficients, $b^*$ and $c^*$.

## *Absorption by organic detritus*

It is not easy to separate the contributions of living phytoplankton and of nonliving detritus to the total particulate absorption as measured by any of the previously mentioned methods. A number of ways to achieve this separation have been investigated: (1) direct examination of individual particles using microspectrophotometry (Iturriaga and Siegel, 1989); (2) filter-pad measurements made before and after chemical extraction of phytoplankton pigments (e.g. Kishino, *et al.*, 1985); (3) modeling based on an assumed ratio of phytoplankton absorption at two wavelengths in the blue

and red (Roesler, *et al.*, 1989); (4) statistical methods based on typical absorption spectra of phytoplankton and detritus (Morrow, *et al.*, 1989); and (5) modeling based on an assumed functional form for detrital absorption (Bricaud and Stramski, 1990).

These diverse measurement methods all yield the same functional form for absorption by detritus, $a_{\text{det}}(\lambda)$, as was seen in Eq. (3.25) for absorption by yellow matter. Roesler, *et al.* (1989) found that the model

$$a_{\text{det}}(\lambda) \; = \; a_{\text{det}}(400) \exp\!\big[-0.011\,(\lambda - 400)\big] \qquad\qquad (3.26)$$

provides a satisfactory fit to detrital absorption curves. Other studies have found detrital exponent coefficients of $-0.006$ to $-0.014$ (Roesler, *et al.,* their Table 1).

Figure 3.8 shows the contributions of absorption by phytoplankton, $a_{\text{ph}}(\lambda)$, and of absorption by detritus, $a_{\text{det}}(\lambda)$, [as partitioned by the method of Iturriaga and Siegel (1989)] to the independently measured (by the filter-pad technique) total particulate absorption, $a_{\text{p}}(\lambda)$, for two depths at the same Atlantic location. The small residual, $\Delta a_{\text{p}}(\lambda) = a_{\text{p}}(\lambda) - a_{\text{ph}}(\lambda) - a_{\text{det}}(\lambda)$ shown in the figure is attributed either to errors in the determination of the phytoplankton and detrital parts (particles smaller than $\sim 3$ μm were not analyzed) or to contamination by dissolved organic matter of the filter-pad measurements of total particulate absorption. Note that at the shallow depth the phytoplankton are relatively more important at blue wavelengths, whereas the detritus is slightly more important at the deeper depth. There is no generality in this result (other locations showed the reverse) – it merely illustrates the variability possible in water samples taken only 60 vertical meters apart. The important feature to note in Fig. 3.8 is the general shape of the spectral absorption curve for detritus.

## *Bio-optical models for absorption*

Depending on the concentrations of dissolved substances, phytoplankton, and detritus, the total spectral absorption coefficient of a given water sample can range from almost identical to that of pure water to one which shows orders-of-magnitude greater absorption than pure water, especially at blue wavelengths. Figure 3.9 shows some $a(\lambda)$ profiles from various natural waters. Figure 3.9(a) shows absorption profiles measured in phytoplankton-dominated waters where chlorophyll concentrations ranged from $C = 0.2$ to $18.4$ mg m$^{-3}$. In essence, the absorption is high in the blue because of absorption by phytoplankton pigments, and high in the red because of absorption by the water. Figure 3.9(b) shows the absorption at
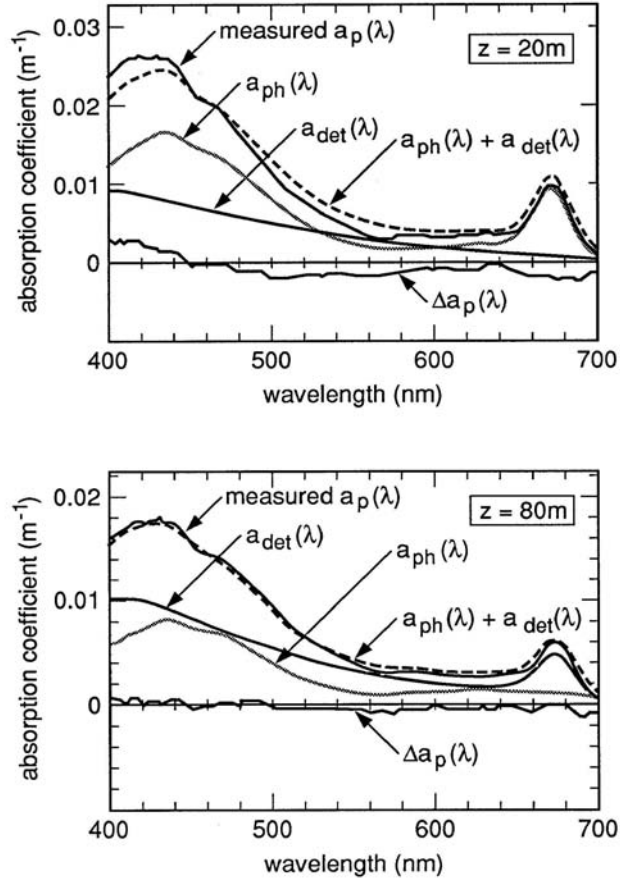
Fig. 3.8. Examples of the relative contributions of absorption by phytoplankton, $a_{ph}(\lambda)$, and by organic detritus, $a_{det}(\lambda)$, to the total particulate absorption $a_p(\lambda)$, from Sargasso Sea waters. [redrawn from Iturriaga and Siegel (1989), by permission]

three locations where $C \approx 2$ mg m$^{-3}$ but where the scattering coefficient $b$ varied from 1.55 to 3.6 m$^{-1}$, indicating that nonpigmented particles were playing an important role in determining the shape of $a(\lambda)$. Figure 3.9(c) shows curves from waters rich in yellow matter, which is causing the high absorption in the blue. One of the goals of bio-optics is to develop predictive models for absorption curves such as those seen in Fig. 3.9.

*Case 1 waters* are waters in which the concentration of phytoplankton is high compared to nonbiogenic particles (Morel and Prieur, 1977). Absorption by chlorophyll and related pigments therefore plays a major role in determining the total absorption coefficient in such waters,
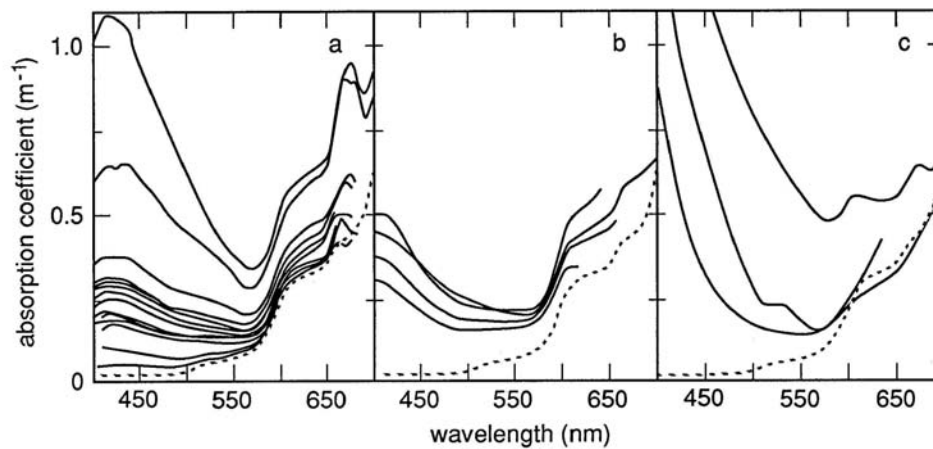
Fig. 3.9. Examples of spectral absorption coefficients $a(\lambda)$ for various waters. Panel (a) shows $a(\lambda)$ for waters dominated by phytoplankton, panel (b) is for waters with a high concentration of nonpigmented particles, and panel (c) is for waters rich in yellow matter. [based on Prieur and Sathyendranath (1981), by permission]

although detritus and dissolved organic matter derived from the phytoplankton also contribute to absorption in case 1 waters. Case 1 water can range from very clear (oligotrophic) water to very turbid (eutrophic) water, depending on the phytoplankton concentration. *Case 2 waters* are "everything else," namely waters where inorganic particles or dissolved organic matter from land drainage dominate, so that absorption by pigments is relatively less important in determining the total absorption. (The case 1 and 2 classifications must not be confused with the Jerlov water *types* 1 and 2, discussed in Section 3.10, below. Note also that "case 1" and "case 2" are *not* synonyms for "open ocean" and "coastal" water.) Roughly 98% of the world's open ocean and coastal waters fall into the case 1 category, and almost all bio-optical research has been directed toward these phytoplankton-dominated waters. However, near-shore and estuarine case 2 waters are disproportionately important to human interests such as recreation, fisheries, and military operations. It is therefore likely that case 2 waters will receive increasing attention in coming years.

Prieur and Sathyendranath (1981) developed a pioneering bio-optical model for the spectral absorption coefficient of case 1 waters. Their model was statistically derived from 90 sets of spectral absorption data taken in various case 1 waters and included absorption by phytoplankton pigments, by

nonpigmented organic particles derived from deceased phytoplankton, and by yellow matter derived from decayed phytoplankton. The contribution of phytoplankton to the total absorption was parameterized in terms of the chlorophyll concentration $C$ (i.e. chlorophyll $a$ plus pheophytin $a$). The contributions of nonpigmented particles and of yellow matter were parameterized in terms of both the chlorophyll concentration and the total scattering coefficient at $\lambda = 550$ nm, $b(550)$. The essence of the Prieur-Sathyendranath model is contained in a more recent and simpler variant given by Morel (1991b):

$$a(\lambda) = \left[ a_w(\lambda) + 0.06\, a_c^{*\prime}(\lambda)\, C^{0.65} \right]\left[ 1 + 0.2 \exp\left( -0.014(\lambda - 440) \right) \right]. \quad (3.27)$$

Here $a_w(\lambda)$ is the absorption coefficient of pure water and $a_c^{*\prime}(\lambda)$ is a nondimensional, statistically derived chlorophyll-specific absorption coefficient; $a_w(\lambda)$ and $a_c^{*\prime}(\lambda)$ values are given in Table 3.7 [these $a_w(\lambda)$ values are slightly different than those of Table 3.5]. When $C$ is expressed in mg m$^{-3}$ and $\lambda$ is in nm, the resulting $a(\lambda)$ is in m$^{-1}$. Figure 3.10 shows $a(\lambda)$ as predicted by Eq. (3.27) for various chlorophyll concentrations. The predicted $a(\lambda)$ values are qualitatively similar to the measured $a(\lambda)$ of Fig. 3.9(a), although the magnitudes sometimes differ, especially for the higher chlorophyll concentrations.

Table 3.7. Absorption by pure sea water, $a_w$, and the nondimensional chlorophyll-specific absorption coefficient, $a_c^{*\prime}$, for use in Eq. (3.27).[a]

| $\lambda$ (nm) | $a_w$ (m$^{-1}$) | $a_c^{*\prime}$ | $\lambda$ (nm) | $a_w$ (m$^{-1}$) | $a_c^{*\prime}$ | $\lambda$ (nm) | $a_w$ (m$^{-1}$) | $a_c^{*\prime}$ |
|---|---|---|---|---|---|---|---|---|
| 400 | 0.018 | 0.687 | 500 | 0.026 | 0.668 | 600 | 0.245 | 0.236 |
| 410 | 0.017 | 0.828 | 510 | 0.036 | 0.618 | 610 | 0.290 | 0.252 |
| 420 | 0.016 | 0.913 | 520 | 0.048 | 0.528 | 620 | 0.310 | 0.276 |
| 430 | 0.015 | 0.973 | 530 | 0.051 | 0.474 | 630 | 0.320 | 0.317 |
| 440 | 0.015 | 1.000 | 540 | 0.056 | 0.416 | 640 | 0.330 | 0.334 |
| 450 | 0.015 | 0.944 | 550 | 0.064 | 0.357 | 650 | 0.350 | 0.356 |
| 460 | 0.016 | 0.917 | 560 | 0.071 | 0.294 | 660 | 0.410 | 0.441 |
| 470 | 0.016 | 0.870 | 570 | 0.080 | 0.276 | 670 | 0.430 | 0.595 |
| 480 | 0.018 | 0.798 | 580 | 0.108 | 0.291 | 680 | 0.450 | 0.502 |
| 490 | 0.020 | 0.750 | 590 | 0.157 | 0.282 | 690 | 0.500 | 0.329 |
|  |  |  |  |  |  | 700 | 0.650 | 0.215 |

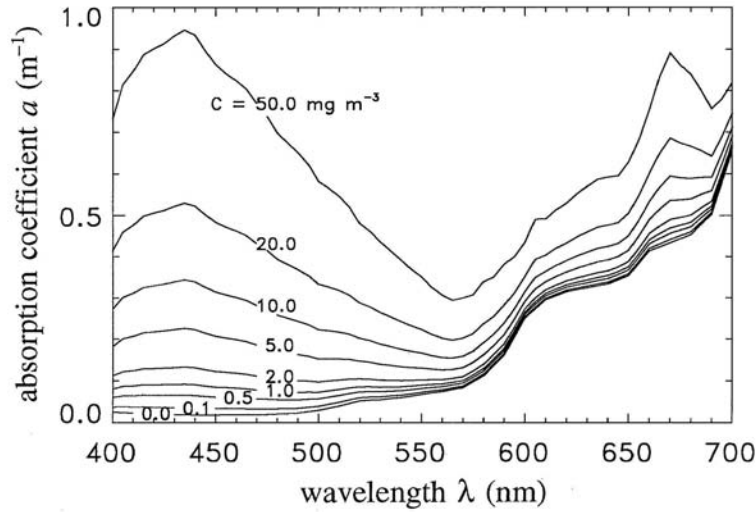[a] Condensed with permission from Prieur and Sathyendranath (1981), who give values every 5 nm.

Fig. 3.10. Total spectral absorption coefficient $a(\lambda)$ for selected chlorophyll concentrations $C$, as predicted by Eq. (3.27).

The bio-optical model for absorption expressed by Eq. (3.27) is frequently used; we shall see it in action in Section 11.8. However, its limitations must be kept in mind. For example, the model assumes that the absorption by yellow matter covaries with that due to phytoplankton; i.e. it assumes that a fixed percentage of the total absorption at a given wavelength always comes from yellow matter. The general validity of this assumption is doubtful even for open ocean waters: Bricaud, *et al.* (1981) show data (their Fig. 5) for which $a(375)$, used as an index for yellow matter concentration, is uncorrelated with chlorophyll concentration even in oceanic regions uninfluenced by fresh-water runoff. The model also assumes that the same (average) chlorophyll-specific absorption coefficient $a_c^{*\prime}(\lambda)$ is valid for all biological particles, which is almost certainly not the case. And finally, the model is intended for use *only* in phytoplankton-dominated, case 1 waters.

Other bio-optical models for absorption have been developed, but each has its own imperfections. Gordon (1992) has developed a model that avoids assuming any relation between yellow matter and phytoplankton. However, his model becomes singular as $C \to 0.01$ mg m$^{-3}$ and cannot be expected to work well for $C$ much less than 0.1 mg m$^{-3}$. A model by Kopelevich (1983) has the chlorophyll contribution proportional to the concentration $C$, whereas the model of Eq. (3.27) has $C^{0.65}$. The exponent

of 0.65 is probably closer to reality, since it reflects a change in the relative contributions to absorption by phytoplankton and by detritus as the chlorophyll concentration changes (absorption by detritus is relatively more important at low chlorophyll concentrations). Moreover, the chlorophyll-specific absorption curve used in the Kopelevich model is based on laboratory cultures of phytoplankton, whereas the work by Prieur and Sathyendranath used *in situ* observations to derive the $a_c^{*\prime}(\lambda)$ values of Table 3.7 – an additional point in favor of Eq. (3.27). Any of these bio-optical models for absorption is useful, but each is imperfect. They may – or may not – give correct *average* values, but they give no information about the *variability* of $a(\lambda)$. It can be anticipated that the simple models now available will in time be replaced, perhaps by models designed for specific regions and seasons, as better understanding of the variability inherent in spectral absorption is achieved.

# 3.8  Scattering

At the most fundamental, microscopic level, all scattering arises from interactions between photons and molecules or atoms. Nevertheless, scattering in natural waters is conveniently viewed as being caused by small-scale ($\ll \lambda$) density fluctuations attributable to random molecular motions, by the ubiquitous large ($> \lambda$) organic and inorganic particles, and by large-scale ($\gg \lambda$) turbulence-induced fluctuations in the real index of refraction. The convenience of these ill-defined size categories lies not in their delineation of fundamental physical processes, but rather in the approximate mathematical theories used to describe scattering in the various size domains.

Small-scale scattering by water molecules (and by salt ions, in seawater) determines the minimum values for the scattering properties. As is the case for absorption, however, the scattering properties of natural waters are greatly modified by the particulate matter that is always present.

## *Measurement of scattering*

Scattering measurements are even more difficult to make than are absorption measurements. The conceptual design of an instrument for measuring the volume scattering function $\beta(\psi;\lambda)$ is no more complicated than Fig. 3.1 and the defining Eq. (3.4), $\beta(\psi;\lambda) = I_s(\psi;\lambda)/[E_i(\lambda)\,\Delta V]$: a collimated beam of known spectral irradiance $E_i(\lambda)$ illuminates a given volume of water $\Delta V$, and the scattered intensity $I_s$ is measured as a function

of scattering angle and wavelength. However, the engineering of instruments capable of the *in situ* determination of $\beta(\psi;\lambda)$ is quite difficult. The magnitude of the scattered intensity typically increases by five or six orders of magnitude in going from $\psi = 90°$ to $\psi = 0.1°$ for a given natural water sample, and scattering at a given angle $\psi$ can vary by two orders of magnitude among water samples. The required dynamic range of an instrument is therefore great. Corrections must be made for absorption within the sample volume, and also for attenuation along the incident and scattered beam paths for *in situ* instruments. The rapid change in $\beta(\psi;\lambda)$ at small scattering angles requires very precise alignment of the optical elements, but rolling ships seem designed to knock things out of alignment – a point that may not be appreciated by those used to the luxury of optical benches. Because of these design difficulties, only a few one-of-a-kind instruments have been built for *in situ* measurement of the volume scattering function, and measurements of $\beta(\psi;\lambda)$ are not routinely made. Petzold (1972) gives the details of two such instruments, one for small scattering angles ($\psi = 0.085°$, $0.17°$, and $0.34°$) and one for larger angles ($10° \leq \psi \leq 170°$); these are the instruments used to obtain the data presented in Table 3.10, below. The large-angle Petzold instrument is still in use over 30 years after its construction. Other instruments are described in Kirk (1983) and in Jerlov (1976).

Commercial instruments are available for laboratory measurement of $\beta(\psi;\lambda)$ at fixed scattering angles, e.g. $\psi$ every $5°$ from ~$20°$ to ~$160°$. These instruments are subject to their own problems, such as degradation of samples between the times of collection and measurement. Moreover, measurements of $\beta(\psi;\lambda)$ over a limited range of $\psi$ are not sufficient for determination of $b(\lambda)$ by integration as in Eq. (3.5). In practice, the scattering coefficient $b(\lambda)$ is usually determined by the conservation of energy relation $b(\lambda) = c(\lambda) - a(\lambda)$, after measurements of beam attenuation and absorption have been made. The backscatter coefficient $b_b(\lambda)$ can be measured in the laboratory using a spectrophotometer combined with an integrating sphere (Bricaud, *et al.*, 1983).

Both *in situ* and laboratory instruments sample small (~1 cm$^3$) volumes of water and therefore may fail to detect the presence of optically significant large aggregates (marine snow), if such particles are too few in number to be reliably captured in the sample volume. Such particles, however, can affect the scattering properties of large volumes of water as are seen, for example, in remote sensing or underwater visibility studies.

Measurements at near forward ($\psi < 1°$) and near backward ($\psi > 179°$) angles are exceptionally difficult to make, yet the behavior of $\beta(\psi;\lambda)$ at these extreme angles is of considerable interest. Accurate determination

of $\beta$ at small angles is crucial to the determination of *b* by integration, since typically one-half of all scattering takes place at angles of less than a few degrees.  Scattering at small angles is important in underwater imaging, and it is of theoretical interest for its connections to scattering theory, particle optical properties, and particle size distributions.  The behavior of $\beta$ very near $\psi = 180°$ is important in laser remote-sensing applications.

Spinrad, *et al.* (1978), Padmabandu and Fry (1990), and Fry, *et al.* (1992b) have reported measurements at very small angles on suspensions of polystyrene spheres, but no such measurements have been published for natural water samples.  The Padmabandu and Fry technique is notable in that it allows the measurement of $\beta$ at $\psi = 0°$ exactly, by use of the coupling of two coherent beams in a photorefractive crystal to measure the phase shift that corresponds to 0° scattering.  Measurement of $\beta(0;\lambda)$ is of theoretical interest because of its relation to attenuation via the optical theorem (Bohren and Huffman, 1983).

Enhanced backscatter has been reported in suspensions of latex spheres; a factor-of-two increase in scattered intensity between $\psi = 179.5°$ and 180.0° is typical (Kuga and Ishimaru, 1989).  Laboratory studies show that small (<300 $\mu$m) air bubbles in water also can generate enhanced backscatter (Arnott and Marston, 1988).  Preliminary measurements in natural waters (Maffione and Honey, 1992) show only about a 10% increase in $\beta(\psi)$ as $\psi$ goes from 179.5° to 180.0°, but this matter is still under investigation.

Very few measurements of the full Mueller scattering matrix have been made in oceanic waters; these are discussed in Section 5.13.

## *Scattering by pure water and by pure sea water*

Raman (1922) and Shuleikin (1922) first pointed out the fundamental role played by small-scale scattering in natural waters.  Raman's delightful paper carefully refuted Lord Rayleigh's assertion that "The much-admired dark blue of the deep sea has nothing to do with the colour of the water, but is simply the blue of the sky seen by reflection."  Raman's paper may still be read with profit.

Morel (1974) has reviewed in detail the theory and observations pertaining to scattering by pure water and by pure sea water.  As we mentioned in Section 3.6, random molecular motions give rise to fluctuations in the number of molecules in a given volume $\Delta V$, where $\Delta V$ is small compared to the wavelength of light but large compared to atomic scales (so that the liquid within the volume is adequately described by statistical thermodynamics).  The Einstein-Smoluchowski theory of

scattering relates these fluctuations in molecule number density to associated fluctuations in the index of refraction, which give rise to scattering. In sea water the basic theory is the same, but random fluctuations in the concentrations of the various ions ($Cl^-$, $Na^+$, etc.) give somewhat greater index of refraction fluctuations, and hence greater scattering. The net result of these considerations is that the volume scattering function for either pure water or for pure sea water has the form

$$\beta_w(\psi; \lambda) = \beta_w(90°; \lambda_o) \left( \frac{\lambda_o}{\lambda} \right)^{4.32} (1 + 0.835 \cos^2 \psi) \qquad (m^{-1} \ sr^{-1}) \,. \quad (3.28)$$

This equation is reminiscent of the form

$$\beta_{Ray}(\psi; \lambda) = \beta_{Ray}(90°; \lambda_o) \left( \frac{\lambda_o}{\lambda} \right)^{4} (1 + \cos^2 \psi) \qquad (m^{-1} \ sr^{-1}) \,, \quad (3.29)$$

which is commonly called Rayleigh scattering. The wavelength dependence of $\lambda^{-4.32}$ (rather than $\lambda^{-4}$) results from the wavelength dependence of the index of refraction. The 0.835 factor (rather than 1) is attributable to the anisotropy of the water molecules.

The phase function corresponding to Eq. (3.28) is

$$\tilde{\beta}_w(\psi) = 0.06225 \, (1 + 0.835 \cos^2 \psi) \qquad (sr^{-1}) \,, \quad (3.30)$$

and the total scattering coefficient $b_w(\lambda)$ is given by

$$b_w(\lambda) = 16.06 \left( \frac{\lambda_o}{\lambda} \right)^{4.32} \beta_w(90°; \lambda_o) \qquad (m^{-1}) \,. \quad (3.31)$$

Table 3.8 gives values of $\beta_w(90°; \lambda)$ and $b_w(\lambda)$ for selected wavelengths, for both pure water and pure sea water ($S = 35 - 39‰$). Note that the pure sea water values are about 30% greater than the pure water values, at all wavelengths. Table 3.9 shows the dependence of $b_w(546 \ nm)$ on pressure, temperature, and salinity. Note that the scattering decreases as decreasing temperature or increasing pressure reduce the small-scale fluctuations.

Oceanographers commonly, and somewhat incorrectly, refer to scattering by pure water as "Rayleigh" scattering because of the previously noted similarity between $\beta_w$ in Eq. (3.28) and $\beta_{Ray}$ in Eq. (3.29). Strictly speaking, though, Rayleigh considered scattering by very small spherical

Table 3.8.  The volume scattering function at $\psi = 90°$, $\beta(90°;\lambda)$, and the scattering coefficient $b(\lambda)$ for pure water and for pure sea water ($S = 35$-$39‰$).  All numbers in the body of the table are times $10^{-4}$, as shown in the first row.[a]

| $\lambda$ (nm) | pure water | | pure sea water | |
| --- | --- | --- | --- | --- |
| | $\beta_w(90°)$ $(m^{-1}\ sr^{-1})$ | $b_w{}^b$ $(m^{-1})$ | $\beta_{sw}(90°)$ $(m^{-1}\ sr^{-1})$ | $b_{sw}{}^b$ $(m^{-1})$ |
| 350 | $6.47 \times 10^{-4}$ | $103.5 \times 10^{-4}$ | $8.41 \times 10^{-4}$ | $134.5 \times 10^{-4}$ |
| 375 | 4.80 | 76.8 | 6.24 | 99.8 |
| 400 | 3.63 | 58.1 | 4.72 | 75.5 |
| 425 | 2.80 | 44.7 | 3.63 | 58.1 |
| 450 | 2.18 | 34.9 | 2.84 | 45.4 |
| 475 | 1.73 | 27.6 | 2.25 | 35.9 |
| 500 | 1.38 | 22.2 | 1.80 | 28.8 |
| 525 | 1.12 | 17.9 | 1.46 | 23.3 |
| 550 | 0.93 | 14.9 | 1.21 | 19.3 |
| 575 | 0.78 | 12.5 | 1.01 | 16.2 |
| 600 | 0.68 | 10.9 | 0.88 | 14.1 |

[a] Reproduced from Morel (1974), with permission.
[b] Computed from $b(\lambda) = 16.0\ \beta(90°;\lambda)$.

Table 3.9.  Computed scattering coefficient $b$ of pure water ($S = 0$) and of pure sea water ($S = 35‰$) at $\lambda = 546$ nm as a function of temperature $T$ and pressure $p$.  Numbers in the body of the table have units of $m^{-1}$.[a]

| $T$ (°C) | $p = 10^5$ Pa (1 atm) | | $p = 10^7$ Pa (100 atm) | | $p = 10^8$ Pa (1000 atm) | |
| --- | --- | --- | --- | --- | --- | --- |
| | $S = 0$ | $S = 35‰$ | $S = 0$ | $S = 35‰$ | $S = 0$ | $S = 35‰$ |
| 0 | 0.00145 | 0.00195 | 0.00140 | 0.00192 | 0.00110 | 0.00167 |
| 10 | 0.00148 | 0.00203 | 0.00143 | 0.00200 | 0.00119 | 0.00176 |
| 20 | 0.00149 | 0.00207 | 0.00147 | 0.00204 | 0.00125 | 0.00183 |
| 40 | 0.00150 | 0.00213 | 0.00149 | 0.00212 | 0.00136 | 0.00197 |

[a] Data extracted from the more extensive table of Shifrin (1989), with permission.

particles, which he modeled as electric dipoles.  (Only much later did Rayleigh identify these particles with molecules.)   Einstein and Smoluchowski considered scattering by small-scale fluctuations.  It is not coincidental that these two different approaches lead to the same general form for $\beta(\psi;\lambda)$. However, to be precise and to give credit where it is due, scattering by pure water as described by Eq. (3.28) should be called "fluctuation" scattering or "Einstein-Smoluchowski" scattering.   Young (1982) gives an interesting history of the erroneous eponomy connected with Rayleigh's name.

## *Scattering by particles*

Heroic efforts are required to obtain water of sufficient purity that the volume scattering function of Eq. (3.28) is observed.  As soon as there is a slight amount of particulate matter in the water – always the case for even the clearest natural water – the volume scattering function becomes highly peaked in the forward direction, and the scattering coefficient increases by at least a factor of ten.

The contribution of the particulate matter to the total volume scattering function $\beta(\psi;\lambda)$ is obtained from

$$\beta_p(\psi;\lambda) \equiv \beta(\psi;\lambda) - \beta_w(\psi;\lambda) . \qquad (3.32)$$

Here the subscript *p* refers to particles, and *w* refers to pure water (if $\beta$ is measured in fresh water) or pure sea water (for oceanic measurements). Figure 3.11 shows several particle volume scattering functions determined from *in situ* measurements of $\beta(\psi;\lambda)$ in a variety of waters ranging from very clear to very turbid.  The particles cause at least a four-order-of-magnitude increase in scattering between $\psi \approx 90°$ and $\psi \approx 1°$.  The contribution of molecular scattering to the total is therefore completely negligible except at backscattered directions ($\psi \geq 90°$) in the clearest natural waters (Morel and Gentili, 1991). The top curve in Fig. 3.11 is shown for small scattering angles in Fig. 3.12. The scattering function shows no indication of "flattening out" even at angles less than 0.01° (see additional data in Honey and Sorenson, 1970).  Note that the scattering function increases by a factor of 100 over only a one-degree range of scattering angle.

Highly peaked forward scattering like that seen in Figs. 3.11 and 3.12 is characteristic of diffraction-dominated scattering in a polydisperse system (a system containing particles of many different sizes).  Scattering by refraction  and  reflection  from  particle  surfaces  becomes  important  at
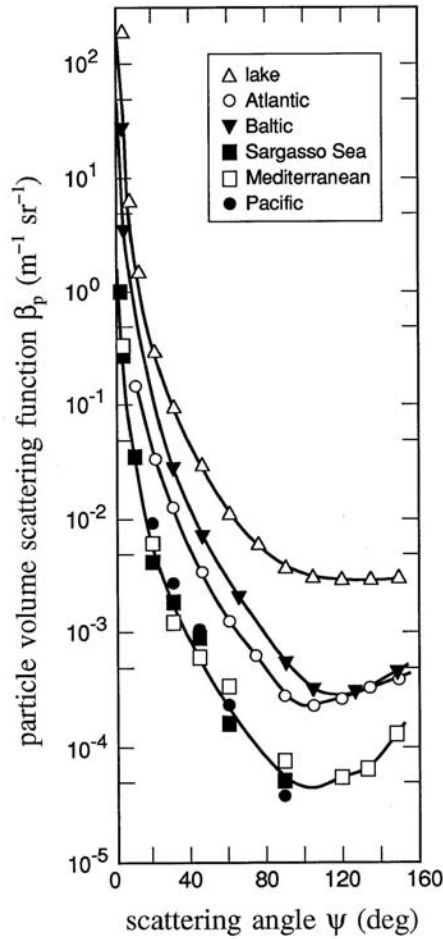
Fig. 3.11. Particle volume scattering functions $\beta_p(\psi;\lambda)$ determined from *in situ* measurements in various waters; wavelengths vary. [redrawn from Kullenberg (1974), by permission]
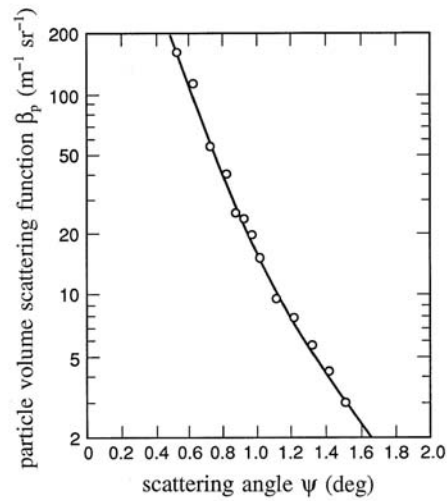
Fig. 3.12. Detail of the forward scattering values of the "lake" volume scattering function seen in the top curve of Fig. 3.11. [redrawn from *H.O. I*]

large scattering angles ($\psi > 15°$). Mie scattering calculations (see Section 3.11) are able to reproduce observed volume scattering functions, except at very small angles, given the proper particle optical properties and size distributions.

## Scattering by turbulence

Mie theory (discussed in Section 3.11) predicts that the volume scattering function should flatten out at very small angles, i.e. $d\beta(\psi)/d\psi \to 0$ as $\psi \to 0$. This behavior has been observed for $\psi \leq 1°$ in laboratory suspensions of polystyrene spheres (Spinrad, *et al.*, 1978) but not in natural waters, even for scattering angles less than 0.01°. Evidence indicates that this continued rise in $\beta(\psi)$ for $\psi < 1°$ may be attributed to turbulence. Small temperature and salinity fluctuations occur in natural waters on scales of millimeters and larger. The associated fluctuations in the real index of refraction cause small angular deviations in light rays propagating through the water.

We can get a feeling for the size of the turbulence-induced fluctuations in the real index of refraction $n$, as follows. Let us hold the wavelength $\lambda$ and pressure $p$ constant, so that $n$ is a function only of the temperature $T$ and salinity $S$. Then taking differentials of $n(T,S)$ gives

$$\Delta n = \left(\frac{\partial n}{\partial T}\right)_S \Delta T + \left(\frac{\partial n}{\partial S}\right)_T \Delta S,$$

where $\Delta T$ and $\Delta S$ are small fluctuations in $T$ and $S$, and $\Delta n$ is the corresponding change in $n$. If we square this equation, average it over many turbulent fluctuations, and assume that the fluctuations in temperature and salinity are uncorrelated, we obtain

$$\langle(\Delta n)^2\rangle = \left(\frac{\partial n}{\partial T}\right)^2 \langle(\Delta T)^2\rangle + \left(\frac{\partial n}{\partial S}\right)^2 \langle(\Delta S)^2\rangle. \tag{3.33}$$

Here $\langle \rangle$ represents the average of the enclosed quantity. The root-mean-square (rms) value of the index-of-refraction fluctuations is then $\langle(\Delta n)^2\rangle^{1/2}$. The derivatives $\partial n/\partial T$ and $\partial n/\partial S$ must be evaluated at particular values of $T, S, \lambda$ and $p$. We can estimate typical values from Fig. 3.5 or, better yet, from the tabulated data in Austin and Halikas (1976), from which this figure was drawn. Let us take $T = 20°C$, $S = 35‰$, $\lambda = 546$ nm, and $p = 1$ atm. Then from the data corresponding to the left-hand panel of Fig. 3.5, we find that

$$\frac{\partial n}{\partial T} \approx \frac{1.3405 - 1.3410}{23°C - 18°C} \approx -10^{-4} \; (°C)^{-1}.$$

From the data underlying the middle panel of Fig. 3.5 we get

$$\frac{\partial n}{\partial S} \approx \frac{1.342 - 1.341}{41‰ - 35‰} \approx 2 \times 10^{-4} \; (‰)^{-1}.$$

Now let us suppose that the temperature fluctuations are of magnitude $\Delta T \approx$ 0.005°C, and that $\Delta S \approx 0.005$‰. Then Eq. (3.33) gives

$$\langle (\Delta n)^2 \rangle^{1/2} \approx \left[ (10^{-4})^2 (0.005)^2 + (2 \times 10^{-4})^2 (0.005)^2 \right]^{1/2} \approx 1 \times 10^{-6}.$$

The turbulence-induced fluctuations in the index of refraction are therefore on the order of parts per million.

Such small changes in $n$ are negligible compared to the 5% "fluctuation" in $n$ when a photon encounters a plankton cell with $n = 1.05$ (relative to the water). However, in the case of particle scattering, we envision photons traveling in straight lines between the occasional encounter with a particle, at which time there may be a large change in direction. In the case of turbulence, we envision many turbulent blobs of water, of many sizes, with the photons slightly but continuously changing direction as they pass through water with a continuously varying index of refraction. It is then possible for the cumulative effect of the turbulent fluctuations to change a photon's direction by a small fraction of a degree. These turbulence-induced deviations manifest themselves in time-averaged scattering measurements as large values of $\beta$ at very small scattering angles.

Turbulence-induced scatter can significantly degrade the quality of underwater images. The effects of turbulence are especially noticeable in motion-picture photography, since the time dependence of the random fluctuations is then apparent, just as it is with the twinkling of stars caused by atmospheric turbulence. Near the boundary between distinctly different water masses, the fluctuations in $T$ and $S$ can be much larger than those assumed above, and even still images can be badly degraded; examples can be seen in Gilbert and Honey (1972).

These turbulence effects have been intensively studied by those interested in atmospheric optics, but have been ignored by most of the hydrologic optics community. This is often justified, since the changes in $n$ within water bodies usually are very small and do not significantly effect the distribution of radiant energy within the water (Duntley, 1974). The exception is found in the community of researchers interested in high-resolution underwater visibility and imaging, and in the behavior of coherent light beams. A pioneering study of the effects of turbulence on underwater images is found in Chilton, *et al.* (1969).

However, turbulence-induced scatter is unimportant in the overall redistribution of radiant energy in lakes and oceans. The purpose of our discussion here is to explain qualitatively the observed small-angle behavior of volume scattering functions. Because the *time-averaged effects of turbulence are included in measured volume scattering functions*, we have

no need to pursue this topic further. We do note, however, that although monochromatic, small-angle measurements of $\beta$ do not distinguish between scattering by particles and by turbulence, it may be possible to separate the two effects by considering the wavelength dependence of $\beta$, differences in polarization, or the time dependence of radiance fluctuations in a narrow collimated beam. Little work has been done along these lines. We also note that detailed numerical simulations of the optical effects of turbulence (Bogucki, *et al.*, 1993) may lead to new applications of "optical turbulence" as a probe of oceanic microstructure.

## *Petzold's measurements of volume scattering functions*

The most carefully made and widely cited scattering measurements are found in Petzold (1972). Figure 3.13(a) shows three of his $\beta(\psi;\lambda)$ curves displayed on a log-log plot to emphasize the forward scattering angles. The same data are displayed on log-linear axes in Fig. 3.13(b). The instruments he used had a spectral response centered at $\lambda = 514$ nm with a bandwidth of 75 nm (full width at half maximum). The top curve was obtained in the very turbid water of San Diego Harbor, California; the center curve comes from near-shore coastal water in San Pedro Channel, California; and the bottom curve is from very clear water in the Tongue of the Ocean, Bahama Islands. The striking feature of these volume scattering functions (and those of Fig. 3.11) from very different waters is the similarity of their shapes.

Although the scattering coefficients $b$ of the curves in Fig. 3.13 vary by a factor of 50 (see Table 3.11), the uniform shapes suggest that it is reasonable to define a "typical" particle phase function $\tilde{\beta}_p(\psi)$. This has been done with three sets of Petzold's data from waters with a high particulate load (one set being the top curve of Fig. 3.13), as follows (Mobley, *et al.*, 1993): (1) subtract $\beta_w(\psi;\lambda=514)$ from each curve to get three particle volume scattering functions $\beta_p^i(\psi)$, $i = 1,2,3$; (2) obtain the corresponding particle scattering coefficients from $b_p^i = b^i - b_w$; (3) compute three particle phase functions via $\tilde{\beta}_p^i(\psi) = \beta_p^i(\psi)/b_p^i$; (4) average the three particle phase functions at each scattering angle to define the typical particle phase function $\tilde{\beta}_p(\psi)$. Table 3.10 displays the three Petzold volume scattering functions plotted in Fig. 3.13, the volume scattering function for pure sea water, and the average particle phase function computed as just described. This particle phase function satisfies the normalization (3.8), if a behavior of $\tilde{\beta}_p \sim \psi^{-m}$ is assumed for $\psi < 0.1°$ and a trapezoidal rule integration is used for $\psi \geq 0.1°$, with linear interpolation used between the tabulated values. Here $m = 1.346$ is the negative of the slope of $\log \tilde{\beta}_p$ vs.
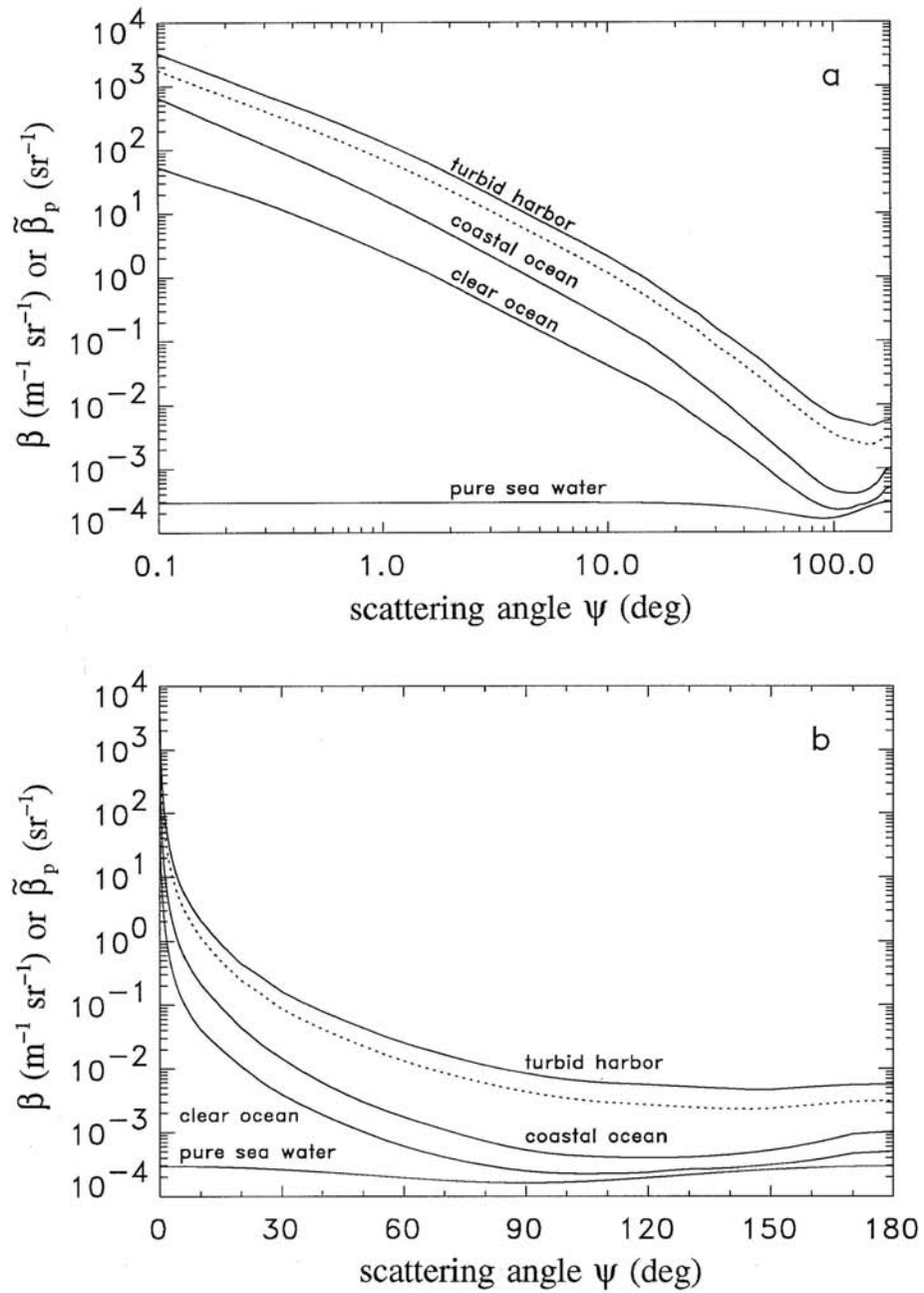
Fig. 3.13. Measured volume scattering functions β (solid lines) from three different natural waters, and the computed volume scattering function for pure sea water, all at λ = 514 nm. The dotted line is the particle phase function $\tilde{\beta}_p$ of Table 3.10. [redrawn from Petzold (1972)]

Table 3.10. Volume scattering functions $\beta(\psi;\lambda)$ for three oceanic waters and for pure sea water, and a typical particle phase function $\tilde{\beta}_p(\psi;\lambda)$, all at $\lambda = 514$ nm. These values are plotted in Fig. 3.13.

| Scattering angle (deg) | Volume scattering functions ($m^{-1}\,sr^{-1}$) | | | | Particle phase function[c] ($sr^{-1}$) |
|---|---|---|---|---|---|
| | clear ocean[a] | coastal ocean[a] | turbid harbor[a] | pure sea water[b] | |
| 0.100 | $5.318\times10^1$ | $6.533\times10^2$ | $3.262\times10^3$ | $2.936\times10^{-4}$ | $1.767\times10^3$ |
| 0.126 | 4.042 | 4.577 | 2.397 | 2.936 | 1.296 |
| 0.158 | 3.073 | 3.206 | 1.757 | 2.936 | $9.502\times10^2$ |
| 0.200 | 2.374 | 2.252 | 1.275 | 2.936 | 6.991 |
| 0.251 | 1.814 | 1.579 | $9.260\times10^2$ | 2.936 | 5.140 |
| 0.316 | 1.360 | 1.104 | 6.764 | 2.936 | 3.764 |
| 0.398 | $9.954\times10^0$ | $7.731\times10^1$ | 5.027 | 2.936 | 2.763 |
| 0.501 | 7.179 | 5.371 | 3.705 | 2.936 | 2.188 |
| 0.631 | 5.110 | 3.675 | 2.676 | 2.936 | 1.444 |
| 0.794 | 3.591 | 2.481 | 1.897 | 2.936 | 1.022 |
| 1.000 | 2.498 | 1.662 | 1.329 | 2.936 | $7.161\times10^1$ |
| 1.259 | 1.719 | 1.106 | $9.191\times10^1$ | 2.935 | 4.958 |
| 1.585 | 1.171 | $7.306\times10^0$ | 6.280 | 2.935 | 3.395 |
| 1.995 | $7.758\times10^{-1}$ | 4.751 | 4.171 | 2.934 | 2.281 |
| 2.512 | 5.087 | 3.067 | 2.737 | 2.933 | 1.516 |
| 3.162 | 3.340 | 1.977 | 1.793 | 2.932 | 1.002 |
| 3.981 | 2.196 | 1.273 | 1.172 | 2.930 | $6.580\times10^0$ |
| 5.012 | 1.446 | $8.183\times10^{-1}$ | $7.655\times10^0$ | 2.926 | 4.295 |
| 6.310 | $9.522\times10^{-2}$ | 5.285 | 5.039 | 2.920 | 2.807 |
| 7.943 | 6.282 | 3.402 | 3.302 | 2.911 | 1.819 |
| 10.0 | 4.162 | 2.155 | 2.111 | 2.896 | 1.153 |
| 15.0 | 2.038 | $9.283\times10^{-2}$ | $9.041\times10^{-1}$ | 2.847 | $4.893\times10^{-1}$ |
| 20.0 | 1.099 | 4.427 | 4.452 | 2.780 | 2.444 |
| 25.0 | $6.166\times10^{-3}$ | 2.390 | 2.734 | 2.697 | 1.472 |
| 30.0 | 3.888 | 1.445 | 1.613 | 2.602 | $8.609\times10^{-2}$ |
| 35.0 | 2.680 | $9.063\times10^{-3}$ | 1.109 | 2.497 | 5.931 |
| 40.0 | 1.899 | 6.014 | $7.913\times10^{-2}$ | 2.384 | 4.210 |
| 45.0 | 1.372 | 4.144 | 5.858 | 2.268 | 3.067 |
| 50.0 | 1.020 | 2.993 | 4.388 | 2.152 | 2.275 |
| 55.0 | $7.683\times10^{-4}$ | 2.253 | 3.288 | 2.040 | 1.699 |
| 60.0 | 6.028 | 1.737 | 2.548 | 1.934 | 1.313 |
| 65.0 | 4.883 | 1.369 | 2.041 | 1.839 | 1.046 |
| 70.0 | 4.069 | 1.094 | 1.655 | 1.756 | $8.488\times10^{-3}$ |
| 75.0 | 3.457 | $8.782\times10^{-4}$ | 1.345 | 1.690 | 6.976 |
| 80.0 | 3.019 | 7.238 | 1.124 | 1.640 | 5.842 |
| 85.0 | 2.681 | 6.036 | $9.637\times10^{-3}$ | 1.610 | 4.953 |
| 90.0 | 2.459 | 5.241 | 8.411 | 1.600 | 4.292 |
| 95.0 | 2.315 | 4.703 | 7.396 | 1.610 | 3.782 |
| 100.0 | 2.239 | 4.363 | 6.694 | 1.640 | 3.404 |
| 105.0 | 2.225 | 4.189 | 6.220 | 1.690 | 3.116 |
| 110.0 | 2.239 | 4.073 | 5.891 | 1.756 | 2.912 |
| 115.0 | 2.265 | 3.994 | 5.729 | 1.839 | 2.797 |
| 120.0 | 2.339 | 3.972 | 5.549 | 1.934 | 2.686 |
| 125.0 | 2.505 | 3.984 | 5.343 | 2.040 | 2.571 |
| 130.0 | 2.629 | 4.071 | 5.154 | 2.152 | 2.476 |
| 135.0 | 2.662 | 4.219 | 4.967 | 2.268 | 2.377 |
| 140.0 | 2.749 | 4.458 | 4.822 | 2.384 | 2.329 |
| 145.0 | 2.896 | 4.775 | 4.635 | 2.497 | 2.313 |
| 150.0 | 3.088 | 5.232 | 4.634 | 2.602 | 2.365 |
| 155.0 | 3.304 | 5.824 | 4.900 | 2.697 | 2.506 |
| 160.0 | 3.627 | 6.665 | 5.142 | 2.780 | 2.662 |
| 165.0 | 4.073 | 7.823 | 5.359 | 2.847 | 2.835 |
| 170.0 | 4.671 | 9.393 | 5.550 | 2.896 | 3.031 |
| 175.0 | 4.845 | 9.847 | 5.618 | 2.926 | 3.092 |
| 180.0 | 5.019 | $1.030\times10^{-3}$ | 5.686 | 2.936 | 3.154 |

[a] Data reproduced from Petzold (1972).
[b] Computed from Eq. (3.28) and Table 3.8.
[c] Data reproduced from Mobley, *et al.* (1993).

$\log\psi$, as determined from the two smallest measured scattering angles. This average particle phase function is adequate for many radiative transfer calculations. However, the user must remember that deviations from the average can be expected in nature (for example, in waters with abnormally high numbers of either large or small particles), although the details of such deviations have not been quantified.

Table 3.11 compares several inherent optical properties for pure sea water and for the three Petzold water samples of Fig. 3.13 and Table 3.10. These data show how greatly different even clear ocean water is from pure sea water. Note that natural water ranges from absorption dominated ($\omega_o = 0.247$) to scattering dominated ($\omega_o = 0.833$) at $\lambda = 514$ nm. The ratio of backscattering to total scattering is typically a few percent in natural waters. However, there is no clear relation between $b_b/b$ and the water type, at least for the Petzold data of Table 3.10. This lack of an obvious relation is likely the result of differing particle types in the three waters. Since refraction and reflection are important processes at large scattering angles, the particle indices of refraction are important in determining $b_b$. Total scattering is dominated by diffraction, and so particle composition has little effect on $b$ values. The last column of Table 3.11 gives the angle $\psi$ such that one half of the total scattering occurs at angles between 0 and $\psi$. This angle is rarely greater than 10° in natural waters.

Table 3.11. Selected inherent optical properties for the waters
presented in Fig. 3.13 and in Table 3.10.
All values are for $\lambda = 514$ nm, except as noted.

| Water[a] | $b$ $(\mathrm{m}^{-1})$ | $c$ $(\mathrm{m}^{-1})$ | $\omega_o$ $(\mathrm{m}^{-1})$ | $b_b/b$ | $\psi(\tfrac{1}{2}b)$ (deg) |
|---|---|---|---|---|---|
| pure sea water | 0.0405[a] | 0.0025[b] | 0.043 | 0.058 | 0.500 | 90.00 |
| clear ocean | 0.114[c] | 0.037 | 0.151[d] | 0.247 | 0.044 | 6.25 |
| coastal ocean | 0.179[c] | 0.219 | 0.398[d] | 0.551 | 0.013 | 2.53 |
| turbid harbor | 0.366[c] | 1.824 | 2.190[d] | 0.833 | 0.020 | 4.68 |

[a] Value obtained by interpolation in Table 3.5.
[b] Value obtained by interpolation in Table 3.8.
[c] Estimated by Petzold (1972) from $c(530) - b(514)$.
[d] Measured by Petzold (1972) at $\lambda = 530$ nm.

It is interesting to compare the particle phase function characteristic of natural waters, $\tilde{\beta}_p$, with a few other phase functions found in nature.  Figure 3.14 plots $\tilde{\beta}_p$ as just defined (dotted line), along with phase functions for atmospheric haze (dashed line), human liver cells (plus signs), and cirrostratus clouds (solid line).  Note especially that the atmospheric haze phase function is much less peaked than $\tilde{\beta}_p$ at small angles:  $\tilde{\beta}_{haze}$ is almost three orders of magnitude less than $\tilde{\beta}_p$ at $\psi = 0.1°$.  However, $\tilde{\beta}_{haze}$ shows more pronounced backscatter than does $\tilde{\beta}_p$.  This more symmetrical (about 90°) behavior of $\tilde{\beta}_{haze}$ reflects its origin in scattering by very small aerosols.  The liver phase function, arising from cells larger than 7 μm in size, appears to show strong forward scatter, although $\tilde{\beta}_{liver}$ was not measured for $\psi < 5°$.  The cirrus cloud phase function is most interesting.  It shows a strong forward peak, arising from diffraction by the large (10–100 μm) ice crystals forming the cloud.  The prominent peaks at $\psi = 22°$ and $46°$ arise from light refraction through the hexagonal ice crystals.  These peaks are
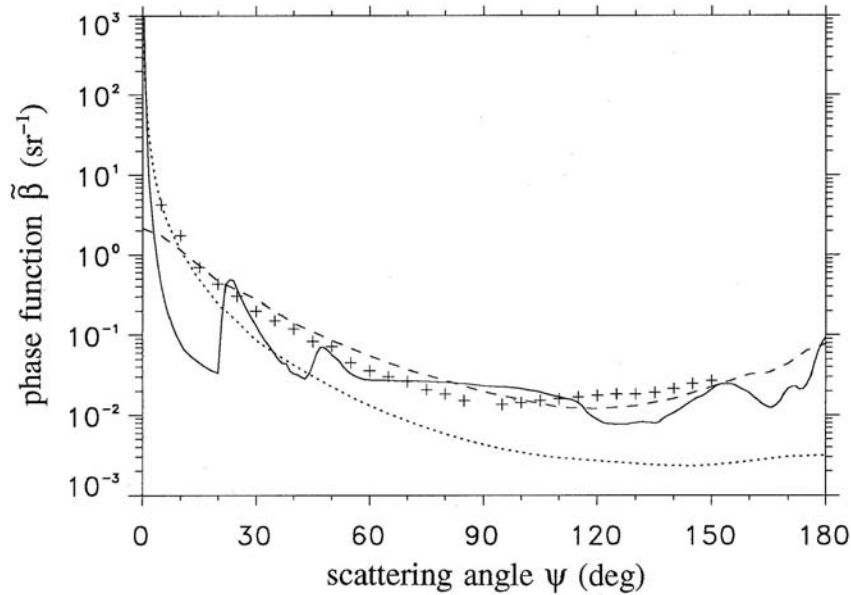


Fig. 3.14  Examples of phase functions.  The dotted line is $\tilde{\beta}_p$ from Fig. 3.13(b); the dashed line is atmospheric haze ["haze L" at $\lambda = 550$ nm, computed by Mie theory using size distribution parameters from Deirmendjian (1969)]; the + signs are human liver tissue [at $\lambda = 635$ nm, redrawn from Marchesini, *et al.* (1989), by permission]; and the solid line is for a cirrostratus cloud [at $\lambda = 550$ nm, drawn from data tabulated in Takano and Liou (1989)].

responsible for the halos sometimes seen around the sun or moon when there is a thin cirrus overcast.  Greenler (1980) gives an excellent explanation of how photon paths passing through ice crystals give rise to the peaks at 22° and 46°.

     We thus see that the $\tilde{\beta}_p$ typical of natural waters lies somewhere in the mid-range of complexity of phase functions.  That is, $\tilde{\beta}_p$ is more highly peaked than say, $\tilde{\beta}_{haze}$, but much less complicated in its $\psi$ dependence than a phase function arising from scattering by ice crystals.  It should be noted that the hexagonal symmetry of the ice crystals leads to a complicated phase function even though the ice crystals are randomly oriented within the cloud.

## *Analytic approximations of phase functions*

     It is often convenient to have a simple analytic formula that approximates the shape of an actual phase function.  The formula most commonly used for this purpose is the Henyey-Greenstein (1941) phase function

$$\tilde{\beta}_{HG}(g;\psi) \equiv \frac{1}{4\pi} \frac{1 - g^2}{\left(1 + g^2 - 2g\cos\psi\right)^{3/2}} . \qquad (3.34)$$

Here $g$ is a parameter that can be adjusted to control the relative amounts of forward and backward scattering in $\tilde{\beta}_{HG}$.  Note that $\tilde{\beta}_{HG}$ satisfies the normalization condition (3.8) for any $g$.

     The physical interpretation of $g$ comes from noting that

$$2\pi \int_{-1}^{1} \tilde{\beta}_{HG}(g;\psi) \cos\psi \, d\cos\psi = g . \qquad (3.35)$$

Thus the Henyey-Greenstein parameter $g$ is just the average of the cosine of the scattering angle for $\tilde{\beta}_{HG}$.  Recall that this asymmetry parameter $g$ was defined for any phase function in Eq. (3.8b).

     The average of $\cos\psi$ for the particle phase function $\tilde{\beta}_p$ of Fig. 3.13 and Table 3.10 is 0.924.  Using $g = 0.924$ in Eq. (3.34) thus gives the "best-fit" Henyey-Greenstein phase function to the particle phase function $\tilde{\beta}_p$, in the sense that each phase function then has the same average cosine.  Figure 3.15 compares $\tilde{\beta}_{HG}(0.924;\psi)$ and $\tilde{\beta}_p$; $\tilde{\beta}_{HG}$ is also shown for $g = 0.7$ and 0.99.  Note that the best-fit $\tilde{\beta}_{HG}$ differs noticeably from $\tilde{\beta}_p$ at scattering angles greater than 150° and less than 20°, and that $\tilde{\beta}_{HG}$ is much too small at angles of less than a few degrees.  The small-angle behavior of Eq. (3.34) is inherently incompatible with $\tilde{\beta}_p$ because $\tilde{\beta}_{HG}$ levels off for small $\psi$,
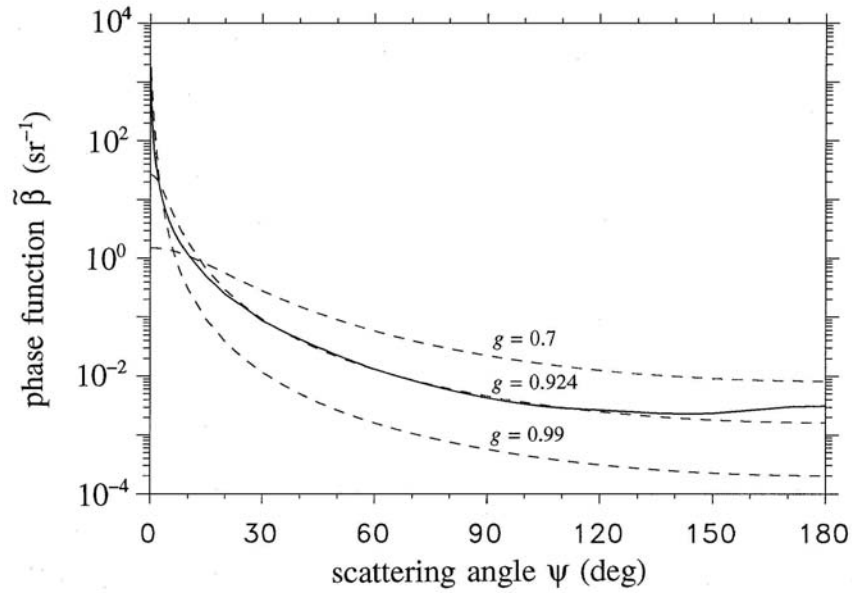
Fig. 3.15 Comparison of the particle phase function $\tilde{\beta}_p$ from Fig. 3.13(b) (solid line) with $\tilde{\beta}_{HG}$ of Eq. (3.34) for three values of $g$ (dashed lines).

whereas $\tilde{\beta}_p$ continues to rise. Even for $g = 0.99$, $\tilde{\beta}_{HG}$ is nearly constant for $\psi < 0.5°$.

It is also possible to choose the Henyey-Greenstein $g$-parameter so as to minimize the mean square difference

$$\int_{-1}^{1} [\beta(\psi) - \beta_{HG}(g;\psi)]^2 \, d\cos\psi$$

between a given $\beta$ and $\beta_{HG}$. Kamiuto (1987) shows how to determine the $g$ value that gives a least-squares best fit to a given phase function.

A linear combination of Henyey-Greenstein phase functions is often used to improve the fit at small and large angles. The so-called two-term Henyey-Greenstein (TTHG) phase function is

$$\tilde{\beta}_{TTHG}(\alpha, g_1, g_2; \psi) \equiv \alpha \, \tilde{\beta}_{HG}(g_1; \psi) + (1 - \alpha) \, \tilde{\beta}_{HG}(g_2; \psi). \tag{3.36}$$

Enhanced small-angle scattering is obtained by choosing $g_1$ near one, and enhanced backscatter is obtained by making $g_2$ negative; $\alpha$ is a weighting factor between zero and one. Kattawar (1975) shows how to determine best-fit values of $\alpha$, $g_1$, and $g_2$ for a given phase function. Excellent fits can

be obtained with the TTHG for phase functions that are not highly peaked, for example the one for atmospheric haze shown in Fig. 3.14 (see Kattawar's paper for example fits).  However, the fit of $\tilde{\beta}_{\text{TTHG}}$ to the highly peaked $\tilde{\beta}_p$ remains unsatisfactory at small angles, for the reason already noted.

Another analytic phase function sometimes seen in the literature is that of Beardsley and Zaneveld (1969).  It has the unnormalized form

$$\tilde{\beta}_{\text{BZ}} \sim \frac{1}{\left(1 - \epsilon_f \cos\psi\right)^4 \left(1 + \epsilon_b \cos\psi\right)^4} .$$

Here $\epsilon_f$ and $\epsilon_b$ are parameters to be used in fitting $\tilde{\beta}_{\text{BZ}}$ to the given phase function.  This formula also has a zero slope as $\psi \to 0$, and is therefore incapable of reproducing $\tilde{\beta}_p$ at small $\psi$.  In fact, $\tilde{\beta}_{\text{BZ}}$ does a poor job of fitting $\tilde{\beta}_p$ at scattering angles of less than several tens of degrees.

A final analytic formula worthy of mention is that of Wells (1973), which has the unnormalized form

$$\tilde{\beta}_{\text{W}}(\psi_o;\psi) \sim \left[1 + \left(\frac{\psi}{\psi_o}\right)^2\right]^{-3/2} . \tag{3.37}$$

Here $\psi_o$ is the parameter to be used in fitting $\tilde{\beta}_{\text{W}}$; $\psi_o = 0.03$ rad is often used for natural waters.  Equation (3.37) is essentially the same as Eq. (3.34) for small $\psi$.  This can be seen by approximating the $\cos\psi$ term in Eq. (3.34) as $\cos\psi \approx 1 - \frac{1}{2}\psi^2$, as is valid for small $\psi$, and comparing the result with Eq. (3.37).  Equating the coefficients of the $\psi^2$ terms reveals the connection

$$\frac{1}{\psi_o^2} = \frac{g}{(1 - g)^2}$$

between the parameters of $\tilde{\beta}_{\text{HG}}$ and $\tilde{\beta}_{\text{W}}$; thus $\psi_o = 0.03$ in Eq. (3.37) corresponds to $g = 0.97$ in Eq. (3.34).  Although Eq. (3.34) gives an overall better fit to any phase function than does Eq. (3.37),  the Wells form is often used in studies where only small-angle ($\psi < 20°$) scattering is of interest.  The reason is that certain integral transforms of the phase function can be computed analytically for $\tilde{\beta}_{\text{W}}$, but not for $\tilde{\beta}_{\text{HG}}$.  Such calculations are seen in the Wells (1973) paper.

## *Wavelength dependence of scattering; bio-optical models*

The strong $\lambda^{-4.32}$ wavelength dependence seen in Eq. (3.28) for pure-water scattering is not seen in natural waters.  This is because scattering is dominated by diffraction from polydisperse particles that are usually much larger than the wavelength of visible light.  Although diffraction depends on the particle size-to-wavelength ratio, the presence of particles of many sizes diminishes the wavelength effects that are seen in diffraction by a single particle.  Moreover, diffraction does not depend on particle composition.  However, some wavelength dependence is to be expected, especially at backward scattering angles where refraction, and hence particle composition, is important.  Molecular scattering also contributes something to the total scattering, and can even dominate the particle contribution at backscatter angles in clear water (Morel and Gentili, 1991).

Morel (1973) presents several useful observations on the wavelength dependence of scattering.  Figure 3.16 shows two sets of volume scattering
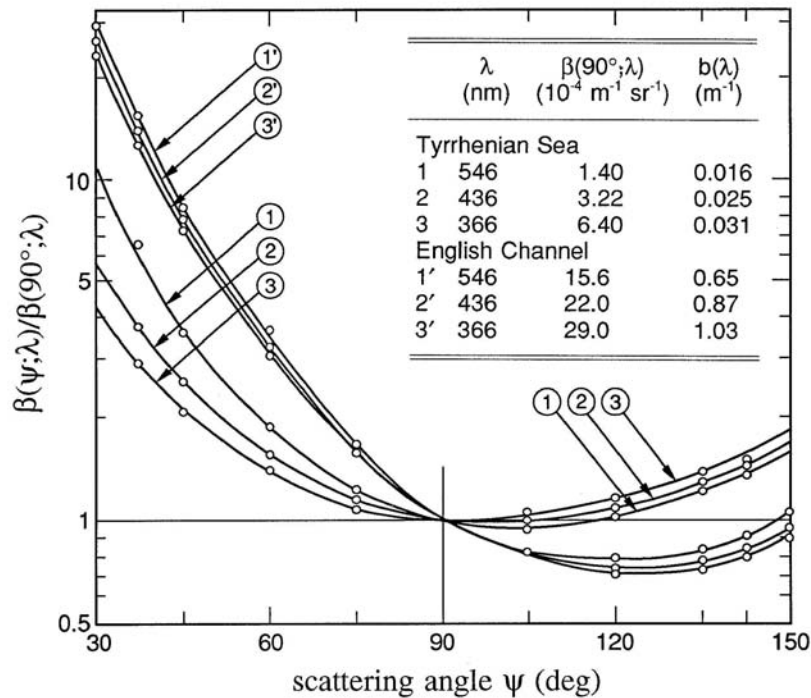


Fig. 3.16   Wavelength dependence of total volume scattering functions measured in very clear (Tyrrhenian Sea) and in turbid (English Channel) waters. [redrawn from Morel (1973)]

functions, one from the very clear waters of the Tyrrhenian Sea and one from the turbid English Channel. Each set displays $\beta(\psi;\lambda)/\beta(90°;\lambda)$ for $\lambda$ = 366, 436, and 546 nm. The clear water shows a definite dependence of the shape of $\beta(\psi;\lambda)$ on $\lambda$, whereas the particle-rich turbid water shows much less wavelength dependence. In each case, the volume scattering function of shortest wavelength is most nearly symmetric about $\psi$ = 90°, presumably because symmetric molecular scattering is contributing relatively more to the total scattering at short wavelengths.

Figure 3.17 shows a systematic wavelength dependence of particle volume scattering functions. Figure 3.17(a) shows average values of $\beta_p(\psi;366)/\beta_p(\psi;546)$ for $N$ samples, as labeled in the figure. The vertical bars are one standard deviation of the observations. Figure 3.17(b) shows the ratio for $\lambda$ = 436 to 546 nm. These ratios clearly depend both on wavelength and scattering angle. Assuming that $\beta_p(\psi;\lambda)$ has a wavelength dependence of

$$\beta_p(\psi;\lambda) = \beta_p(\psi;546)\left(\frac{546}{\lambda}\right)^n,$$

the data of Fig. 3.17 imply values for $n$ as seen in Table 3.12. As
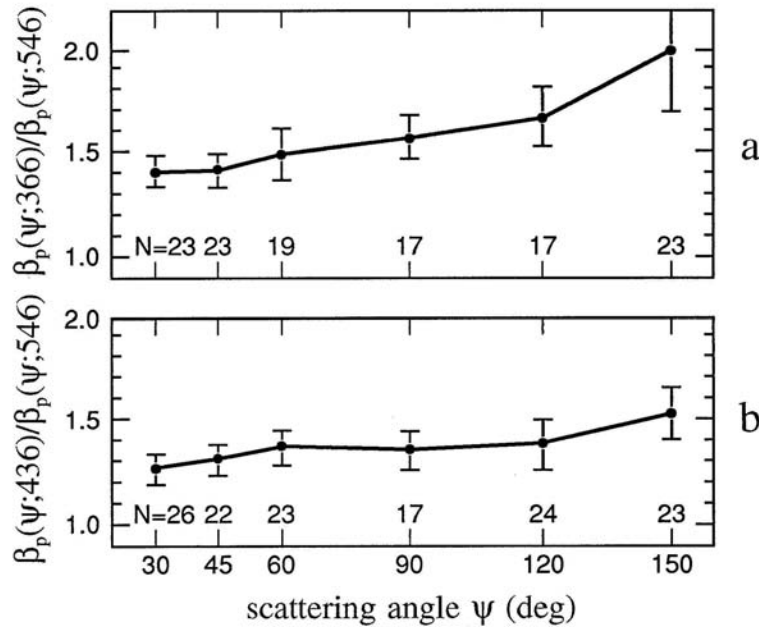


Fig. 3.17. Wavelength dependence of particle volume scattering functions. $N$ is the number of samples. [redrawn from Morel (1973)]

Table 3.12. Exponents *n* required to fit the data of Fig. 3.17, assuming that $\beta_p(\psi;\lambda) = \beta_p(\psi;546)(546/\lambda)^n$.[a]

| Wavelength $\lambda$ (nm) | Scattering angle $\psi$ | | |
| --- | --- | --- | --- |
| | 30° | 90° | 150° |
| 366 | 0.84 | 1.13 | 1.73 |
| 436 | 0.99 | 1.33 | 1.89 |

[a] Reproduced from Mobley (1994), by permission.

anticipated, the wavelength dependence is strongest for backscatter ($\psi = 150°$) and weakest for forward scatter ($\psi = 30°$).

Kopelevich (1983) and Kopelevich and Mezhericher (1983) have statistically derived a two-parameter model for spectral volume scattering functions (VSF's). This model separates the contributions by "small" and "large" particles to the particulate scattering. Small particles are taken to be mineral particles less than 1 μm in size and having an index of refraction (relative to water) of $n = 1.15$; large particles are biological particles larger than 1 μm in size and having an index of refraction of $n = 1.03$. The model is defined by

$$\beta(\psi;\lambda) = \beta_w(\psi;\lambda) + v_s\beta_s^*(\psi)\left(\frac{550}{\lambda}\right)^{1.7} + v_\ell\beta_\ell^*(\psi)\left(\frac{550}{\lambda}\right)^{0.3}, \qquad (3.38)$$

with the following definitions:

$\beta_w(\psi;\lambda)$     the VSF of pure sea water, given by Eq. (3.28) with $\lambda_o = 550$ nm and an exponent of 4.30,

$v_s$     the volume concentration of small particles, with units of $cm^3$ of particles per $m^3$ of water, i.e. parts per million (ppm),

$v_\ell$     the analogous volume concentration of large particles,

$\beta_s^*(\psi)$     the small-particle VSF per unit volume concentration of small particles, with units of $m^{-1}\ sr^{-1}\ ppm^{-1}$,

$\beta_\ell^*(\psi)$     the analogous large-particle concentration-specific VSF.

The concentration-specific VSF's for small and large particles are given in Table 3.13. Equation (3.35) can be evaluated as is if the two parameters $v_s$ and $v_\ell$ are known; the ranges of values for oceanic waters are $0.01 \leq v_s \leq 0.20$ ppm and $0.01 \leq v_\ell \leq 0.40$ ppm. However, these two parameters are themselves parameterized in terms of the total volume scattering function measured at $\lambda$ = 550 nm for $\psi = 1°$ and $45°$:

$$v_s = -1.4 \times 10^{-4} \beta(1°; 550) + 10.2 \beta(45°; 550) - 0.002$$
$$v_\ell = 2.2 \times 10^{-2} \beta(1°; 550) - 1.2 \beta(45°; 550) \qquad (3.39)$$

Thus $\beta(\psi; \lambda)$ can also be determined from two measurements of the total VSF.

The mathematical form of the Kopelevich model reveals its underlying physics. Large particles give diffractive scattering at very small angles, thus $\beta_\ell^*(\psi)$ is highly peaked for small $\psi$ and the wavelength dependence of the large particle term is weak ($\lambda^{-0.3}$). Small particles contribute more to scattering at large angles and thus have a more symmetric VSF and a stronger wavelength dependence ($\lambda^{-1.7}$).

Table 3.13.  The concentration-specific volume scattering functions for small ($\beta_s^*$) and large ($\beta_\ell^*$) particles, for use in Eq. (3.38).[a]

| $\psi$ (deg) | $\beta_s^*$ $\left(\dfrac{m^{-1} sr^{-1}}{ppm}\right)$ | $\beta_\ell^*$ $\left(\dfrac{m^{-1} sr^{-1}}{ppm}\right)$ | $\psi$ (deg) | $\beta_s^*$ $\left(\dfrac{m^{-1} sr^{-1}}{ppm}\right)$ | $\beta_\ell^*$ $\left(\dfrac{m^{-1} sr^{-1}}{ppm}\right)$ |
|---|---|---|---|---|---|
| 0 | 5.3 | 140 | 45 | $9.8 \times 10^{-2}$ | $6.2 \times 10^{-4}$ |
| 0.5 | 5.3 | 98 | 60 | 4.1 | 3.8 |
| 1 | 5.2 | 46 | 75 | 2.0 | 2.0 |
| 1.5 | 5.2 | 26 | 90 | 1.2 | $6.3 \times 10^{-5}$ |
| 2 | 5.1 | 15 | 105 | $8.6 \times 10^{-3}$ | 4.4 |
| 4 | 4.6 | 3.6 | 120 | 7.4 | 2.9 |
| 6 | 3.9 | 1.1 | 135 | 7.4 | 2.0 |
| 10 | 2.5 | 0.20 | 150 | 7.5 | 2.0 |
| 15 | 1.3 | $5.0 \times 10^{-2}$ | 180 | 8.1 | 7.0 |
| 30 | 0.29 | $2.8 \times 10^{-3}$ | $b^* =$ | 1.34 m$^{-1}$/ppm | 0.312 m$^{-1}$/ppm |

[a] Reproduced from Kopelevich (1983).

A qualitative comparison of Eq. (3.38) with the Petzold measurements of Fig. 3.13 is worthwhile.  If we arbitrarily choose mid-range values of $v_s$ = 0.1 ppm and $v_\ell$ = 0.2 ppm, then the total scattering associated with Eq. (3.38) at the Petzold wavelength of $\lambda$ = 514 nm is $b$ = 0.216 m$^{-1}$ [from Eq. (3.42), below].  This is nearly equal to the total scattering for the Petzold coastal water case, $b$ = 0.219 m$^{-1}$ (from Table 3.11).  Figure 3.18 shows the individual contributions of pure sea water, small particles, and large particles to $\beta(\psi;514)$ as predicted by Eq. (3.38), along with the Petzold coastal water $\beta(\psi;514)$ of Table 3.11.  We see that the model of Eq. (3.38) underpredicts $\beta$ at small scattering angles and overpredicts $\beta$ at large angles, when compared to the Petzold measurements.

Figure 3.19 shows the predictions of Eq. (3.38) for very clear water ($v_s$ = $v_\ell$ = 0.01 ppm) and for very turbid water ($v_s$ = 20 ppm and $v_\ell$ = 40 ppm), for the wavelengths seen in the Morel data of Fig. 3.16.  Comparison of these two figures shows that the Kopelevich model for $\beta(\psi;\lambda)$ qualitatively reproduces the wavelength behavior observed in the clear (Tyrrhenian Sea) and turbid (English Channel) waters of Fig. 3.16.  Shifrin (1988, his Fig. 5.20) also claims that Eq. (3.38) gives a reasonably good
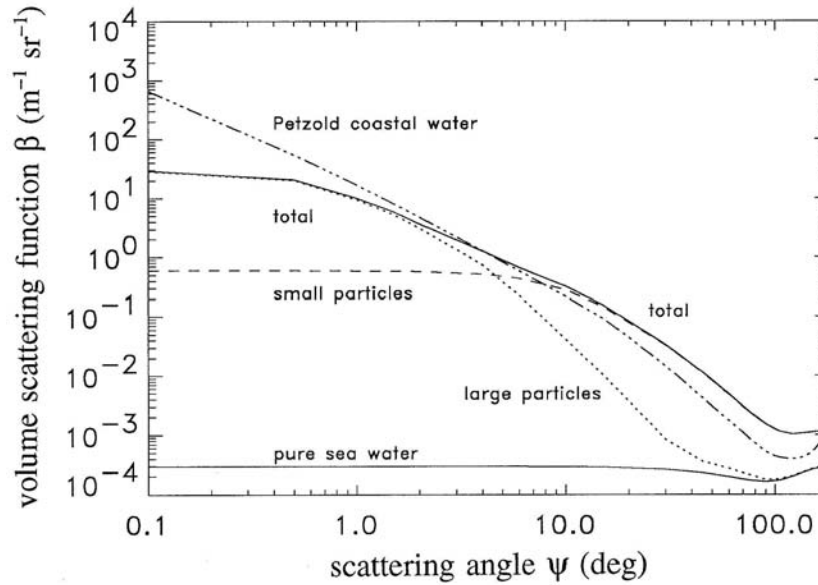


Fig. 3.18.  Comparison of the Kopelevich model for the volume scattering function, Eq. (3.38), with a volume scattering function as measured by Petzold (Table 3.10).   The pure-sea-water, small- particle, and large-particle components of Eq. (3.38) are shown.
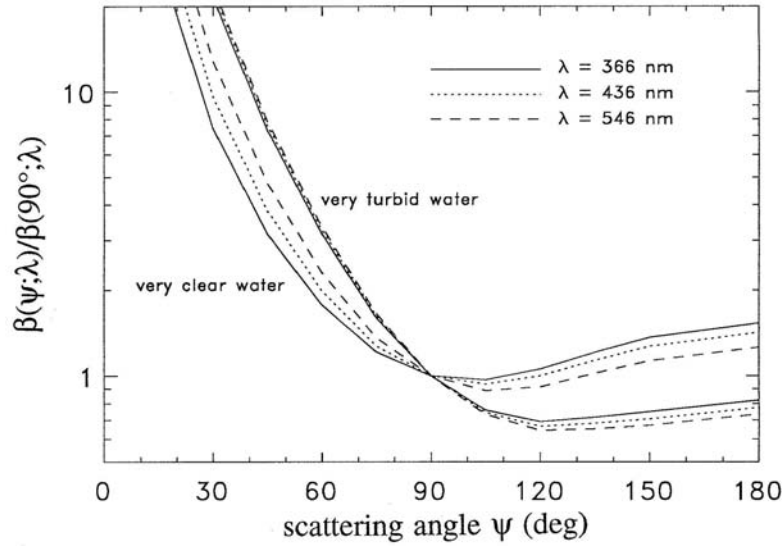
Fig. 3.19. Wavelength dependence of the Kopelevich model, Eq. (3.38), for very clear and very turbid waters. Compare to Fig. 3.16.

description of VSF's observed in a variety of waters. Unfortunately, the data upon which the model (3.38) is based have never been published.

Several simple models are available for the total scattering coefficient $b(\lambda)$. A commonly employed bio-optical model for $b(\lambda)$ is that of Gordon and Morel (1983):

$$b(\lambda) = \left( \frac{550}{\lambda} \right) 0.30 \, C^{0.62} \qquad (\text{m}^{-1}) . \tag{3.40}$$

Here $\lambda$ is in nm, and $C$ is the chlorophyll concentration in mg m$^{-3}$. This model includes the contribution of pure water to the total scattering; this contribution is negligible except at very low chlorophyll values. Morel (1991b) adds a pure-water term, $b_w(\lambda)$, to the right-hand side of Eq. (3.40), so that the model gives the correct value at $C = 0$. We shall use this model in Section 11.8.

A related bio-optical model for the total backscatter coefficient $b_b(\lambda)$ is found in Morel (1988; see also Stramski and Kiefer, 1991):

$$b_b(\lambda) = \tfrac{1}{2} b_w(\lambda)$$
$$+ \left[ 0.002 + 0.02 (\tfrac{1}{2} - \tfrac{1}{4} \log C) \left( \frac{550}{\lambda} \right) \right] \left[ 0.30 \, C^{0.62} - b_w(550) \right]. \tag{3.41}$$

This model explicitly shows the contributions by pure water and by particles. The first factor in brackets in the second term on the right-hand side of the equation represents the probability of backscatter by a particle; the second factor in brackets is the total scattering by particles. The ($\frac{1}{2}$ − $\frac{1}{4}$log$C$) factor gives the particle contribution a $\lambda^{-1}$ wavelength dependence in very clear ($C$ = 0.01 mg m$^{-1}$) water and no wavelength dependence in very turbid ($C$ = 100 mg m$^{-3}$) water. The empirically derived models (3.40) and (3.41) are intended for use only in case 1 waters.

A feeling for the accuracy of the $b(\lambda)$ model of Eq. (3.40) can be obtained from Fig. 3.20, which plots measured $b(550)$ values versus chlorophyll concentration $C$ in both case 1 and case 2 waters. Note that even when the model is applied to the case 1 waters from which it was derived, the predicted $b(550)$ value easily can be wrong by a factor of two. If the model is misapplied to case 2 waters, the error can be an order of magnitude. Note that for a given $C$ value, $b(550)$ is higher in case 2 waters
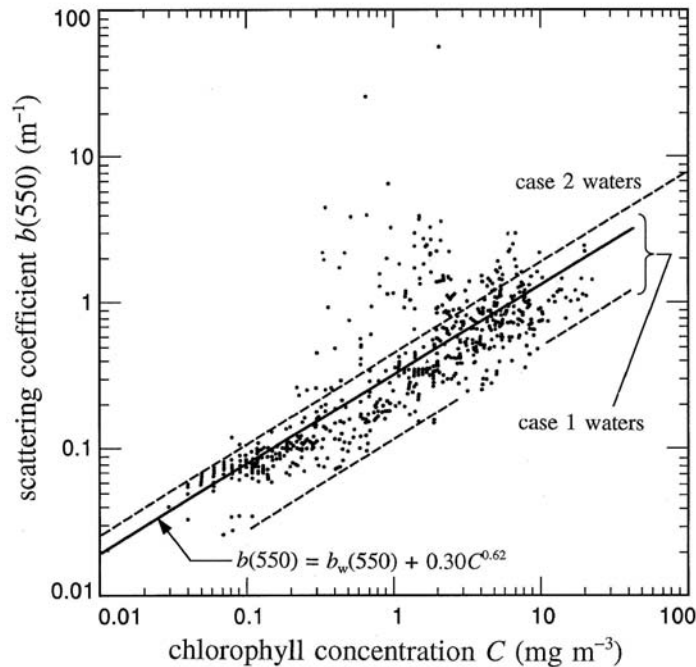


Fig. 3.20. Measured scattering coefficients at $\lambda$ = 550 nm, $b(550)$, as a function of chlorophyll concentration $C$. Case 1 waters lie between the dashed lines. Case 2 waters lie above the upper dashed line, which is defined by $b(550) = 0.45C^{0.62}$. The solid line is the model of Eq. (3.40). [redrawn from Gordon and Morel (1983), by permission]

than in case 1 waters, presumably because of the presence of additional particles that do not contain chlorophyll.

Integration over $\psi$ of the Kopelevich $\beta(\psi;\lambda)$ model of Eq. (3.38) yields another model for $b(\lambda)$:

$$b(\lambda) = 0.0017\left(\frac{550}{\lambda}\right)^{4.3} + 1.34\, v_s \left(\frac{550}{\lambda}\right)^{1.7} + 0.312\, v_\ell \left(\frac{550}{\lambda}\right)^{0.3} \quad (\text{m}^{-1}) \quad (3.42)$$

where $v_s$ and $v_\ell$ are given by Eq. (3.39). Kopelevich claims that the accuracy of this model is ~30%.

An extension of the Kopelevich model is found in Haltrin and Kattawar (1991, their notation):

$$b(\lambda) = b_w(\lambda) + b_{ps}^o(\lambda)P_s + b_{p\ell}^o(\lambda)P_\ell. \qquad (3.43)$$

Here $b_w(\lambda)$ is given by

$$b_w(\lambda) = 5.826 \times 10^{-3}\left(\frac{400}{\lambda}\right)^{4.322}, \qquad (3.44)$$

which is essentially the same as Eq. (3.31) and the data in Table 3.8. The terms $b_{ps}^o(\lambda)$ and $b_{p\ell}^o(\lambda)$ are the specific scattering coefficients for small and large particles, respectively, and are given by

$$b_{ps}^o(\lambda) = 1.1513\left(\frac{400}{\lambda}\right)^{1.7} \qquad (\text{m}^2\text{g}^{-1})$$

$$b_{p\ell}^o(\lambda) = 0.3411\left(\frac{400}{\lambda}\right)^{0.3} \qquad (\text{m}^2\text{g}^{-1}).$$

$P_s$ and $P_\ell$ are the concentrations in g m$^{-3}$ of small and large particles, respectively. These quantities are parameterized in terms of the chlorophyll concentration $C$, as shown in Table 3.14. This work also presents a model for backscattering:

$$b_b(\lambda) = \tfrac{1}{2}b_w(\lambda) + B_s b_{ps}^o(\lambda)P_s + B_\ell b_{p\ell}^o(\lambda)P_\ell. \qquad (3.45)$$

Here $B_s = 0.039$ is the backscattering probability for small particles and $B_\ell = 0.00064$ is the backscattering probability for large particles.

The bio-optical models for scattering just discussed are useful but very approximate. The reason for the frequent large discrepancies between model predictions and measured reality likely lies in the fact that scattering depends not just on particle concentration (as parameterized in terms of

Table 3.14. Parameterization of the concentrations of small ($P_s$) and large ($P_\ell$) particles in terms of the chlorophyll concentration $C$, for use in Eqs. (3.43) and (3.45).[a]

| $C$ (mg m$^{-3}$) | $P_s$ (g m$^{-3}$) | $P_\ell$ (g m$^{-3}$) |
|---|---|---|
| 0.00 | 0.000 | 0.000 |
| 0.03 | 0.001 | 0.035 |
| 0.05 | 0.002 | 0.051 |
| 0.12 | 0.004 | 0.098 |
| 0.30 | 0.009 | 0.194 |
| 0.60 | 0.016 | 0.325 |
| 1.00 | 0.024 | 0.476 |
| 3.00 | 0.062 | 1.078 |

[a] Reproduced from Haltrin and Kattawar (1991), with permission.

chlorophyll concentration), but also on the particle index of refraction and on the details of the particle size distribution, which are not well parameterized in terms of the chlorophyll concentration alone. Whether or not the Kopelevich model or its derivative Haltrin-Kattawar form, which at least partition the scattering into large and small particle components, is in some sense better than the Gordon-Morel model is not known at present. Another consequence of the complexity of scattering is seen in the next section.

# 3.9 Beam Attenuation

The spectral beam attenuation coefficient $c(\lambda)$ is just the sum of the spectral absorption and scattering coefficients: $c(\lambda) = a(\lambda) + b(\lambda)$. Since both $a(\lambda)$ and $b(\lambda)$ are highly variable functions of the nature and concentration of the constituents of natural waters, so is $c(\lambda)$. Beam attenuation near $\lambda = 660$ nm is the only inherent optical property of water

that is easily, accurately and routinely measured. This wavelength is used both for engineering reasons (the availability of a stable LED light source) and because absorption by yellow matter is negligible in the red. Thus the quantity

$$c_p(660) \equiv c(660) - a_w(660) - b_w(660) \equiv c(660) - c_w(660) \qquad (3.46)$$

is determined by the nature of the suspended particulate matter. The particulate beam attenuation $c_p(660)$ is highly correlated with total particle volume concentration (usually expressed in parts per million, ppm), but it is much less well correlated with chlorophyll concentration (Kitchen, *et al.*, 1982). The particulate beam attenuation can be used to estimate the total particulate load [often expressed as g m$^{-3}$; see Bishop (1986)]. However, the dependence of the particulate beam attenuation on particle properties is not simple. Spinrad (1986) used Mie theory to calculate the dependence of the volume-specific particulate beam attenuation (particulate beam attenuation coefficient $c_p$ in m$^{-1}$, per unit of suspended particulate volume in ppm) on the relative refractive index and on the slope $s$ of an assumed Junge size distribution, for particles in the size range 1-80 µm. (See Section 3.11 for a description of how such calculations are made.) Figure 3.21 shows the results. Although the details of the figure are sensitive to the
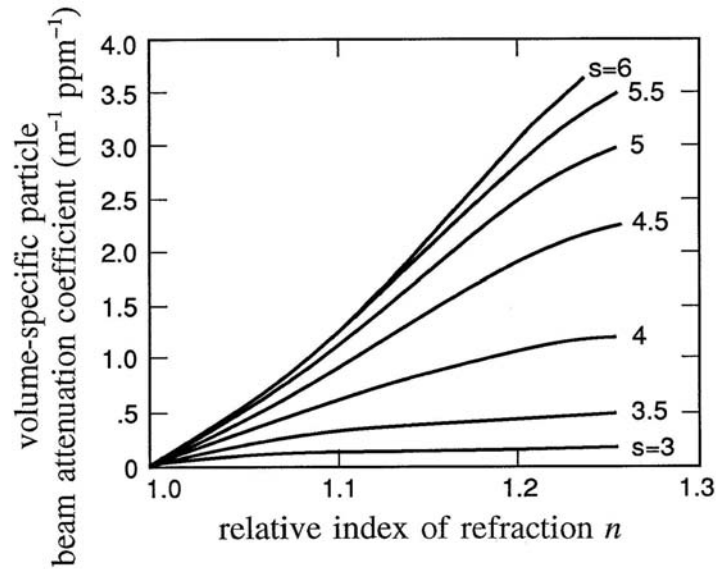


Fig. 3.21. Computed relationship between the volume-specific particle beam attenuation coefficient, relative index of refraction, and slope *s* of a Junge number size distribution. [reproduced from Spinrad (1986), by permission]

choice of upper and lower size limits in the Mie calculations [see Eq. (3.53)], the qualitative behavior of the curves is generally valid and supports the statements made in the closing paragraph of the previous section.

Because of the complicated dependence of scattering, and hence of beam attenuation, on particle properties, the construction of bio-optical models for $c(\lambda)$ is not easy. The reason, as just seen, is that chlorophyll concentration alone is not sufficient to parameterize scattering (Kitchen and Zaneveld, 1990a). Figure 3.22 illustrates this insufficiency. The figure plots vertical profiles of $c(665)$, water density (proportional to the oceanographic variable $\sigma_t$), and chlorophyll concentration (proportional to fluorescence by chlorophyll and related pigments). Note that the maximum in beam attenuation at 46 m depth coincides with the interface (pycnocline) between
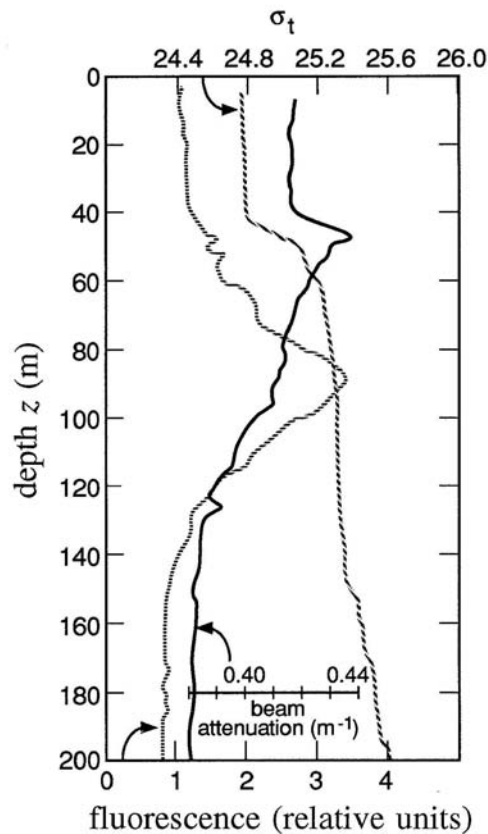


Fig. 3.22. Example from Pacific Ocean water of the depth dependence of beam attenuation (solid line), water density ($\sigma_t$, dashed line), and chlorophyll concentration (fluorescence, dotted line). [reproduced from Kitchen and Zaneveld (1990a), by permission]

less dense water above and more dense water below.  Peaks in beam attenuation are commonly observed at density interfaces, because particle concentrations are often greatest there.  The maximum in chlorophyll concentration occurs at a depth of 87 m. The chlorophyll concentration depends not just on the number or volume of chlorophyll bearing particles, but also on their photoadaptive state, which depends on nutrient availability and ambient lighting.  Thus chlorophyll concentration cannot be expected to correlate well with total scattering or with particulate beam attenuation $c_p(\lambda)$.

Voss (1992) has developed an empirical model for $c(\lambda)$ given a measurement of $c$ at $\lambda = 490$ nm:

$$c(\lambda) = c_w(\lambda) + [c(490) - c_w(490)][1.563 - 1.149{\times}10^{-3}\lambda], \qquad (3.47)$$

where $\lambda$ is in nm and $c$ is in $m^{-1}$.  The attenuation coefficient for pure sea water, $c_w = a_w + b_w$, is given by the Smith-Baker data of Table 3.5.  This model was statistically derived from data of global extent.  Testing of the model with independent data usually gave errors of less than 5%, although occasional errors of ~20% were found.

Voss also determined a least-squares fit of $c(490)$ to the chlorophyll concentration.  The result,

$$c(490) = c_w(490) + 0.39\,C^{0.57}, \qquad (3.48)$$

is similar in form to the chlorophyll dependence of the $a(\lambda)$ and $b(\lambda)$ models seen in Eqs. (3.27) and (3.40), respectively.  Figure 3.23 shows the spread of the data points used to determine Eq. (3.48).  Note that for a given value of $C$, there is an order-of-magnitude spread in values of $c(490)$.  The user of Eq. (3.48), or of the models for $b(\lambda)$, must always keep in mind that large deviations from the predicted values will be found in natural waters.

# 3.10 Diffuse Attenuation and Jerlov Water Types

As we saw in Section 3.2,  there is a so-called diffuse attenuation coefficient for any radiometric variable.  The most commonly used diffuse attenuation coefficients are those for downwelling plane irradiance, $K_d(z;\lambda)$, and for PAR, $K_{PAR}(z)$. Although the various diffuse attenuation coefficients are conceptually distinct, in practice they are often numerically similar, and they all asymptotically approach a common value at great depths in homogeneous water.  The monograph by Tyler and Smith (1970) gives
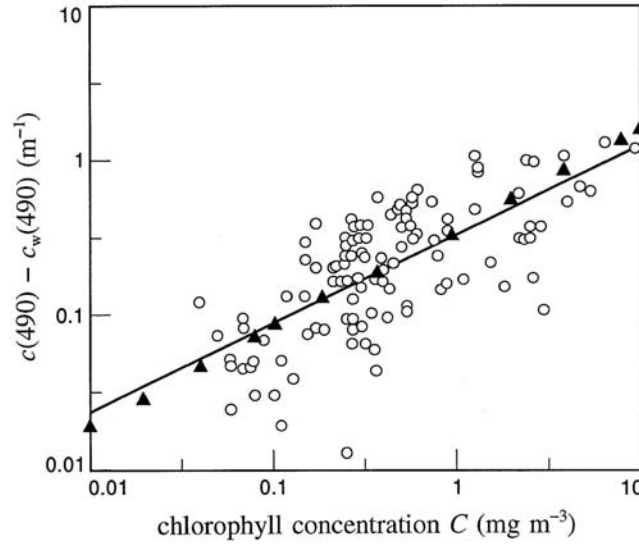
Fig. 3.23. Particle beam attenuation at 490 nm (open circles) as a function of chlorophyll concentration $C$, as used to determine Eq. (3.47), which is given by the solid line. Triangles give values as predicted by the sum of Eqs. (3.27) and (3.40). [redrawn from Voss (1992), by permission]

tabulations and plots of $E_d(z;\lambda)$, $E_u(z;\lambda)$, and the associated $K_d(z;\lambda)$, $K_u(z;\lambda)$, and $R(z;\lambda)$ measured in a variety of waters.

   Observation shows that $K_d(z;\lambda)$ varies systematically with wavelength over a wide range of waters from very clear to very turbid. Moreover, $K_d(z;\lambda)$ is often rather insensitive to environmental effects (Baker and Smith, 1979) except for extreme conditions (such as the sun near the horizon), and in most cases correction can be made for the environmental effects that are present in $K_d$ (Gordon, 1989a, as discussed in Section 3.2). $K_d$ therefore is regarded as a quasi-inherent optical property whose variability is governed primarily by changes in the inherent optical properties of the water body and not by changes in the external environment.

   Jerlov (1976) exploited this benign behavior of $K_d$ to develop a frequently used classification scheme for oceanic waters based on the spectral shape of $K_d$. The *Jerlov water types* are in essence a classification based on water clarity as quantified by $K_d(w;\lambda)$, where $z = w$ is a depth just below the sea surface. This classification scheme can be contrasted with the case 1 and case 2 classification described in Section 3.7, which is based on the nature of the suspended matter within the water. The Jerlov water types

are numbered I, IA, IB, II and III for open ocean waters, and 1 through 9 for coastal waters. Type I is the clearest and type III is the most turbid open ocean water. Likewise, for coastal waters, type 1 is clearest and type 9 is most turbid. The Jerlov types I-III generally correspond to case 1 water, since phytoplankton predominate in the open ocean. Types 1-9 correspond to case 2 waters, where yellow matter and terrigenous particles dominate the optical properties. A rough correspondence between chlorophyll concentration and Jerlov oceanic water type is given by Morel (1988):

$$C: \quad 0\text{-}0.01 \sim 0.05 \sim 0.1 \sim 0.5 \sim 1.5\text{-}2.0 \text{ mg m}^{-3}$$
$$\text{water type:} \quad \text{I} \quad \text{IA} \quad \text{IB} \quad \text{II} \quad \text{III}$$

Table 3.15. Downwelling irradiance diffuse attenuation coefficients $K_d(\lambda)$ used to define the Jerlov water types, as determined by Austin and Petzold.[a] All quantities in the body of the table have units of m$^{-1}$.

| $\lambda$ (nm) | Jerlov water type | | | | | |
|---|---|---|---|---|---|---|
| | I | IA | IB | II | III | 1 |
| 350 | 0.0510 | 0.0632 | 0.0782 | 0.1325 | 0.2335 | 0.3345 |
| 375 | 0.0302 | 0.0412 | 0.0546 | 0.1031 | 0.1935 | 0.2839 |
| 400 | 0.0217 | 0.0316 | 0.0438 | 0.0878 | 0.1697 | 0.2516 |
| 425 | 0.0185 | 0.0280 | 0.0395 | 0.0814 | 0.1594 | 0.2374 |
| 450 | 0.0176 | 0.0257 | 0.0355 | 0.0714 | 0.1381 | 0.2048 |
| 475 | 0.0184 | 0.0250 | 0.0330 | 0.0620 | 0.1160 | 0.1700 |
| 500 | 0.0280 | 0.0332 | 0.0396 | 0.0627 | 0.1056 | 0.1486 |
| 525 | 0.0504 | 0.0545 | 0.0596 | 0.0779 | 0.1120 | 0.1461 |
| 550 | 0.0640 | 0.0674 | 0.0715 | 0.0863 | 0.1139 | 0.1415 |
| 575 | 0.0931 | 0.0960 | 0.0995 | 0.1122 | 0.1359 | 0.1596 |
| 600 | 0.2408 | 0.2437 | 0.2471 | 0.2595 | 0.2826 | 0.3057 |
| 625 | 0.3174 | 0.3206 | 0.3245 | 0.3389 | 0.3655 | 0.3922 |
| 650 | 0.3559 | 0.3601 | 0.3652 | 0.3837 | 0.4181 | 0.4525 |
| 675 | 0.4372 | 0.4410 | 0.4457 | 0.4626 | 0.4942 | 0.5257 |
| 700 | 0.6513 | 0.6530 | 0.6550 | 0.6623 | 0.6760 | 0.6896 |

[a] Reproduced from Austin and Petzold (1986), with permission.

Austin and Petzold (1986) re-evaluated the Jerlov classification using an expanded data base and slightly revised the $K_d(\lambda)$ values used by Jerlov in his original definition of the water types.  Table 3.15 gives the revised values for $K_d(\lambda)$ for the water types commonly encountered in oceanography.  These values are recommended over those found in Jerlov (1976).  Figure 3.24 shows the percent transmittance of $E_d(\lambda)$ per meter of water for selected Jerlov water types.  Note how the wavelength of maximum transmittance shifts from blue in the clearest open ocean water (type I) to green (types III and 1) to yellow in the most turbid, yellow-matter-rich coastal water (type 9).  Figure 3.25 shows the color of the various Jerlov water types as a function of depth within the water body.  The color was computed by using $E_d(\lambda)$ in Eqs. (2.10) and (2.11).  Note that the open-ocean types I-III are blue, coastal waters of types 1-5 are green, and the very turbid type 9 is distinctly yellow.  For each water type, the color is a very impure mixture near the surface.  As one descends into the water body, only the wavelengths of minimum absorption are left, and the color becomes purer.

Austin and Petzold also presented a simple model that allows the determination of $K_d(\lambda)$ at all wavelengths from a value of $K_d$ measured at any single wavelength.  This model is defined by

$$K_d(\lambda) = \frac{M(\lambda)}{M(\lambda_o)}\left[K_d(\lambda_o) - K_{dw}(\lambda_o)\right] + K_{dw}(\lambda). \tag{3.49}$$


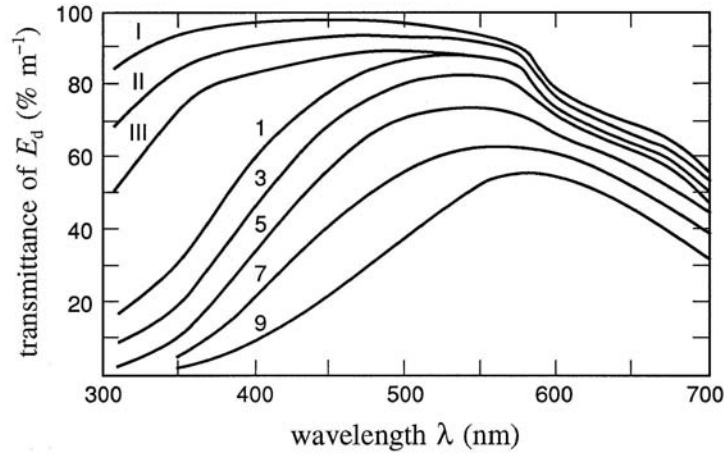
Fig. 3.24.  Percentage transmittance of downwelling irradiance $E_d$, per meter of water, as a function of wavelength, for selected Jerlov water types. [reproduced from Jerlov (1976), by permission]
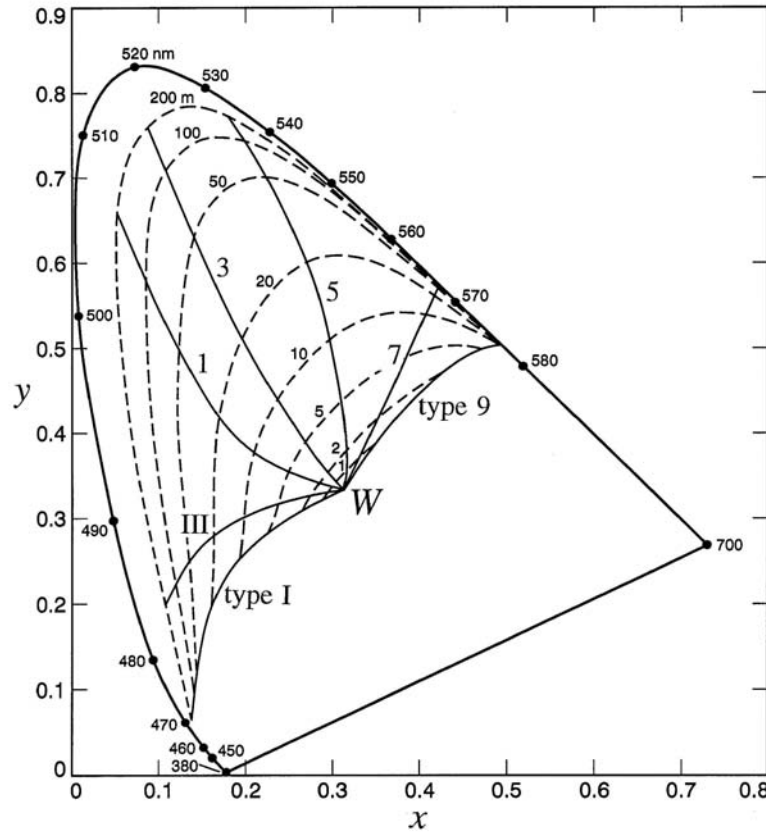
Fig. 3.25. Water color computed from $E_d(\lambda)$, as a function of the Jerlov water type and depth within the water body, displayed on a C.I.E. chromaticity diagram. The dashed curves are lines of constant depth, in meters, and the solid curves emanating from the white light point $W$ give the colors for their respective Jerlov water types. [redrawn from Jerlov (1976), by permission]

Here $\lambda_o$ is the wavelength at which $K_d$ is measured, and $K_{dw}$ refers to values for pure sea water. $K_{dw}(\lambda)$ and the statistically derived coefficients $M(\lambda)$ are given in Table 3.16. (These $K_{dw}$ values differ slightly from those seen in Table 3.5.) This model is valid in waters where $K_d(490) \le 0.16 \text{ m}^{-1}$, which corresponds to a chlorophyll concentration of $C \le 3 \text{ mg m}^{-3}$.

Unlike the beam attenuation coefficient $c(\lambda)$, the diffuse attenuation $K_d(z;\lambda)$ is highly correlated with chlorophyll concentration. The reason is seen in the approximate formula (Gordon, 1989a)

Table 3.16. Values of the coefficient $M(\lambda)$ and of the downwelling diffuse attenuation coefficient for pure sea water, $K_{dw}(\lambda)$, for use in Eq. (3.49).[a]

| $\lambda$ (nm) | $M$ (m$^{-1}$) | $K_{dw}$ (m$^{-1}$) | $\lambda$ (nm) | $M$ (m$^{-1}$) | $K_{dw}$ (m$^{-1}$) | $\lambda$ (nm) | $M$ (m$^{-1}$) | $K_{dw}$ (m$^{-1}$) |
|---|---|---|---|---|---|---|---|---|
| 350 | 2.1442 | 0.0510 | 470 | 1.1982 | 0.0179 | 590 | 0.4840 | 0.1578 |
| 360 | 2.0504 | 0.0405 | 480 | 1.0955 | 0.0193 | 600 | 0.4903 | 0.2409 |
| 370 | 1.9610 | 0.0331 | 490 | 1.0000 | 0.0224 | 610 | 0.5090 | 0.2892 |
| 380 | 1.8772 | 0.0278 | 500 | 0.9118 | 0.0280 | 620 | 0.5380 | 0.3124 |
| 390 | 1.8009 | 0.0242 | 510 | 0.8310 | 0.0369 | 630 | 0.6231 | 0.3296 |
| 400 | 1.7383 | 0.0217 | 520 | 0.7578 | 0.0498 | 640 | 0.7001 | 0.3290 |
| 410 | 1.7591 | 0.0200 | 530 | 0.6924 | 0.0526 | 540 | 0.7300 | 0.3559 |
| 420 | 1.6974 | 0.0189 | 540 | 0.6350 | 0.0577 | 660 | 0.7301 | 0.4105 |
| 430 | 1.6108 | 0.0182 | 550 | 0.5860 | 0.0640 | 670 | 0.7008 | 0.4278 |
| 440 | 1.5169 | 0.0178 | 560 | 0.5457 | 0.0723 | 680 | 0.6245 | 0.4521 |
| 450 | 1.4158 | 0.0176 | 570 | 0.5146 | 0.0842 | 690 | 0.4901 | 0.5116 |
| 460 | 1.3077 | 0.0176 | 580 | 0.4935 | 0.1065 | 700 | 0.2891 | 0.6514 |

[a] Condensed with permission from Austin and Petzold (1986), who give values every 5 nm.

$$K_d(\lambda) \approx \frac{a(\lambda) + b_b(\lambda)}{\cos\theta_{sw}},$$

where $\theta_{sw}$ is the solar angle measured within the water. Since $a(\lambda) \gg b_b(\lambda)$ for most waters, $K_d(\lambda)$ is largely determined by the absorption properties of the water, which are fairly well parameterized by the chlorophyll concentration. Beam attenuation on the other hand is proportional to the total scattering which, as seen above, is not well parameterized by chlorophyll concentration. Observations show that the beam attenuation at 660 nm is not in general correlated with diffuse attenuation (Siegel and Dickey, 1987).

A bio-optical model for $K_d(\lambda)$ is given by Morel (1988):

$$K_d(\lambda) = K_{dw}(\lambda) + \chi(\lambda)\,C^{e(\lambda)}. \qquad (3.50)$$

Here $K_{dw}(\lambda)$ is the diffuse attenuation for pure sea water, and $\chi(\lambda)$ and $e(\lambda)$ are statistically derived functions that convert the chlorophyll concentration $C$ in mg m$^{-3}$ into $K_d$ values in m$^{-1}$. Table 3.17 gives the $K_{dw}$, $\chi$ and $e$ values used in the Morel model. This model is applicable to case 1 waters with

Table 3.17. Values of the coefficients $\chi(\lambda)$ and $e(\lambda)$, and of the downwelling diffuse attenuation coefficient for pure sea water, $K_{dw}(\lambda)$, for use in Eq. (3.50).[a]

| $\lambda$ (nm) | $\chi(\lambda)$ | $e(\lambda)$ | $K_{dw}(\lambda)$ $(m^{-1})$ | $\lambda$ (nm) | $\chi(\lambda)$ | $e(\lambda)$ | $K_{dw}(\lambda)$ $(m^{-1})$ |
|---|---|---|---|---|---|---|---|
| 400 | 0.1100 | 0.668 | 0.0209 | 550 | 0.0410 | 0.650 | 0.0640 |
| 410 | 0.1125 | 0.680 | 0.0196 | 560 | 0.0390 | 0.640 | 0.0717 |
| 420 | 0.1126 | 0.693 | 0.0183 | 570 | 0.0360 | 0.623 | 0.0807 |
| 430 | 0.1078 | 0.707 | 0.0171 | 580 | 0.0330 | 0.610 | 0.1070 |
| 440 | 0.1041 | 0.707 | 0.0168 | 590 | 0.0325 | 0.618 | 0.1570 |
| 450 | 0.0971 | 0.701 | 0.0168 | 600 | 0.0340 | 0.626 | 0.2530 |
| 460 | 0.0896 | 0.700 | 0.0173 | 610 | 0.0360 | 0.634 | 0.2960 |
| 470 | 0.0823 | 0.703 | 0.0175 | 620 | 0.0385 | 0.642 | 0.3100 |
| 480 | 0.0746 | 0.703 | 0.0194 | 630 | 0.0420 | 0.653 | 0.3200 |
| 490 | 0.0690 | 0.702 | 0.0217 | 640 | 0.0440 | 0.663 | 0.3300 |
| 500 | 0.0636 | 0.700 | 0.0271 | 650 | 0.0450 | 0.672 | 0.3500 |
| 510 | 0.0578 | 0.690 | 0.0384 | 660 | 0.0475 | 0.682 | 0.4050 |
| 520 | 0.0498 | 0.680 | 0.0490 | 670 | 0.0515 | 0.695 | 0.4300 |
| 530 | 0.0467 | 0.670 | 0.0518 | 680 | 0.0505 | 0.693 | 0.4500 |
| 540 | 0.0440 | 0.660 | 0.0568 | 690 | 0.0390 | 0.640 | 0.5000 |
|  |  |  |  | 700 | 0.0300 | 0.600 | 0.6500 |

[a] Condensed with permission from Morel (1988), who gives values every 5 nm.

$C \le 30$ mg m$^{-3}$, although the $\chi$ and $e$ values are somewhat uncertain for $\lambda > 650$ nm because of sparse data available for their determination. Some feeling for the accuracy of the Morel $K_d(\lambda)$ model can be obtained from Fig. 3.26, which shows predicted (the line) and observed $K_d(450)$ values as a function of $C$. Errors can be as large as a factor of two in case 1 waters (dots), and can be much larger if the model is misapplied to case 2 waters (open circles). The Morel model (3.50) allows the determination of $K_d(\lambda)$ if $C$ is measured; the Austin and Petzold model (3.49) determines $K_d(\lambda)$ from a measurement at one wavelength.

Morel (1988) also presents a very simple bio-optical model for $\overline{K}_{PAR}(0;z_{eu})$, the value of $K_{PAR}(z)$ averaged over the euphotic zone $0 \le z \le z_{eu}$:

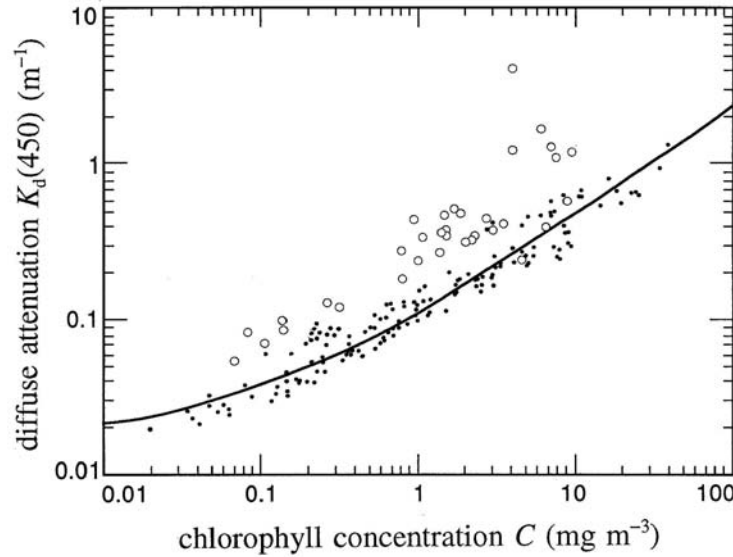$$\overline{K}_{PAR}(0;z_{eu}) = 0.121\,C^{0.428}, \tag{3.51}$$

Fig. 3.26.   Measured $K_d$ values at 450 nm as a function of chlorphhyll concentration $C$.  Dots are measurements from case 1 waters; open circles are from case 2 waters.  The solid line gives $K_d(450)$ as predicted by the Morel bio-optical model, Eq. (3.50).  [redrawn from Morel (1988), by permission]

where $C$ is chlorophyll concentration in mg m$^{-3}$ and $\bar{K}_{PAR}$ is in m$^{-1}$.  The euphotic zone is the region where there is sufficient light for photosynthesis to take place; it extends roughly to the depth where $E_{PAR}(z)$ is one percent of its surface value, i.e. $E_{PAR}(z_{eu}) = 0.01\ E_{PAR}(0)$.  Table 3.18 gives $z_{eu}$ as a function of $C$, as determined by the Morel model, Eq. (3.51).

# 3.11 Single-particle Optics

In the preceding sections of this chapter, we have discussed the optical properties of large volumes of water.  We have only commented that these bulk properties are determined by the combined effects of the myriad particles found within the water.  We now briefly outline how the connection is made between many individual particles, each with its own optical properties, and the bulk properties as measured by oceanographic instruments and as used in radiative transfer theory.

Table 3.18. Approximate depth of the euphotic zone, $z_{eu}$, in homogeneous case 1 water as a function of the chlorophyll concentration $C$.[a]

| $C$ (mg m$^{-3}$) | $z_{eu}$ (m) | $C$ (mg m$^{-3}$) | $z_{eu}$ (m) |
|---|---|---|---|
| 0.0 | 183 | 1 | 39 |
| 0.01 | 153 | 2 | 29 |
| 0.03 | 129 | 3 | 24 |
| 0.05 | 115 | 5 | 19 |
| 0.1 | 95 | 10 | 14 |
| 0.2 | 75 | 20 | 10 |
| 0.3 | 64 | 30 | 8 |
| 0.5 | 52 | | |

[a] Data extracted from Morel (1988), with permission.

## *Mie theory*

Let us consider the following problem. We have given a single, homogeneous sphere of diameter $D$, whose material has a complex index of refraction $m_s = n_s - ik_s$. The sphere is imbedded in an infinite, uniform, non-absorbing medium whose index of refraction is therefore real: $m_m = n_m$. The sphere is illuminated by a collimated beam of monochromatic light of wavelength $\lambda_m = \lambda_{vac}/n_m$, where $\lambda_{vac}$ is the wavelength *in vacuo* of light corresponding to the given frequency. The beam is much larger in diameter than the sphere. We wish to find how the incident light is absorbed and scattered by the sphere, including the angular distribution of the scattered intensity and the state of polarization of the scattered light. The so-called *Mie theory* give a rigorous solution to this problem.

The stated problem is most easily attacked using the electromagnetic-field viewpoint of light. The collimated light beam is described as an electromagnetic plane wave, and the sphere is treated as a dielectric. Maxwell's equations are then solved subject to boundary conditions at the surface of the sphere. The solution of Maxwell's equations gives the electromagnetic field – in other words, the light field – both within the sphere and throughout the surrounding medium.

The solution of this geometrically simple problem is surprisingly difficult.  Indeed, this is one of the classic problems of applied mathematics, and its solution was attempted (and achieved in various forms) by many of the most illustrious figures of nineteenth-century physics.  For historical reasons, which can be found in Logan (1990), Mie (1908) commonly gets credit for the solution of the problem.  His general solution is *exact and valid for all sizes of spheres, indices of refraction, and wavelengths*.  The solution is in the form of infinite series of complicated mathematical functions, and we shall not present the equations here.  Details of the solution are given in the texts by van de Hulst (1957) and by Bohren and Huffman (1983); the latter book includes computer programs for numerical evaluation of the various formulas.

Calculations based on Mie theory are playing an increasingly important role in hydrologic optics, primarily because modern computers make it convenient to perform the necessary computations.  We should therefore at least acquaint ourselves with the terminology, even if we skip the mathematics. Moreover, a brief discussion of Mie theory and of "single-particle" optics serves to tie together several topics discussed earlier in this chapter.

Mie's solution often is presented in terms of various *absorption* and *scattering efficiencies*.  The absorption efficiency $Q_a$, for example, gives the fraction of radiant energy incident on the sphere that is absorbed by the sphere. By "energy incident on the sphere," we mean the energy passing through an area equal to the cross-sectional (projected, or "shadow") area of the sphere, $A_s = \pi D^2/4$.  Likewise, the total scattering efficiency $Q_b$ gives the fraction of incident energy that is scattered into all directions.  Other efficiencies can be defined: $Q_c = Q_a + Q_b$ for total attenuation, $Q_{bb}$ for backscattering, and so on.

The Mie solution also can be presented in terms of *absorption* and *scattering cross sections*.  The physical interpretation of these cross sections is simple.  The absorption cross section $\sigma_a$, for example, is the cross sectional area of the incident beam that has power equal to the power absorbed by the sphere.  The absorption and scattering cross sections are  therefore related to the corresponding efficiencies by the geometrical cross section of the sphere. Thus

$$\sigma_a \equiv Q_a A_s = Q_a \pi D^2/4 \qquad (m^2).$$

Likewise, $\sigma_b = Q_b A_s$, and so on for $\sigma_c$, $\sigma_{bb}$, etc.

These efficiencies and cross sections depend on the various parameters of the problem as follows.  The relevant parameter describing the

*material* of the sphere and of the surrounding medium is the *relative* complex index of refraction, $m_r$, defined by [see Supplementary Note 2]

$$m_r \equiv \left( \frac{n_s}{n_m} \right) - i \left( \frac{k_s}{n_m} \right) \equiv n_r - i k_r .$$

Note that $n_r$ can be less than one: a spherical air bubble in water would have $n_r \approx 1/1.34 \approx 0.75$. The relevant parameter describing the *size* of the sphere is its diameter $D$ relative to the wavelength of the incident light within the medium. The size parameter usually is written as

$$\alpha \equiv \frac{\pi D}{\lambda_m} = \frac{\pi D n_m}{\lambda_{vac}} .$$

Some of the Mie formulas also involve the *phase-shift parameter*

$$\rho \equiv 2\alpha(n_r - 1),$$

and the *absorption thickness*

$$\rho' \equiv 4 k_r \alpha = a_s D .$$

It is important to note, when computing $\rho'$, that $a_s$ is the absorption coefficient of the material forming the sphere. Phytoplankton cells typically have $a_s$ values of $10^4$–$10^5$ m$^{-1}$ at visible wavelengths. This $a_s$ must not be confused with the bulk absorption coefficient for natural waters containing phytoplankton – the quantity seen, for example, in Eq. (3.27). As an example of the Mie parameter values, consider a phytoplankton cell with $D = 8$ μm, $n_s = 1.4$, and $a_s = 4 \times 10^5$ m$^{-1}$. If the cell is floating in water with $n_m = 1.34$, and if the incident light has $\lambda_{vac} = 500$ nm, we then have $\alpha = 67.4$, $\rho = 6.0$, and $\rho' = 3.2$.

## *Computing bulk IOP's*

The various single-particle cross sections obtained from Mie theory are the cornerstones upon which we construct the equations that give us the bulk inherent optical properties. These equations are not complicated.

Consider, for example, the computation of the total scattering coefficient $b(\lambda)$ from the single-particle cross section $\sigma_b(D;m_r;\lambda)$. The arguments of $\sigma_b$ remind us that the cross section depends on the particle's size and relative index of refraction, and on the wavelength of the incident light. We could equally well write $\sigma_b(\alpha;\rho;\rho')$.

We next observe that for even the most numerous oceanic particles, e.g. viruses or colloids at a concentration of $10^{15}$ m$^{-3}$, the average distance between particles is greater than ten wavelengths of visible light. For the optically most significant phytoplankton, the average separation is thousands of wavelengths. Moreover, these particles usually are randomly distributed and oriented. Ocean water therefore can be treated as a very dilute suspension of random scatterers, and consequently the intensity of light scattered by an ensemble of particles is given by the sum of the intensities due to the individual particles. Coherent scattering effects are negligible, except at extremely small scattering angles (Shifrin, 1988; Fry, *et al.*, 1992b).

Because of this optical independence of the individual particles, we can simply "sum up" their individual contributions to scattering:

$$b(\lambda) \;=\; \int\limits_{\text{all } m_r} \int\limits_{\text{all } D} \sigma_b(D; m_r; \lambda)\, n(D)\, dD\, dm_r \,.$$

(3.52)

Here $n(D)$ is the particle number size distribution discussed in Section 3.4. Recall that $n(D)dD$ is the number of particles per unit volume with diameters between $D$ and $D + dD$. Examples of $n(D)$ were seen in Eqs. (3.23) and (3.24). Equation (3.51) shows the key role played by the size distribution in connecting particles of all different sizes and indices of refraction with the bulk scattering coefficient. Equations such as (3.52) were used to generate Fig. 3.21.

In practice, Eq. (3.52) usually is evaluated separately for each type of particle. By particle type, we mean particles that have the same index of refraction (particles that are made of the same material), but which differ in size. For the $i^{th}$ particle type, which might be cyanobacteria or clay mineral particles, we then have

$$b_i(\lambda) \;=\; \int\limits_{D_{min}^{i}}^{D_{max}^{i}} \sigma_b^{i}(D; m_r^{i}; \lambda)\, n^{i}(D)\, dD$$

(3.53)

$$=\; \int\limits_{D_{min}^{i}}^{D_{max}^{i}} Q_b^{i}(D; m_r^{i}; \lambda)\, \frac{\pi D^2}{4}\, n^{i}(D)\, dD \,.$$

Here $D_{min}^{i}$ and $D_{max}^{i}$ are the minimum and maximum diameters of particles of type $i$. For cyanobacteria, for example, these values might be $D_{min}^{i} = 0.5$ µm and $D_{max}^{i} = 2.5$ µm. The value of $b_i(\lambda)$ is the contribution by the $i^{th}$ particle type to the total scattering coefficient $b(\lambda)$, as was seen in Eq. (3.11). Corresponding equations can be written for other quantities, such as

absorption and backscattering.  Mie theory also gives us a cross section for scattering through angle $\psi$, $\sigma_d(\psi;\lambda)$ with units of $m^2\ sr^{-1}$.  This cross section yields the volume scattering function $\beta(\psi;\lambda)$ via the same formalism as Eq. (3.53).

Mie calculations applied to hydrologic optics have a venerable history. Early efforts at predicting bulk properties from assumed particle properties and size distributions are seen in Kullenberg (1974) and in Brown and Gordon (1974). Brown and Gordon were unable to reproduce observed backscattering values using measured particle size distributions.  However, their instruments were unable to detect submicrometer particles.  They found that Mie theory properly predicted backscattering if they assumed the presence of numerous, submicrometer, low-index-of-refraction particles.   We may reasonably speculate that bacteria and the recently discovered colloids are the particles whose existence was inferred by Brown and Gordon.  Recent Mie calculations have used three-layered spheres to model the structure of phytoplankton (cell wall, chloroplasts, and cytoplasm core) and have used polydisperse mixtures of both organic and inorganic particles (Kitchen and Zaneveld, 1990b).

Much of the utility of Mie theory lies in the fact that it gives us an overall theoretical structure for the analysis and modeling of IOP's.  It is not possible to measure directly all desired quantities.  Therefore, we measure what we can, e.g. beam attenuation, absorption, and particle size distributions.  Mie theory then can be used to determine consistent values for the missing pieces, e.g. particle refractive index and phase functions.  The comprehensive paper by Stramski and Kiefer (1991) shows how this  can be done.  Their paper is a good  example  of  the  sophisticated  level  of  Mie-based  computations  now employed in optical oceanography.

Considerable effort is now being expended in determining the optical properties of microbial particles, which are needed as input to the Mie calculations. The optical properties of living cells depend in complicated ways on the cells' physiological state, which in turn depends on age, nutrient availability, ambient lighting, and the like.  Recent papers by Ackleson, *et al*. (1986), Bricaud and Morel (1986), Morel and Bricaud (1986), Stramski and Morel (1990), Morel (1991a), Ahn, *et al*. (1992), Stramski, *et al*. (1992),  and Morel, *et al*. (1993) will connect the reader with the current literature on this fundamental topic.

Further discussion of single-particle optics would take us beyond the immediate needs of radiative transfer theory.  Our point has been made, and we must proceed.

# 3.12  Closure

One of the guiding principles of any science is the achievement of closure.  This means nothing more than making sure that "all the numbers add up" in a proper fashion.  Researchers in hydrologic optics commonly speak of three types of closure.

*Measurement closure* refers to making accurate measurements.  Consider, for example, the simple conservation-of-energy relation (3.3):

$$a(\lambda) + b(\lambda) = c(\lambda).$$

We have commented on the difficulties in measuring $a(\lambda)$, and on the extreme difficulty of measuring $b(\lambda)$.  For these reasons, $b$ almost always is determined as $c - a$.  However, we can never be sure that a value of $b$ so determined is correct, because there may be undetected random or systematic errors in the measured values of $c$ or, especially, of $a$.  However, *if* we could *independently* measure $a$, $b$, and $c$, so that $a + b = c$ to high accuracy, *then* we could be confident that our instruments and measurement methodologies were giving correct values for $a$ and $c$.  We could then confidently use $b = c - a$ for routine determinations of $b$.

Another example of measurement closure would be to make independent measurements of $b$ and $\beta(\psi)$, and then see if the measured $b$ agrees with $b$ computed as $2\pi \int \beta(\psi)\sin\psi d\psi$.

Making the transition from the optical properties of single particles to the bulk properties, as discussed in the previous section, is an example of *scale closure*, because the calculations connect the smallest and largest size scales.  This form of scale closure provides a strenuous test of our understanding of the properties of the various constituents of natural waters and of the ways in which these constituents contribute to the overall properties of these waters.

Another form of scale closure occurs when we measure IOP's on small samples of water, and then relate those IOP's to measured AOP's, which are determined by large volumes of water.

The third type of closure is called *model closure.*  Here we ask whether analytical or numerical models for computing underwater light fields do indeed make correct predictions, given the IOP's and boundary conditions of a water body.  Errors in models can arise from simple coding errors in computer programs, or from the omission of relevant physics in the equations being solved.  For example, a model that omits fluorescence effects cannot be expected to provide accurate predictions for waters that

contain high concentrations of yellow matter or chlorophyll, both of which fluoresce strongly at certain wavelengths.

Closure is in many ways the Holy Grail of hydrologic optics – always sought, never achieved. Instrumental difficulties in measuring $b$ and $\beta$ keep measurement closure just out of reach. Single-particle-to-bulk-IOP scale closure via Mie theory requires a complete determination of the optical properties of the individual particles, which cannot be made. Checking model closure requires comprehensive measurements of IOP's, boundary conditions, and underwater light fields (preferably the full spectral radiance distribution). The IOP's and boundary conditions are needed as input to the models, and the light field is needed for comparison with the models' predictions. Such data sets have never been collected.

In spite of its elusive nature, the goal of closure provides a valuable framework for prioritizing instrument development, for planning field experiments, and for guiding the development of ever-more-sophisticated numerical models. Zaneveld (1994) discusses closure in more detail.

## 3.13 Summary

We have now defined and briefly surveyed various inherent and apparent optical properties of natural waters. The optical properties of the constituents of natural waters are under active investigation, and we may anticipate that the crude models now available for absorption and scattering will be improved as time goes by. However, the data and models presented in the chapter will be more than adequate for our subsequent discussions of radiative transfer.

Figure 3.27 summarizes the relationships between the various radiometric quantities, IOP's and AOP's that we have discussed. Note in the figure that radiative transfer theory, as expressed by the radiance transfer equation, is the mathematical structure that links the IOP's and the external environment of a water body to the radiometric quantities and AOP's of the water body. We now turn our attention to the development of this theory.

## 3.14 Problems

3.1. Compute $\bar{\mu}_d$ for the cardioidal radiance distribution of Problem 1.5.

3.2. Compute $\bar{\mu}_d$, $\bar{\mu}_u$, $\bar{\mu}$, and $R$ for the radiance distribution of Problem 1.7.
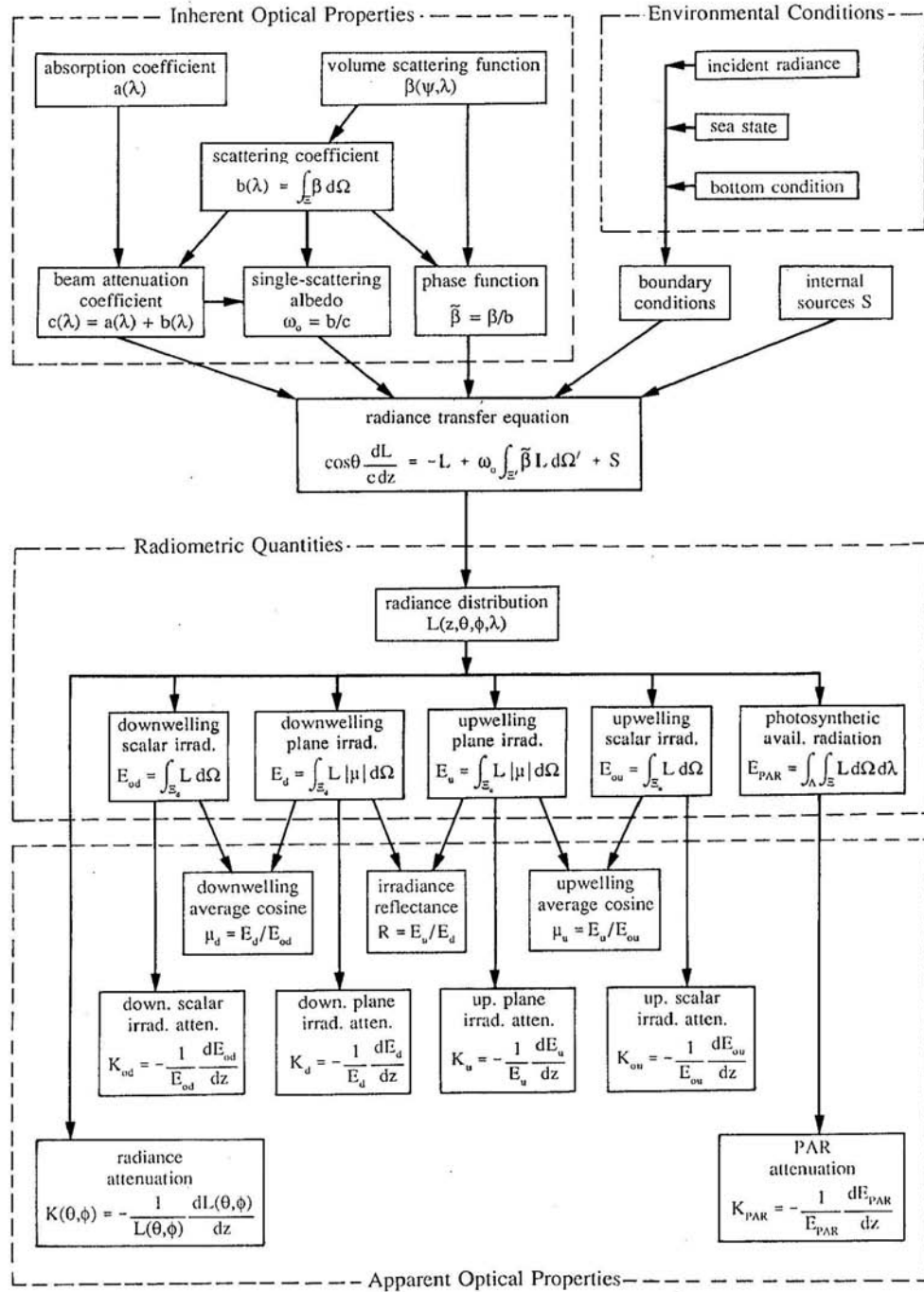
Fig. 3.27. Relationships among the various quantities commonly used in hydrologic optics. [reproduced from Mobley (1994), by permission]

3.3.  At sea level on a clear day at noon, the solar irradiance in the "blue-green window" of greatest water transparency is about 50 W m$^{-2}$.  How much of this irradiance will reach a depth of 1000 m in the clearest ocean water (use water properties for 450 nm)?  How does this compare with the irradiance at sea level at night?  At about what depth would there be only 1 photon m$^{-2}$ s$^{-1}$ of sunlight left?  Assume that the water surface transmits all of the sunlight.  If the sun were 10 times as bright, would the light reach 10 times as deep into the ocean?

3.4.  You are working off of the west coast of North Africa.  On the first day of the cruise, you measure the inherent optical properties *a, b,* and $\tilde{\beta}$.  On the second day, a strong wind brings a severe dust storm from the Sahara Desert. The dust consists of very small ($\leq 0.1$ μm diameter) particles of clear quartz. After the storm, you measure the IOP's again.  Would you expect the absorption coefficient *a* (at a given wavelength) to increase, decrease, or stay about the same?  How about the scattering coefficient *b* (at a given wavelength)?  Would the wavelength dependence of $b(\lambda)$ become stronger, weaker, or stay about the same?  What changes would you expect in the shape of the phase function $\tilde{\beta}$ (e.g. relatively more/less/same forward scatter; more/less/same backscatter)?  Explain your reasoning for all of the above questions. How would the above answers change if the dust particles consisted of opaque clay instead of quartz?

3.5.  Roughly how far does near-infrared radiation of wavelength $\lambda = 1$ μm penetrate into a lake before 99.9% of the radiation is absorbed?  How about thermal radiation of wavelength 10 μm?  You can estimate the needed values of $a(1$ μm$)$ and $a(10$ μm$)$ from Fig. 3.4.